# Lidar and MCP in Wind Resource Estimations above Measurement-Mast Height

N.D. Waars

August 2017

TU Delft

Ventolines
Bevlogen windspecialisten

DTU Danmarks Tekniske Universitet

# Lidar and MCP in Wind Resource Estimations above Measurement-Mast Height

by

N.D. Waars

to obtain the degree of Master of Science
at the Delft University of Technology, and the Technical University of Denmark,
to be defended publicly on 29 August 2017

Student number: 4226275 (TU Delft)
s152218 (DTU)

Thesis committee:

| | |
|---|---|
| Prof. dr. G. J. W. van Bussel, | TU Delft, chair of the thesis committee |
| Dr. Ir. W. A. A. M. Bierbooms, | TU Delft, supervisor |
| Dr. M. C. Kelly, | DTU, supervisor |
| Ir. T. A. Walvis | Ventolines, supervisor |

An electronic version of this thesis is available at http://repository.tudelft.nl/.

TU Delft

Ventolines
Bevlogen windspecialisten

DTU Danmarks Tekniske Universitet

# Acknowledgements

This thesis is the last step in completing the European Wind Energy Master, and it is the end of my study period in Delft. This final project, and the master in total, have been a great experience and I would like to thank various people that have been involved.

First of all, I would like to thank my supervisors for their feedback and guidance. Thank you Mark Kelly, for your help with structuring the project at the start at DTU, and for your advice during our Skype meetings. Thank you Ardaan Walvis, for giving me an insight in wind resource assessment in practice and your help during the project. Thank you Wim Bierbooms, for the constructive feedback. It helped me to write down my work, and to look critically to my report.

I want to thank the people at Ventolines for giving me the opportunity to work on my thesis in a company that is actively involved in the development of wind farms. Being at Ventolines allowed me to get a practical view on the wind energy industry. The people at Ventolines together have an incredible amount of knowledge about the wind energy industry, and it has been a valuable experience to work with you.

My study in Delft and Lyngby has been an amazing experience due to the friends I made. I want to thank them for their contribution to a wonderful study period.

Last, but foremost, I want to express my gratitude to my family and girlfriend. I thank them for their confidence, and for their support for my ambitions. They provided me with invaluable advice when it was most needed and thereby made a great contribution to this project and my personal development.

*N.D. Waars*
*Delft, August 2017*

# Abstract

Modern multi-megawatt wind turbines are tall and may reach heights of 200 meter. Tall wind turbines require measurements above typical measurement mast height. As tall measurement masts are expensive and cumbersome to install, wind measurements at hub height are scarce. Currently, the use of lidars in wind measurement campaigns is increasing. Lidars provide wind measurements over the full wind turbine rotor, but lidars are not always available for an extended period. This thesis investigates the possibility of applying the measure-correlate-predict (MCP) method to short-term lidar measurements in order to extrapolate wind shear statistics.

The first step was to compare the wind shear derived from lidar measurements with wind shear derived from mast measurements because the instruments have a different measurement principle. Wind data from mast-lidar pairs at Høvsøre (DK) and Breezanddijk (NL) are used for the analyses. Subsequently, a detailed study of the seasonality of wind shear, as the seasonality becomes a concern when the measurement period is shorter than one year. The MCP model has been implemented and validated using the commercially available software WindPRO. The data from the measurement sites have been used to test the new approach of estimating the mean wind shear exponent using short-term lidar measurements and MCP. Lastly, the uncertainty in the wind shear exponent is propagated to uncertainty in the annual energy production.

Although the wind shear statistics are subject to seasonality, this thesis shows that the proposed method has the potential to significantly reduce the error in the estimate of the mean wind shear exponent. As the error in the mean wind shear exponent is decreased, the uncertainty in the vertical extrapolation of the wind resource can be reduced. This reduction ultimately leads to a decrease of the uncertainty in the annual energy production.

# Contents

# List of Figures

# List of Tables

# Nomenclature

## Latin Symbols

| Symbol | Description | Unit |
|---|---|---|
| $A$ | Weibull scale parameter | [m/s] |
| $b_0$ | Slope from linear regression | |
| $b_1$ | Intercept from linear regression | |
| $\mathbb{C}$ | Covariance matrix | [-] |
| $c_i$ | Count in bin $i$ | [-] |
| $f$ | Frequency | [1/s] |
| $g$ | Gravitational acceleration | [m/s$^2$] |
| $k$ | Weibull shape parameter | |
| $L$ | Obukhov length | [m] |
| $M$ | Total number of bins | [-] |
| $N$ | Total number of samples | [-] |
| $p$ | Exponent of the AEP model | [-] |
| $r$ | Ratio of prediction height over observation height | [-] |
| $R$ | Pearson's correlation coefficient | [-] |
| $R^2$ | Coefficient of determination | [-] |
| $u$ | Wind speed | [m/s] |
| $u_*$ | Friction velocity | [m/s] |
| $u_{ref}$ | Wind speed at reference height | [m/s] |
| $V_{rat}$ | Rated wind speed | [m/s] |
| $w$ | Weight | [-] |
| $x$ | Wind speed at reference site | [m/s] |
| $\hat{y}$ | Predicted wind speed at target site | [m/s] |
| $z$ | Height above ground level | [m] |
| $z_0$ | Roughness length | [m] |
| $z_{ref}$ | Reference height | [m] |

## Greek Symbols

| Symbol | Description | Unit |
|---|---|---|
| $\alpha$ | Wind shear exponent | [-] |
| $\hat{\alpha}$ | Predicted wind shear exponent | [-] |
| $\Gamma(x)$ | Gamma function of $x$ | [-] |
| $\Delta\alpha$ | Bin width of the shear exponent histogram | [-] |
| $\epsilon$ | Error or difference | |
| $\tilde{\epsilon}$ | Normalised error or difference | |
| $\kappa$ | Von Karman constant | [-] |
| $\lambda_0$ | Wavelength | [m] |
| $\mu_x$ | Mean of random variable $x$ | [-] |
| $\tilde{\mu}_x$ | Normalised mean of random variable $x$ | |
| $\sigma_x$ | Standard deviation of random variable $x$ | |
| $\tilde{\sigma}_x$ | Normalised standard deviation of a random variable $x$ | [-] |
| $\chi^2$ | Chi-squared goodness of fit statistic | [-] |
| $\tilde{\chi}^2$ | Normalised chi-squared goodness of fit statistic | [-] |

# Abbreviations

| | |
|---|---|
| **ABL** | Atmospheric Boundary Layer |
| **AEP** | Annual Energy Production |
| **ANNs** | Artificial Neural Networks |
| **CW** | Continuous Wave |
| **LR** | Linear Regression |
| **LT** | Long-term |
| **MCP** | Measure Correlate Predict |
| **NaN** | Not a Number |
| **SL** | Surface Layer |
| **ST** | Short-term |
| **VRM** | Variance Ratio Method |
| **wLR** | Weighted Linear Regression |
| **wVRM** | Weighted Variance Ratio Method |

# 1 Introduction

## 1.1. Project context

In pursuit of an entirely sustainable electricity generation, it is necessary to increase the amount of installed wind power. An important aspect of increasing the amount of installed wind power, is reducing the cost of wind energy by making wind turbines more efficient. Over the last years, the design of more efficient wind turbines has lead to an increased rotor size and higher wind turbine hub heights. Two main reasons are identified for the increase in size. Firstly, large multi-megawatt wind turbines are more efficient per produced megawatt-hour, and these turbines require large rotors. Secondly, wind turbines have become taller to make wind energy projects profitable in areas with a lower natural wind resource. When the wind resource at greater heights can be utilised, new, inland areas become suitable for wind energy generation.

As wind turbines grow taller, wind measurements at greater heights are required. For wind resource assessment, it is currently advised to install a measurement mast, which has a height of at least two thirds of the wind turbine hub height [28]. An illustration of the relevant heights in wind resource assessment are shown in Fig. 1.1. The installation of the appropriate met mast becomes cumbersome and expensive for wind energy projects involving tall wind turbines.

Lidar is becoming a popular tool for measuring over expected turbine rotor heights [32]. The employment of lidars is expensive, and often less than a year of lidar measurements are available in industrial wind farm developments. This project focuses on how lidar measurements, in combination with Measure Correlate Predict (MCP) methods, can be used in wind resource assessment to improve the wind resource estimations above measurement mast height. Reduction of the measurement period using MCP methods would reduce the costs of the measurement campaign and allows the use of the portability of the lidar.

As the rotor size and hub height of wind turbines increase, the wind shear has significant effects on power performance and fatigue loading. Regarding wind resource assessment, the wind shear affects the available wind power. Due to the large rotor, there can be a significant difference in the available wind power in the lower and in the upper half of the rotor plane. This provide another argument for evaluating the wind shear distribution at a potential wind farm site.

A complication that appears due to increasing turbine heights, is the presence of the turbine in different regimes of the atmospheric boundary layer (ABL). As the height of the ABL is varying, the height of the atmospheric surface layer (ASL), which is approximately 10% of the ABL height, is varying as well. Tall turbines are more often present above the ASL, where different formulations are needed to describe the wind profile [12]. Lidars are able to measure the wind over the full wind turbine height, and could support the understanding of wind at higher heights.

This thesis contributes to the knowledge about the benefits and usability of lidars in a wind measurement campaign. The focus of this thesis is on the wind shear measured by lidars, and how MCP can be used to use short-term lidar measurements to improve the wind resource estimation above measurement mast height.

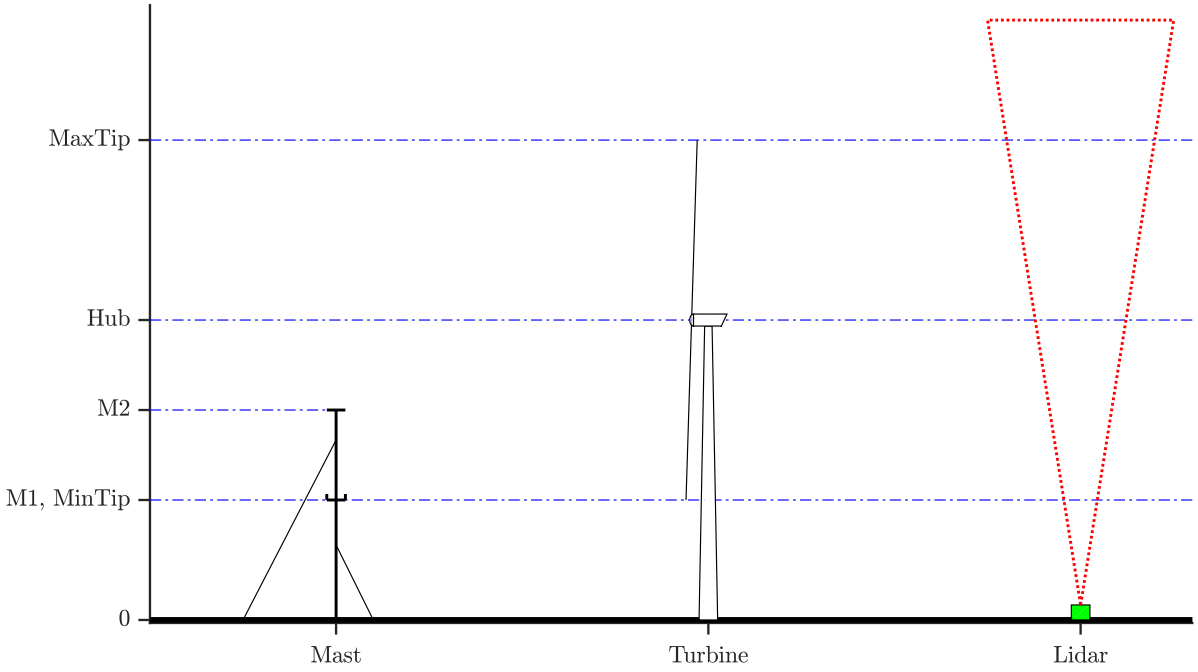


Figure 1.1: Illustration of relevant heights in wind resource assessment and wind turbine siting. Fictive situation for a wind turbine with a hub height of 100 m and a rotor diameter of 120 m. The mast measures at 40 m and 75 m.

## 1.2. Objectives

The project goal is formulated as follows:

**" To improve wind resource assessment above measurement mast height by statistical extrapolation using lidar measurements."**

And is split into sub-objectives:

1. Compare the wind profiles and shear exponent distributions obtained via lidar measurements with the ones obtained via met mast measurements
2. Estimate wind shear exponent distribution and long-term wind profile using lidar measurements and MCP method
3. Determine effect of shorter measurement period on the obtained wind speed and wind shear distribution

## 1.3. Scope

The wind energy resource is often vertically extrapolated using the logarithmic wind profile or the power law profile. The focus of this project is the extrapolation using the power law. A drawback of the logarithmic law is the need for the specification of a roughness length. An advantage of the logarithmic law is that it can be adapted to fit diabetic wind profiles. However, this requires determination of the atmospheric stability and this may be complicated as the installation of instruments required for the evaluation of the atmospheric stability is not current practice in the industry.

It is known that wind shear influences the wind turbine performance. Wind shear over a wind turbine rotor affects the loading on the turbine and therefor the power production. The focus of this thesis is on the role of the wind shear in wind resource assessment and vertical extrapolation of the wind resource. The effects of wind shear on the loads on the wind turbines are outside the scope of this study. Also, the effects of the wind shear on a wind turbine power curve are outside the scope of this study.

## 1.4. Outline

In Chapter 2 the results of the literature study are presented. Three main topics are distinguished in the literature study, respectively wind profiles, lidars, and MCP methods. The research set-up is discussed in Chapter 3. Definition of the research questions, and description of the measurement sites are included. Data of the sites is firstly used in Chapter 4 to compare the wind shear derived from mast measurement with the wind shear derived from lidar measurements. Secondly, in Chapter 5 the wind measurements are analysed on seasonal trends of the wind shear exponent.

The implementation and validation of the MCP code are presented in Chapter 6. This chapter also considers two improvements over standard MCP methods for the current application on wind shear exponents. The implemented MCP method is applied in Chapter 7. In order to evaluate its performance, the MCP result is compared with long-term measurements. Further, the effect of the measurement period on the MCP outcome is studied. Lastly, the effect of the wind shear exponent on the Annual Energy Production (AEP) is considered in Chapter 8.

# 2

# Literature Review

An overview of the relevant background theory and a literature review are provided in this chapter. Firstly, the vertical wind profile discussed in Section 2.1. Secondly, lidars are discussed in Section 2.2. The working principle of lidars, and the difference between lidars and the traditional met mast measurements are reviewed. Measure-correlate-predict methods, which are used to obtain the long-term wind characteristics at a wind site are discussed in Section 2.3.

## 2.1. Wind profiles

Wind speed and direction change with height above the ground level. The variation of the wind with height is depicted in a wind profile. The wind profile is influenced by the geostrophic wind, the surface roughness and buoyancy effects. Additionally, local effects change the wind profile, for example roughness changes, flow inclination, or speed-up.

### 2.1.1. Wind in the atmospheric boundary layer

The atmospheric boundary layer (ABL) is the part of the atmosphere that is directly influenced by the Earth's surface. The height of the ABL is in the range from a few hundred meters to a few kilometres and can change over time. The structure of the atmospheric boundary layer over land and its diurnal variation are shown in Fig. 2.1. By definition, the lower ten percent of the ABL is called the surface layer (SL) [37].

During the day the sun heats up the surface and there is a positive heat flux from the relatively warm surface. During the night the opposite process takes place, the surface is relatively cold and a negative heat flux from the air towards the surface exists. This process cools down the air and enhances the atmospheric stability.

Buoyancy effects on the wind profile are indicated by the static stability of the atmospheric boundary layer. Stull defines an unstable, neutral and stable stratification. An unstable ABL is characterised by turbulence and convective processes, which are enhanced by the unstable air. Vertical mixing of the air takes place and the wind shear is limited. In the stable case the turbulence and convective processes are suppressed. The vertical mixing is limited and wind shear is enhanced. This condition allows higher wind shear. The stable stratification means a decoupling of the flow and surface [37].

The Obukhov length $L$ is used to quantify the static stability:

$$L = -\frac{\overline{\theta_v} {u_*}^3}{\kappa g (w'\theta')_s} \tag{2.1}$$

In the equation $\theta_v$ is the virtual temperature, $u_*$ is the friction velocity, $\kappa$ is the Von Karman constant, $g$ is the gravitational acceleration, and $(w'\theta')_s$ represents the virtual potential heat flux [15]. The quantification of the stability allows further classification. Various classifications of the atmospheric stability exist, an example is given in Table 2.1. In the example five stability classes are distinguished.

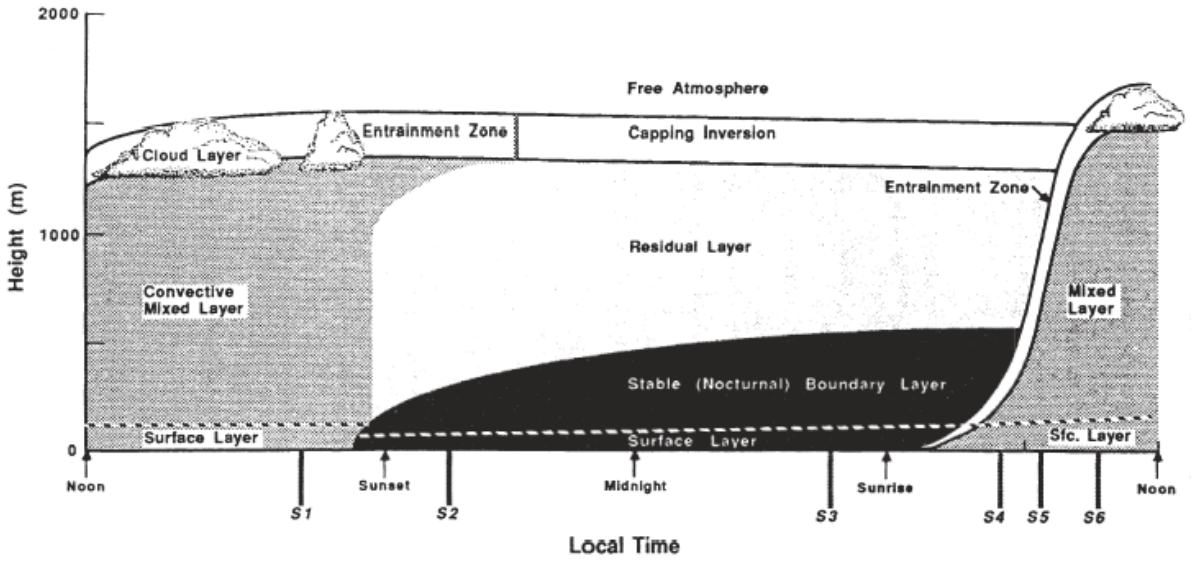


Figure 2.1: Structure of the atmospheric boundary layer over time. Adopted from [37]

Table 2.1: Stability classes and their respective boundaries, as defined by Holtslag et al. [15]

| Class Name | Class Boundaries |
|---|---|
| Very Unstable (VU) | -200 $\leq L <$ 0 |
| Unstable (U) | - 500 $\leq L <$ -200 |
| Neutral (N) | $\|L\| >$ 500 |
| Stable (S) | 200 $< L \leq$ 500 |
| Very Stable (VS) | 0 $< L \leq$ 200 |

The connection between the atmospheric stability and the wind shear has been described in literature for different sites. For example, 2006 Verkaik described the wind profiles at Cabauw, The Netherlands[40]. More recently, the relationship between atmospheric stability and wind shear has been investigated regarding wind energy. Holtslag et al. observed the influence of atmospheric stability on the wind shear at an offshore wind farm site in the Netherlands [15].

Kelly et al. derived a general formulation for the distributions of atmospheric stability in the SL [19], and applied it to extend the mean wind profile above the surface layer [18].

### 2.1.2. The logarithmic wind profile

The neutral logarithmic wind profile is given by Eq. (2.2). It is derived by applying Buckingham Pi Theory. Alternatively, it can be derived using mixing length theory [37].

$$u(z) = \frac{u_*}{\kappa} \ln\left(\frac{z}{z_0}\right) \tag{2.2}$$

In which $u_*$ is the friction velocity, $\kappa$ is the Von Karman constant, $z$ the respective height above ground level, and $z_0$ is the (aerodynamic) roughness length. As Eq. (2.2) yields for neutral atmospheric stability only, it has to be adapted to represent a wind profile in stable or unstable atmospheric conditions. According to Monin-Obukhov similarity theory, the neutral logarithmic wind profile can be rewritten to account for stable and unstable conditions and is given by:

$$u(z) = \frac{u_*}{\kappa}\left[\ln\left(\frac{z}{z_0}\right) - \psi_m\left(\frac{z}{L}\right)\right] \tag{2.3}$$

In which $\psi_m$ is the correction function and $\frac{z}{L}$ the stability parameter. The form of the correction function depends on the sign of $L$ i.e. the stability class. The Monin-Obukhov similarity theory is valid for homogeneous surface layers [41].

### 2.1.3. The power law profile

An alternative to the logarithmic wind profile is the power law. This empirical function is often used for engineering purposes because of its simplicity. The power law is also used in the IEC standards for wind turbine design. Contrary to the logarithmic law, the power law does not include an aerodynamic roughness length. Instead, over a limited vertical extent the shear exponent $\alpha$ is defined.

$$u(z) = u_{ref}\left(\frac{z}{z_{ref}}\right)^{\alpha} \tag{2.4}$$

The shear exponent is obtained by fitting the power law to wind speed measurements at two or more heights. When only two points are used for the fit or when none of the measurements were above hub height, the shear exponent may result in an unrepresentative wind profile [41]. As the shear exponent varies over time, the shear characteristic of a site can be shown using a $P(\alpha)$ distribution. The $P(\alpha)$ distribution shows a dependence on wind speed. For higher wind speeds the peak of the $P(\alpha|U)$ is located at smaller shear exponents. This observation is explained by the reduced effect of the atmospheric stability at high wind speeds [22].

In the SL, the stable side of the distribution of the stability can be used to map the distribution of the wind shear exponent from stability. Above the SL mapping of shear from stability does not result in a correct shear distribution, as the MO theory does not apply, and the flow can be decoupled from the flow in the SL [22].

### 2.1.4. Vertical extrapolation in wind resource assessment

The wind resource assessment is essential in the assessment of the financial feasibility of a wind energy project. Before a wind turbine is erected at a site, its future energy production is to be estimated. The estimations are complex and uncertain. Uncertainty arises due to different factors, among those is vertical extrapolation. According to Clifton et al., vertical extrapolation of the wind resource accounts for an uncertainty up to 6 % in a gross energy estimate. Advanced measurement techniques like remote sensing could mitigate the uncertainty [4].

The annual energy production (AEP) estimate is based on the power curve of the wind turbine generator. As the power curve is a function of the wind speed at hub height, it is essential to know the wind speed distribution at hub height. However, wind measurements at hub height are not always available and vertical extrapolation of the wind resource is necessary to improve the AEP estimation. Methods for vertical extrapolation are based on the logarithmic law (Eq. (2.2)) and the power law (Eq. (2.4)). Both methods introduce uncertainty in the wind statistics.

A simple method for quantification of the vertical extrapolation uncertainty is given by Kwon [24]. In this work only the variation of the shear exponent $\alpha$ is taken into account. A more elaborated method to quantify the uncertainty, and a comparison of the uncertainty due to vertical extrapolation via the WAsP method and the power law are provided by Kelly [18]. The uncertainty in the wind speed due to the vertical extrapolation is dependent on the relative extrapolation distance $(z_{pred}/z_{obs})$. The comparison shows that for small relative extrapolation distances the differences between the WAsP method and the power law are small. However, for larger relative extrapolation distances, the WAsP method results in lower uncertainties.

### 2.1.5. Extension of the wind profile

New wind turbines are tall and reach above the atmospheric surface layer. The logarithmic wind profile, Eq. (2.3) is based on the assumption of a constant friction velocity $u_*$, which is true for the surface layer only. Therefore the logarithmic wind profile is only valid for heights up to 80m. To describe the wind profile above the surface layer, different formulations of the wind profile are needed. Extended wind profile forms have been suggested by Etling, and Gryning et al. [12, 14], with Kelly et al. further developing mean wind profiles and extrapolation above the SL based on statistics of stability and ABL-depth [19, 21, 22].

## 2.2. Light Detection and Ranging

As new wind turbines are tall, high met masts are required for the wind resource assessment. Installation of tall meteorological masts is cumbersome and expensive, therefore remote sensing techniques have become more attractive to be used in the wind resource assessment. Lidars are remote sensing devices, which make use of the Doppler shift in back-scattered light. Previous research has established that current wind lidars can be an alternative to the installation of tall meteorological masts [32].

### 2.2.1. Working Principle

Lidars utilize the wave characteristic of light to measure the wind speed and direction. A laser emits light, which is back-scattered by moving aerosols and molecules in the air. The back-scattered light is collected by a detector and the Doppler shift of the frequency is measured. The Doppler shift relates to the velocity of the moving particles, following Eq. (2.5).

$$\Delta f = f_{bs} - f_{ref} = \frac{\vec{U}}{\lambda_0} \tag{2.5}$$

Where $\lambda_0$ is the wavelength of the emitted laser light $\vec{U}$ is the velocity of the particle along the beam direction. This implies that no Doppler shift is observed when the particle moves perpendicular to the beam.

A common applied technique to find the Doppler shift is heterodyne (coherent) detection. At the detector the back-scattered light is mixed with the reference signal. As the Doppler shift is small, the mixed signal shows beats. The beats are appearing at the frequency of the Doppler shift, so $\Delta f$ can be measured directly and the flow velocity along the beam direction can be calculated using Eq. (2.5).

A single measurement provides only the flow velocity along the beam direction. To establish a three dimensional wind velocity vector the lidar needs to measure the flow velocity along multiple beam directions. It is common to use beams that form a cone, as is shown in Fig. 2.2. By keeping the cone angle constant and varying the azimuthal angle of the beam, the lidar measures multiple velocity vectors and a wind velocity vector can be constructed. A cone angle of approximately 60 degrees is often applied [32].

The majority of currently deployed lidars can be divided into two groups: Continuous Wave (CW) lidars and pulsed lidars. Both techniques have their specific advantages and disadvantages. Dependent on the application one may prefer one technique over the other.

**Continuous Wave Lidar** The laser of a continuous wave lidar continuously emits laser light. The optics of the lidar focus the laser beam at the desired measurement height.A rotating wedge is used to vary the azimuthal angle. In this way measurements are made for a range of azimuthal angles. The CW lidar addresses one measurement height at a time. In approximately 1 second, the lidar measures the flow velocity height along the beam direction at one height for different azimuthal angles, see the right side of Fig. 2.2. Subsequently, it focuses on the next measurement height and again measures the flow velocity along the beam direction for different azimuthal angles in approximately 1 second.

Back-scattered light is scattered by particles from a confined volume. This volume is called the probe volume. The probe volume depends on the probe length and beam diameter. For CW lidars both the probe length and beam diameter depend on the measurement range. As the measurement range increases, the beam diameter increases linearly with the range and the probe length increases roughly quadratically with the range. The quadratic increase is caused by focusing the Gaussian laser beam, which causes a spatial sensitivity in the axial direction of the beam. The spatial sensitivity can be approximated by a Lorentzian function [32].

The disadvantage of the increase in probe length is that it can lead to biased wind speed measurements. Under conditions of non-linear shear, spatial averaging leads to a small bias in the wind speed measurement. At greater measurement ranges, the probe lengths are longer, and the bias could be more severe [36].

**Pulsed Lidar** The pulsed lidar emits strong laser pulses, that have a duration in the order of hundreds of nanoseconds. The frequency at which the pulsed lidar emits the pulses is limited by the time the light needs to travel from the emitter to the detector. The lidar uses one pulse to measure the wind speed at all the programmed heights. The focus of the laser is optimised to receive signals from all the heights.

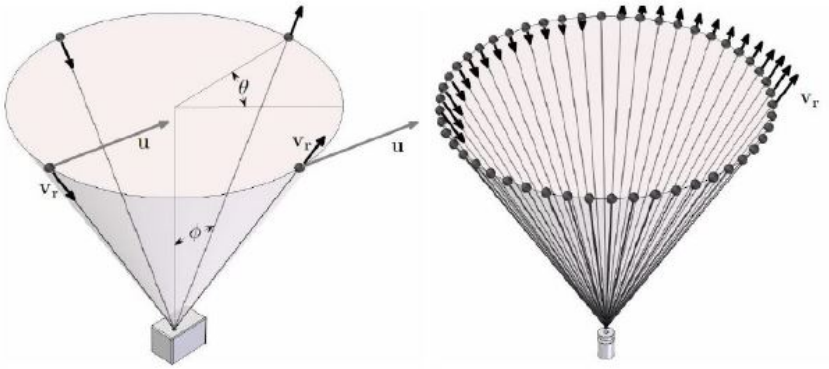


Figure 2.2: Comparison of the scanning techniques of a pulsed lidar(left) and a scanning lidar, where $\phi$ is the cone half angle, $u$ is the velocity of the particle, $v_r$ its radial component, and $\theta$ is the azimuthal angle. Adopted from [6]

The travel time of the signal is used to determine the height that corresponds to the received signal. Due to the short travel time for low heights, the pulsed lidar has a minimum measurement height around 40 metres, whereas the CW lidar does not have the disadvantage of a minimum measurement height. On the opposite, the advantage of a pulsed lidar is that the probe length does not increase with measurement height [32].

The scanning technique used by pulsed lidars is often different from the scanning technique used by CW lidar. To construct the wind speed vector, the pulsed lidar uses three to five fixed beam directions, as shown on the left side of Fig. 2.2 The advantage of this method, is that it offers the possibility to remove a rotating part from the lidar [32].

### 2.2.2. Comparison of Lidar measurements and mast measurements

The method of measuring the wind using lidars is significantly different from the method using cup anemometers or sonic anemometers. The wind velocity measured by the lidar is volume averaged, whereas the velocity vectors measured by a cup anemometer or a sonic anemometer can be considered as a point measurement. Several studies have compared lidar measurements and tower measurements, because understanding the difference between the methods is essential in the process of replacing meteorological towers by lidars. Experiments with all-fibre lidars at DTU Wind Energy started in 2003 and numerous studies on lidars have been carried out. Currently new applications of lidars are investigated, e.g. wind turbine control using lidars and power curve verifications [29].

Comparison of scanning lidar and met mast measurements have been carried out extensively, e.g. by Courtney et al., and Smith et al. [7, 36]. The studies show good agreement of wind speed measured by the lidar and by the measurement mast. Courtney concluded that the pulsed lidar (Windcube) is better suited for measurements above 130m, whereas the CW lidar (ZephIR) is better for wind measurements below 80 meters. Furthermore, an advantage of the pulsed lidar over the CW lidar is that it is not affected by back-scatter from clouds [7].

The relation between lidars and met masts in complex terrain is still a relevant research topic. As the flow in complex terrain can be non-uniform across the lidar measurement disk, the measured wind speed can be significantly different [32]. Recently, lidars and met masts have been compared in multi-site experiments, e.g. by Rodrigo et al. [35] [23]. It was observed that the lidar error increases with terrain complexity.

### 2.2.3. Shorter measurement campaigns

The portability of remote sensing devices as lidars provides the possibility of a new type of wind resource assessment, in which the device is moved around within a measurement year. Short measurement periods are distributed over the year to measure the wind during the different seasons within a year. As a result, the lidar can measure at different sites within a year, resulting in a reduction of the cost of the wind resource assessment.

Lackner et al. tested this type of wind resource assessment in 2007 and called the method ”round robin site assessment method”[26]. In his study long-term measurement data from weather station pairs were used to assess the quality of the prediction using the round robin site assessment method. One of the weather stations was assumed to be a remote sensing device and its data was used for the short-term measurement periods. The other weather station was used as a reference site. The results showed that the new method performs well in comparison to the standard method in terms of accuracy and uncertainty, and that the method can enhance the efficiency of the wind resource assessment campaign.

Later, in 2010 Lackner investigated a method in which short-term hub height wind speed measurements are used to correct the wind shear model applied to met mast measurement. As measurements from remote sensing devices were not available, Lackner used measurements from a met mast to test the method. The measurement from the top anemometer was assumed to be a measurement from a remote sensing device. The measurement was used to establish a shear correction factor, which is applied to the shear measured from the lower anemometers. Basically, a kind of measure-correlate-predict method is applied to correct the shear. The results show that the short-term hub height measurements can be used to improve the estimation of the wind speed, although the method may not be effective every time it is applied [27].

Crockford studied the effect of a shorter wind measurement campaign using lidar in 2013. It was concluded that the wind climate derived from 6 months measurement time, distributed over the four seasons in a year, differs by only 1 % from the wind climate derived from full year of measurements. At the same time, the costs of the measurement campaign were reduced by 35% [8].

## 2.3. Measure-correlate-predict methods

Wind measurements at a wind farm site are often only available for a relative short period, i.e. approximately a year. Based on the measurements of the short period, the energy production for 20 years has to be estimated. As the wind resource varies from year to year, a method to correct for the long-term wind resource is necessary. In wind resource assessment the measure-correlate-predict (MCP) methods are commonly applied to correct for the long-term. At first a reference site, which has good quality data for a long period of time, is needed. Secondly, a correlation between the target site and the reference site is established. The correlation is based on the concurrent measurement period. Lastly, the long-term data of the reference site and the correlation are used to predict the wind resource at the target site.

### 2.3.1. Correlation methods

A variety of MCP methods exists to establish the correlation between the target site and the reference site. In 2005, Rogers et al. compared the performance of four MCP methods. The methods are [34]:

1. Linear Regression
2. Mortimer method
3. Vector regression method
4. Variance ratio method

In his work Roger concluded that the linear regression method succeeds at predicting the average wind speed. However, as the predicted wind speed has lower variance, the method does predict a biased wind speed distribution. Furthermore it was concluded that the variance ratio method and the Mortimer method performed best in predicting the different metrics. The variance ratio performed slightly better, since the Mortimer method results in biased predictions for the Weibull shape parameter $k$. Below, the working principles of different MCP methods are explained.

The linear regression was suggested by Derrick [9]. The method assumes that there exists a relationship between the wind speed at the target site and the reference site of the form:

$$\hat{y} = ax + b \tag{2.6}$$

In which $\hat{y}$ is the predicted wind speed, $x$ is the wind speed measured at the reference site, and $a$ and $b$ are the fitting constants determined via linear regression. Clive [5] notes that there is a non-linearity in the relation between two Weibull distributions and proposes to use the form of Eq. (2.7), in which $m$, $a$ ,and $c$ are fitting constants. However, if $c \neq 0$, linear regression cannot be applied.

$$\hat{y} = mx^a + c \tag{2.7}$$

Secondly, the Mortimer method is an empirical method proposed by Mortimer [30]. The wind speed measurements are binned according to the wind speed and wind direction at the reference site. Then, two matrices are constructed: a matrix which provides the average of ratios of the wind speed at the target site to the wind speed at reference site per wind speed and wind direction bin , and a matrix containing the corresponding standard deviations. Subsequently a relation of the form shown in Eq. (2.8) is used to predict the wind speed at the target site.

$$\hat{y} = (r + e)x \tag{2.8}$$

In this relation, $r$ is the average of the wind speed ratios corresponding to the speed and direction at the target site, and $e$ is a random variable given by a triangular distribution corresponding to the standard deviation of the ratios.

Thirdly, the vector regression method has been introduced by Nielsen et al. [31]. A vector model of the form of Eq. (2.9) is set up to correlate the orthogonal wind speed components at the target site to the wind speed components at the reference site.

$$\begin{bmatrix} \hat{y}_1 \\ \hat{y}_2 \end{bmatrix} = \begin{bmatrix} a_1 \\ a_2 \end{bmatrix} + \begin{bmatrix} b_{11} & b_{12} \\ b_{21} & b_{22} \end{bmatrix} \begin{bmatrix} x_1 \\ x_2 \end{bmatrix} \tag{2.9}$$

In which $x_1, x_2$ are the orthogonal wind speed components at the reference site and $\hat{y}_1, \hat{y}_2$ the predicted wind speed components at the target site. The advantage of the vector regression method, is that the wind data is not binned into direction bins.

The last method used by Rogers et al. is the variance ratio method. They have introduced the variance ratio method, because simple linear regression leads to an underestimation of the long-term variance in the predicted wind speed. The expression used for predicting the wind speed is:

$$\hat{y} = \mu_y - \frac{\sigma_y}{\sigma_x}\mu_x + \frac{\sigma_y}{\sigma_x}x \tag{2.10}$$

In which $\mu_y$ and $\mu_x$ are the mean wind speed at the target site and the reference site, respectively. And $\sigma_y$ and $\sigma_x$ are the respective standard deviations of the wind speed at the target site and the reference site. Using Eq. (2.10), the variance of the predicted wind speeds, $\sigma^2(\hat{y})$, is equal to the variance of the observed wind speeds $\sigma^2(y)$. Using Eq. (2.10) for the correlation, results in better prediction of the wind speed distribution at the target site [34].

Thøgersen et al. describe MCP methods incorporated in the software WindPRO, which is widely used for wind resource assessments in the industry. The regression method in WindPRO is extended by adding a random error term to the regression model, see Eq. (2.11) [38].

$$\hat{y} = f(x) + e \tag{2.11}$$

In which $e$ is a Gaussian-distributed random variable.

In addition the matrix method is introduced by Thøgersen. Similar to the Mortimer method, the wind speed data is binned based on the wind speed and direction at the reference site. The mean wind speed-up and mean wind-veer at the target site are modeled by a joint distribution conditioned on the wind speed and wind direction at the reference site. To predict the wind speed at the target site the the joint distribution is to be known for all wind conditions at the reference site, i.e. the full matrix needs to be constructed. When the joint distribution for certain wind conditions cannot be acquired from the measured wind data, polynomials are used to interpolate the mean and standard deviation and to fill the matrix [38].

Artificial Neural Networks (ANNs) are as well applied as correlation technique, since the ANNs are useful for pattern recognition. The performance of ANNs in long-term wind prediction has been subject in different studies [3, 39, 43]. However, the ANNs are currently not among the standard methods for long-term correction used in wind resource assessment. More information can be found in an extensive overview of MCP methods by Carta et al. [2].

The traditional MCP methods use one reference site. New correlation methods have been developed to predict the long-term wind characteristics using data from multiple reference sites. Zhang developed a hybrid MCP method which combines wind data from multiple reference sites. To account for the different stations, a weight based on the distance and the elevation difference was assigned to each reference station. He found that the hybrid MCP method has the potential to improve the accuracy of the predictions. However the best hybrid strategy is highly dependent on the stations and the data [43]. Another hybrid MCP method is provided by Dinler, who developed a MCP method that improves the prediction for the cases in which only low-correlation reference sites are available or when no concurrent data is available [11]. ’

### 2.3.2. Uncertainty in MCP predictions

The quantification of uncertainties is an important part of the wind resource assessment, as it has a direct effect on the financial feasibility of a wind project. Frameworks for quantifying the uncertainty in wind resource assessment have been provided by e.g. Lackner and Kwon [24, 25]. These frameworks include methods to estimate the uncertainty due to the MCP method. However, both frameworks assume the variance ratio method is used for the wind resource assessment. Further research on the uncertainty propagation through the MCP methods is still relevant, as this would increase the credibility of wind resource assessment and energy production estimates [43].

# 3

# Research Set-Up

In this chapter the master thesis project is further outlined. The research questions are presented in Section 3.1. The research questions provide structure to the study, and assist in obtaining the knowledge required to achieve the research objectives stated in Section 1.2. The data which is required for the stufy is obtained from two measurement sites. The surrounding of the sites and the instrumentation are described in Section 3.2.

## 3.1. Research questions

Three main research questions have been defined. Those are divided in sub-questions.

1. How do the wind profile and shear distribution obtained via lidar compare to the wind profile and shear distribution obtained via met mast?
   (a) How do lidar measurements compare to measurements from a met mast?
   (b) What definition of wind shear is used?
   (c) What methods for vertical extrapolation of the wind profile are used and what are the implications and shortcomings of the current methods?
2. To what extent can statistical extrapolation methods estimate the shear exponent distribution?
   (a) What metrics are used to assess the quality of the estimation?
   (b) What statistical extrapolation methods exist?
   (c) How do the estimations from different extrapolation methods compare?
   (d) What changes in the extrapolation method could be made to improve the estimation of the shear exponent distribution?
3. What is the effect of shorter measurement campaigns on the obtained long-term wind profile and shear distribution?
   (a) What duration for short-term measurement periods can be used?
   (b) Does distribution of measurement time within a year improve the estimation?
   (c) Does seasonality of the wind affect the estimation?

## 3.2. Measurement site descriptions

Wind data from two measurement sites wind data from two measurement sites is used: Høvsøre, and Breezanddijk. At both locations lidar data and met mast data are available. A brief overview of the available wind data/instruments is given in Table 3.1.

Table 3.1: Overview of the available measurement instruments. The heights at Høvsøre refer to height above ground level. The heights at Breezanddijk refer to the height above the average water level of the lake (IJsselmeer).

| | Measurement period | Instrument | Measurement heights [m] |
|---|---|---|---|
| **Høvsøre** | | | |
| 1. Met Mast | 01-01-2009 to 01-06-2017 | Cup anemometer<br>Wind vane | 10, 40, 60, 80, 100, 116.5<br>10, 60, 100 |
| 2. Lightning Mast | 01-01-2009 to 01-06-2017 | Sonic Anemometer | 60, 100, 160 |
| 3. Lidar | 17-5-2011 to 04-04-2012 | Windcube | 40, 60, 80, 100, 160, 200 |
| **Breezanddijk** | | | |
| 1. Met Mast | 23-06-2016 to 01-06-2017 | Cup anemometer<br>Wind vane | 40, 60, 70, 75<br>36, 67 |
| 2. Lidar | 01-01-2016 to 01-06-2017 | ZephIR 300 | 20, 40, 47, 60, 75, 95, 110, 120, 135, 182, 200 |

The quality and usability of the wind data depend on the surroundings and lay-out of the measurement site. Obstacles, e.g buildings and wind turbines, distort the wind flow and cause a change in the vertical wind profile. How the obstacles influence the wind profile is illustrated in Fig. 3.1. Other roughness changes like the land-sea interface affect the wind profile as well.

Local effects should be taken into account. It is desired that the measurement used for the analysis are not influenced by obstacles or wind turbine wake. Therefore a description of the measurement sites is necessary and suitable wind direction sectors need to be defined.

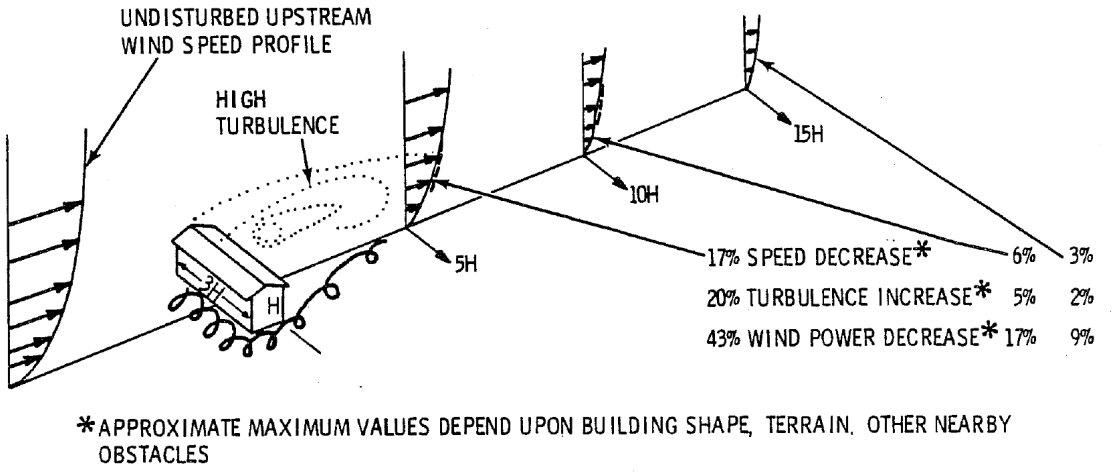


Figure 3.1: The effect of obstacles on an undisturbed airflow [42]

### 3.2.1. Høvsøre

The Høvsøre measurement site is located in Jutland, in the western part of Denmark. As shown on the map of Fig. 3.3, the site is surrounded by farmland. Approximately 1.7 km to the west of the site, is the coastline of the land with the North Sea. One kilometer to the south of the measurement site the Bøvling Fjord is located.

Five wind turbines are present at the Høvsøre site. The wind turbines are aligned in a row from north to south, as can be seen on the map. Each wind turbine has its own power curve met mast, which is located on the west side of the turbine.

Next to the wind turbines, two major obstacles are located at the site:

- The village of Bøvlingbjerg is located at approximately 3 km to the east of the site.
- Between the site and the coastline is a sand dune with a height of 12 m and a width of 40 to 50 m [33].

At the south end of the wind turbine row, a 116.5m-high meteorological met mast is located. This met mast is used in this analysis. The mast contains several types of instruments. The available cup anemometers and wind vanes are listed in Table 3.1.

Within the row of wind turbines, two lightning protection masts are located. One of the lightning masts is equipped with sonic anemometers. A detailed description of the Høvsøre test facility and an overview of the research performed at the site are provided by Pena et al. [33].

Wind speed and direction measurements of the met mast have been used to construct the wind rose of Fig. 3.4. It is clear that winds from the west are more common than winds from the east. The prevailing wind direct is west-northwest.

To avoid the wakes of turbines and the effect of the obstacles, two wind direction sectors will be used: the eastern wind sector from 60 to 120 degrees, and the western wind direction from 240 to 300 degrees. An overview of the selected wind directions is provided in Fig. 3.2 and Table 3.2.

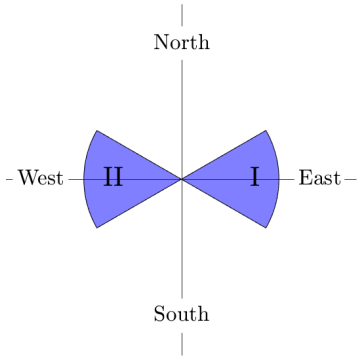


Figure 3.2: Direction sectors used for analysis at Høvsøre

Table 3.2: Overview of direction sectors at Høvsøre

| Sector | Description |
|---|---|
| I. 60 - 120 deg | Wind coming from the farmland |
| II. 240-300 deg | Wind coming from the North Sea, over the sand dune |


Figure 3.3: Overview of the Høvsøre test site. In the centre of the map the row of wind turbines, the lightning mast, and the measurement mast are located. Furthermore the coastline of the North Sea and the coastline of the Bøvling Fjord are visible.

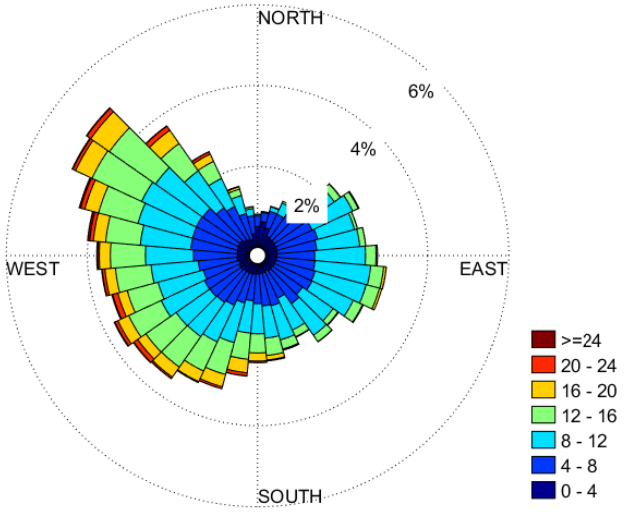


Figure 3.4: Wind rose of wind speeds at 100 m at Høvsøre. The wind rose is constructed using eight years of data (2009-2017).

### 3.2.2. Breezanddijk

Breezanddijk is located in the northern part of the Netherlands, at the Afsluitdijk, which is the dyke between the Waddenzee and the IJsselmeer. Apart from the dyke the site is surrounded by water. The shortest distance to the mainland is 15 km to the southwest and 12 km to the northeast. The measurement set-up consists of a lidar and a met mast, which are approximately 110m separated from each other. A map of the site is provided in Fig. 3.6.

The lidar at Breezanddijk is a ZephIR300 continuous wave lidar. It measures the wind at eleven altitudes, ranging from 20m to 200m above the average water level (see Table 3.1). As the lidar was installed in December 2015, more than a year of lidar data is available. The exact location of the lidar is on top of a gas station. Therefore the wind measurements at lower heights are influenced by the building. The met mast has a height of 70m. It measures the wind speed at four heights and the wind direction at two heights. The met mast was set-up six months later than the lidar, in June 2016. Therefore less than a year of met mast data is available.

The lidar data has been used to construct the wind rose for the Breezanddijk site. The wind rose is shown in Fig. 3.7. It indicates that the prevailing wind direction is south-west.

At the Breezanddijk measurement site various obstacles are present:

- Gas station building: The lidar is on top of the gas station. The mast is located approximately 100 m to the east of the building.
- Telecommunication mast is located between the lidar and the met mast. The distance to both the met mast and the lidar is approximately 50 m. The telecom mast is approximately 40 m high and affects the cup anemometer at 36 m.
- Road overpass: At 200 m distance from the lidar a road overpass is located. The height of the overpass is approximately 10 m.
- Dyke: The dyke is located north of the mast and lidar. It is approximately 10 m high and could influence the measurements at lower heights.

To avoid the influence of the obstacles and to avoid the interaction between the wind and the booms of the met mast, three wind direction sectors are distinguished. An overview of the sectors used for is provided in Fig. 3.5 and Table 3.3. Sector 1 is relatively open and without obstacles. The only obstacle in this sector is the dyke. It is expected that the dyke only affects the wind profile at lower heights. Unfortunately, the wind does not frequently blow from the directions in sector 1. The wind profile in sector 2 can be affected by the presence of the camping site, but as this is the prevailing wind direction, the sector is included. The wind profile in sector 3 could be affected by the harbour and the dyke.

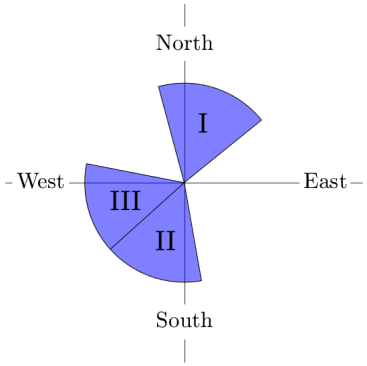


Figure 3.5: Breezanddijk direction sectors used for analysis

Table 3.3: Overview of sectors at Breezanddijk

| Sector | Description |
|---|---|
| I. 345 - 51 deg | Wind coming from the sea, coming over the dyke |
| II. 170-228 deg | Wind coming from the Ijsselmeer, flowing over the harbour and camping site |
| III. 228-281 deg | Wind coming from the sea, flowing over the harbour and the dyke |


Figure 3.6: Overview of the Breezanddijk measurement site. The location of the lidar and the location of the met mast are indicated. The harbour and the camping site are also visible on the map.

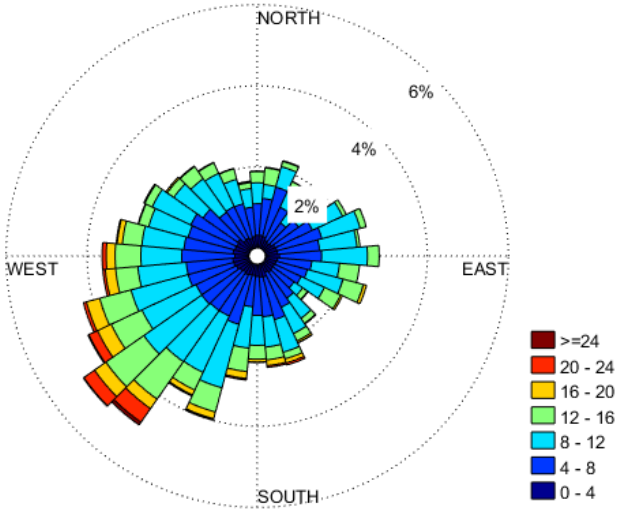


Figure 3.7: Wind rose of wind speeds at 95 m at Breezanddijk. The wind rose is constructed using one year of data (2016).

# 4

# Comparison of Wind Profiles observed by Lidar and Measurement Mast

Lidars use a different measurement principle than met masts. As explained in Chapter 2, traditional cup anemometers measure the wind speed at a point, whereas lidars measure the wind speed over a volume. As most lidars use a conical scan, the measurement volume increases with the height. Measuring over a volume instead of measuring at a point could lead to a difference between the wind shear derived from mast measurements and the wind shear derived from lidar measurements.

Whether the difference in measurement principle leads to a significant difference between the mast and lidar is studied in this chapter. The observations from the lidar and mast pairs at Høvsøre and Breezanddijk are used for the comparison. In Section 4.1 the approach used for the comparison is outlined. The results of the analysis are presented per measurement site in Section 4.2. Subsequently, the results are summarised and discussed in Section 4.3.

## 4.1. Method

For the comparison of the lidar profiles and the met mast profiles, the lidar and met mast pairs at Breezanddijk and Høvsøre are used. In the ideal measurement set-up for the comparison, the mast and the lidar would be located directly next to each other, thereby minimising the difference due to spatial variation in the wind. At Høvsøre this is the case: the lidar was located approximately 10 m to the west of the met mast. However, at Breezanddijk the lidar and mast are further away from each other: the lidar is located 110 m to the west of the met.

The wind speed data for the comparison is filtered on wind speed and wind direction. The selected data points are concurrent 10-minute averages for which both wind speed and wind direction measurements are available at the mast and the lidar. Two selection criteria are applied. Firstly, the wind direction at both the lidar and the mast should be within the selected sector. Secondly, the 10-minute averages of wind speed below 1 m/s have been left out of the comparison.

In the comparison, the wind shear exponent measured by the lidar is compared with the wind shear exponent measured by the met mast. The definition of the wind shear exponent which is used, is the two point log-ratio fit:

$$\alpha = \frac{\ln(u_2/u_1)}{\ln(h_2/h_1)} \tag{4.1}$$

Examples of the power law representation of wind profiles are provided in Appendix C.

To compare the lidar and the met mast on the measured wind shear, the time series of wind shear exponents are compared using four metrics:

1. Bias: the difference between the means of the time series.
2. Root Mean Squared Error (RMSE) gives an indication of the deviation of shear measured by the lidar from the shear measured by the met mast.

3. Slope: the slope of a linear fit through the origin (intercept is zero).
4. Pearson's correlation coefficient, $R$, provides an indication of the linear dependence of the time series of the lidar and the met mast.

## 4.2. Results

The results of the analysis are presented in this section. First the results obtained from the Høvsøre measurement campaign are discussed. Secondly the results obtained at Breezanddijk are discussed.

### 4.2.1. Høvsøre

The lidar at Høvsøre has been measuring for almost a full year. The data is used to calculate two shear exponents: $\alpha_{40-100}$ and $\alpha_{100-160}$. The $\alpha_{40-100}$ from the lidar is compared with the $\alpha_{40-100}$ from the met mast. The met mast and the lidar can be considered collocated. The lightning mast is located 400m north of the Lidar, but has the advantage that it measures the wind speed at 160m height, so the shear exponent at higher height can be compared as well. As it turned out that the lidar measurements for the eastern sector are significantly influenced by the presence of the mast structure, the focus of the comparison is on the western sector.

In Fig. 4.1 the observed $\alpha_{40-100}$ are plotted for the western sector at Høvsøre. According to the figure, the shear exponent from the mast and the lidar are similar. The slope of the fit is 1.00, and most of the data points are located along the line. It stands out that the deviation of the data points from the fitted line is larger for the lower shear exponents. The cloud of data points is wider for shear exponents in the range of 0.0 to 0.2 than it is for the range of 0.2 to 0.5.

The corresponding metrics are shown in Table 4.1. A bias of 0.0036 is observed in the measurements, implying that the shear measured by the Windcube is slightly higher. The slope is 1.0, and the correlation coefficient is 0.97. These metrics are confirming the very good agreement of the shear exponents from the lidar and mast.

Table 4.1: Comparison of the shear exponent $\alpha_{40-100}$ measured by the lidar and by the met mast per direction sector at Høvsøre

| | | **East** | | **West** | |
|---|---|---|---|---|---|
| **Parameter** | **Indicator** | MM | Windcube | MM | Windcube |
| | # Samples | 4340 | 4309 | 9179 | 9142 |
| | # vs MM | | 4309 | | 9140 |
| $\alpha$ 40-100 | Mean [-] | 0.2252 | 0.2476 | 0.1602 | 0.1638 |
| | BIAS [-] | | 0.0224 | | 0.0036 |
| | RMSE [-] | | 0.0484 | | 0.0187 |
| | Slope [-] | | 1.0385 | | 0.9951 |
| | $R$ [-] | | 0.8989 | | 0.9669 |

Secondly, $\alpha_{100-160}$ from the lidar measurements is compared with $\alpha_{100-160}$ measured by the sonic anemometers. The results are presented in Fig. 4.2 and Table 4.2. The plot shows that for this case there is a larger difference between the shear exponent from the lidar and from the mast. This observation is also pointed out by the higher RMSE and lower correlation coefficient in the table. An explanation for the difference in the shear exponents is the horizontal distance between the sonic anemometers and the lidar.

In order to assess the effect of the horizontal distance without changing from a mast to a lidar, a comparison between the measurement from the two masts is made. Although the met mast and the lightning mast use different types of anemometers, both measurement can be considered a point measurement, whereas the lidar measurement is a volume measurement. The overview of the results of this analysis are included in Appendix D.

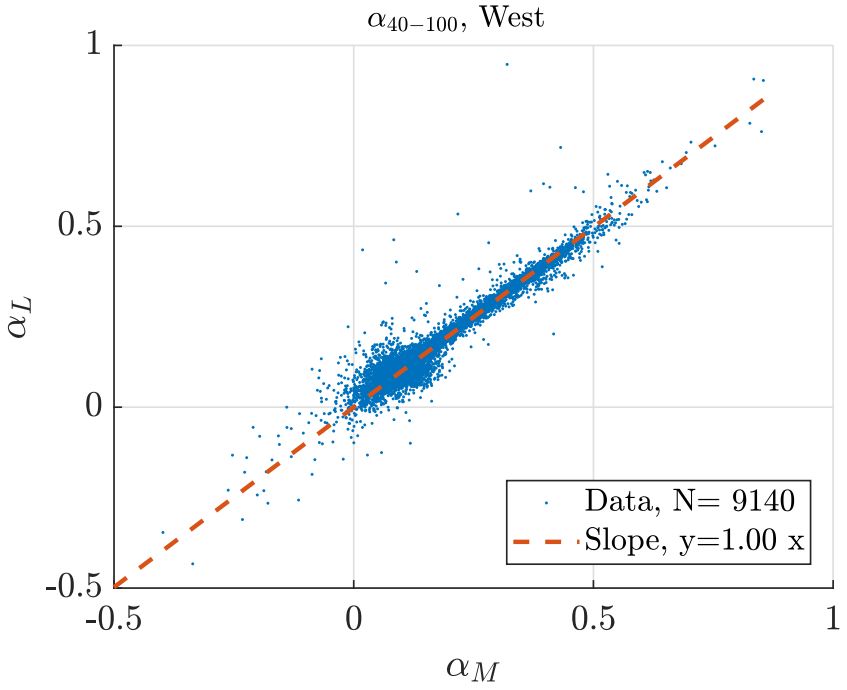


Figure 4.1: Comparison of $\alpha_{40-100}$ measured by the lidar and by the met mast at Høvsøre. The result of the western sector is shown.

The comparison of the two masts is based on data recorded during approximately the same period as the lidar was measuring at Høvsøre, and over 13,000 data points were included in the comparison for the western sector. The bias between the met mast and the lightning mast is -0.0015, and the RMSE is 0.0336. As shown in Table 4.2, the bias and RMSE for the western sector are 0.0224, and 0.0382 respectively. It is remarkable that the bias in the lidar-mast comparison is significantly higher than in the mast-mast comparison, but the RMSE is similar.

Table 4.2: Comparison of the shear exponent $\alpha_{100-160}$ measured by the lidar and by the met mast per direction sector at Høvsøre

| | | **East** | | **West** | |
|---|---|---|---|---|---|
| **Parameter** | **Indicator** | Sonic | Windcube | Sonic | Windcube |
| | # Samples | 3983 | 3774 | 9827 | 9831 |
| | # vs Sonic | | 3772 | | 9766 |
| $\alpha$ 100-160 | Mean [-] | 0.2111 | 0.2421 | 0.0779 | 0.1003 |
| | BIAS [-] | | 0.0310 | | 0.0224 |
| | RMSE [-] | | 0.0868 | | 0.0382 |
| | Slope [-] | | 1.0029 | | 1.0175 |
| | $R$ [-] | | 0.7656 | | 0.8778 |

### 4.2.2. Breezanddijk

Over seven months of wind measurements at Breezanddijk have been included in the analysis. Data has been collected in the period from the start of July 2016 til early February 2017.The lidar and met mast are compared for three different direction sectors, as the surroundings of the lidar and the mast are not homogeneous. The direction sectors are described in Section 3.2.2. For each direction sector the four metrics are calculated and are shown in Table 4.3.

The table indicates that the mast recorded more 10-min averages than the lidar. The discrepancy is mainly because the lidar occasionally fails to record a wind speed and wind direction due to a low signal to noise ratio. Possible causes of the low signal to noise ratio are precipitation, and fog.

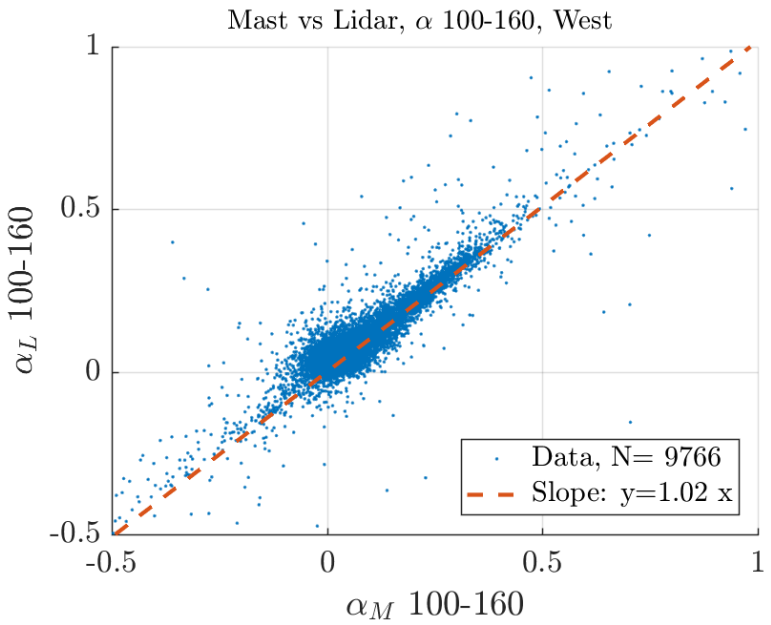


Figure 4.2: Comparison of $\alpha_{100-160}$ measured by the lidar and by the met mast at Høvsøre. The result of the western sector is shown.

The RMSE in sector 2 is significantly larger than for sector 1 and 3. This observation can be explained by two factors. Firstly, the upwind terrain in sector 2 differs between the mast and the lidar. The wind measurements in sector 2 are affected by the camping site, the road overpass and the marina. As the lidar is closer to these obstacles than the met mast, a deviation in the wind speed measurements can be expected. Secondly, it appeared that objects had been affecting the mast measurement at 40 m, but were not affecting the lidar measurements leading to inconsistencies in the derived shear exponents. The deviations result in a large spread in the plot of the shear exponents (see Fig. 4.3b).

Table 4.3: Comparison of the shear exponent measured by the lidar and by the met mast per direction sector at Breezanddijk

| | | **Sector I** | | **Sector II** | | **Sector III** | |
|---|---|---|---|---|---|---|---|
| **Parameter** | **Indicator** | MM | ZephIR | MM | ZephIR | MM | ZephIR |
| | # Samples | 2883 | 2782 | 8166 | 7879 | 7316 | 7166 |
| | # vs MM | | 2749 | | 7651 | | 7133 |
| $\alpha$ 40-75 | Mean [-] | 0.1023 | 0.0955 | 0.1130 | 0.1367 | 0.1278 | 0.1162 |
| | BIAS [-] | | -0.0068 | | 0.0238 | | -0.0116 |
| | RMSE [-] | | 0.0438 | | 0.0592 | | 0.0443 |
| | Slope [-] | | 0.9285 | | 0.9077 | | 0.8593 |
| | $R$ [-] | | 0.9038 | | 0.8387 | | 0.8826 |

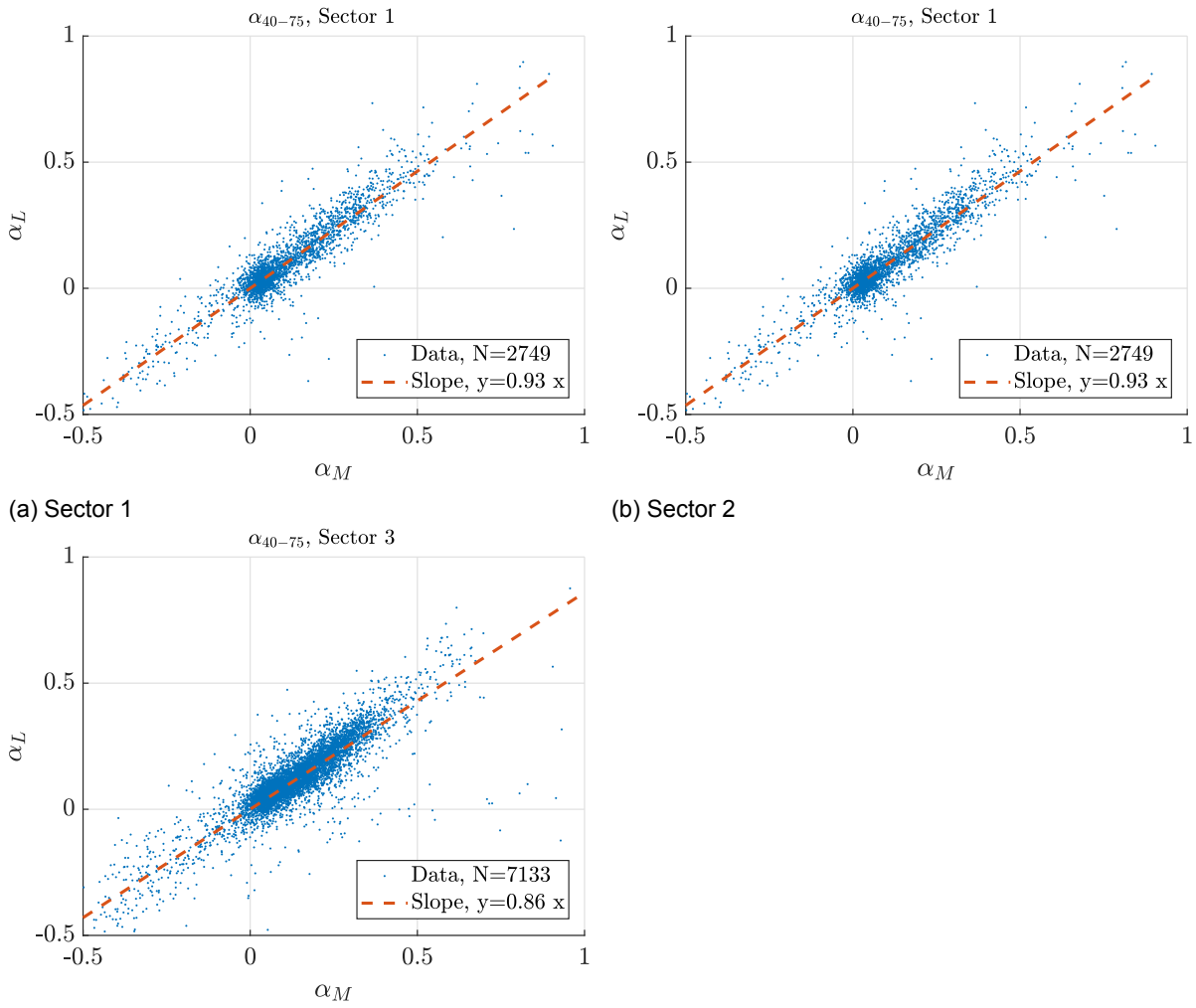


(a) Sector 1

(b) Sector 2

(c) Sector 3

Figure 4.3: Comparison of the wind shear exponent from 40 to 75m, $\alpha_{40-75}$ measured by the met mast, $\alpha_M$ and by the lidar, $\alpha_L$ at Breezanddijk

## 4.3. Discussion and Conclusion

The findings show that the shear measured by the mast and by the lidar is comparable. To place the results in perspective, a comparison with results found in the literature is made. Unfortunately, the majority of the lidar validation studies leaves the shear exponent out of the validation and focuses on wind speed and turbulence intensity instead. An exception is a study by Rodrigo et al., which includes the wind shear in the lidar validation study [35]. They performed a lidar validation study at two locations: Høvsøre, and Alaiz, which is a complex terrain site in Spain. In the study a pulsed lidar and a continuous-wave lidar were compared to the met mast. It is noted that the mast and lidar at Høvsøre that were used by Rodrigo et al., are different from the mast and lidar used in this study. Only the results obtained at Høvsøre are used for comparison, because the terrain is comparable.

Rodrigo et al. found a bias between the mast and lidars of 0.005 and 0.011 for the CW and pulsed lidar respectively. From the tables, it can be observed that the bias found in this validation study is 0.0036, and 0.0224 for the shear exponents in the western sector at Høvsøre. The latter one is affected by the horizontal distance between the mast and the lidar.

At Breezanddijk the bias for sector 1 is -0.0068. This bias is comparable in size to the 0.005 that Rodrigo found. Sectors 2 and 3 result in higher biases of 0.0238 and -0.0116 respectively. The increase of the bias can be attributed to the surroundings of the measurement set-up. Sector 1 is open and very similar for the mast and lidar. On the contrary, sector 2 and 3 are different for the mast and the lidar in terms of distance to obstacles and roughness changes.

Rodrigo et al. also calculated the RMSE of the shear exponents compared to the mast. They found a RMSE of 0.034, and 0.031 for the CW lidar and pulsed lidar. Høvsøre western sector in same order. At Breezanddijk the RMSE is in the order of 0.044 for sector 1 and 3, and 0.06 for sector 2, so larger than the RMSE found at Høvsøre.

In conclusion, the shear measured by the mast and lidar show a proper agreement, especially in the ideal measurement set-up at Høvsøre, where the lidar was located directly next to the mast. At an actual potential wind farm site, like Breezanddijk, the location of the lidar and met mast are dependent on the surroundings, and the ideal measurement set-up is not always feasible. The data from Breezanddijk shows that the shear measured by the mast and lidar deviates. The deviation is explained by two factors. Obstacles cause deviations in the measured wind profile. Secondly, differences in the roughness of the upwind terrain cause differences in the wind profile.

# 5

# Intra-annual Variability of the Wind-Shear Exponent

The vertical wind profile at a potential wind farm site varies within the year. The profile is affected by temperature changes and changes of the surface. In this chapter the intra-annual variability of the shear exponent at Høvsøre and Breezanddijk is studied. Two main aspects are discussed. Firstly the extent of monthly variation of the shear exponent is discussed, because the variation is an important factor in the possibility of reducing the measurement time. Significant intra-annual variation confirms the need for a long-term correction when the measurement time is shorter than a year. The MCP method could be the long-term correction.

Secondly, the variation of the relation between shear exponents at different heights is analysed. Relating shear exponents at different heights is a first step towards the vertical extrapolation of the shear exponent which is discussed in Section 6.2. It could potentially improve the estimation of wind shear above measurement mast height.

## 5.1. Method

Variability of the wind shear exponent is studied by calculating the monthly average shear exponent, and the shear exponent distribution per month. The wind shear is analysed per direction sector, because the wind shear can significantly change with the wind direction due to terrain differences and obstacles. The direction sectors for both Høvsøre and Breezanddijk are described in Section 3.2.

The monthly average of the shear exponent shows the variation of the shear exponent over the year. By plotting the monthly mean of shear exponents from various heights, a comparison of monthly averages of shear exponents at different heights is possible.

The shear exponent distribution, $P(\alpha)$, is calculated for each month and compared with the shear exponent distribution of a full year. In this way, it becomes clear what part of the shear exponent distribution is measured in a certain month, and how this month relates to the full year. The distributions are calculated using Matlab's built-in histogram function, which bins the data, and estimates the probability corresponding to the bin using:

$$P(\alpha_i) = \frac{c_i}{N} \tag{5.1}$$

In which $c$ is the number of bin elements, $i$ is indicating the bin, and $N$ is the total number of elements. This is a direct way of estimating the shear exponent distribution. Another way of estimating the distribution would be to estimate the parameters of a given probability density function. However, there is no standard probability density function for wind shear exponent distributions.

For each month the number of data points, $N_{\text{month}}$, and a weight, $w$ is assigned. The $w$, is calculated to assess how much each month contributes to the yearly shear exponent distribution, and depends on the wind direction distribution for each month.

$$w = \frac{N_{\text{month}}}{N_{\text{year}}} \tag{5.2}$$

## 5.2. Observations

The shear variability is discussed per measurement site. First the observations at Høvsøre are analysed, subsequently the observations at Breezanddijk are discussed.

### 5.2.1. Høvsøre

Measurement data from the met mast and the lightning mast are used for this analysis, because only short-term lidar data is available. In total, seven years of measurement data have been included. Two shear exponents are investigated:

- $\alpha_{40-100}$ is evaluated at the met mast. It could represent a shear exponent which is derived using a tall met mast in a wind measurement campaign.
- $\alpha_{60-160}$ is evaluated at the lightning mast. As this mast provides measurement above typical met mast height, this could represent a shear exponent derived using a lidar. Besides, this shear exponent could be used to represent the wind profile over a full rotor plane

The mean shear exponent per month for the eastern sector at Høvsøre is shown in Fig. 5.1. It is observed that the monthly means vary in the range of 0.15 to 0.32 with a few outliers reaching as high as 0.41. In general, the shear from 40 to 100 m is greater than the shear from 60 to 160m, which is expected due to high shear in the surface layer and lower shear above the surface layer. The variation of the mean shear does not show a seasonal trend. Fluctuations appear only on a monthly scale.

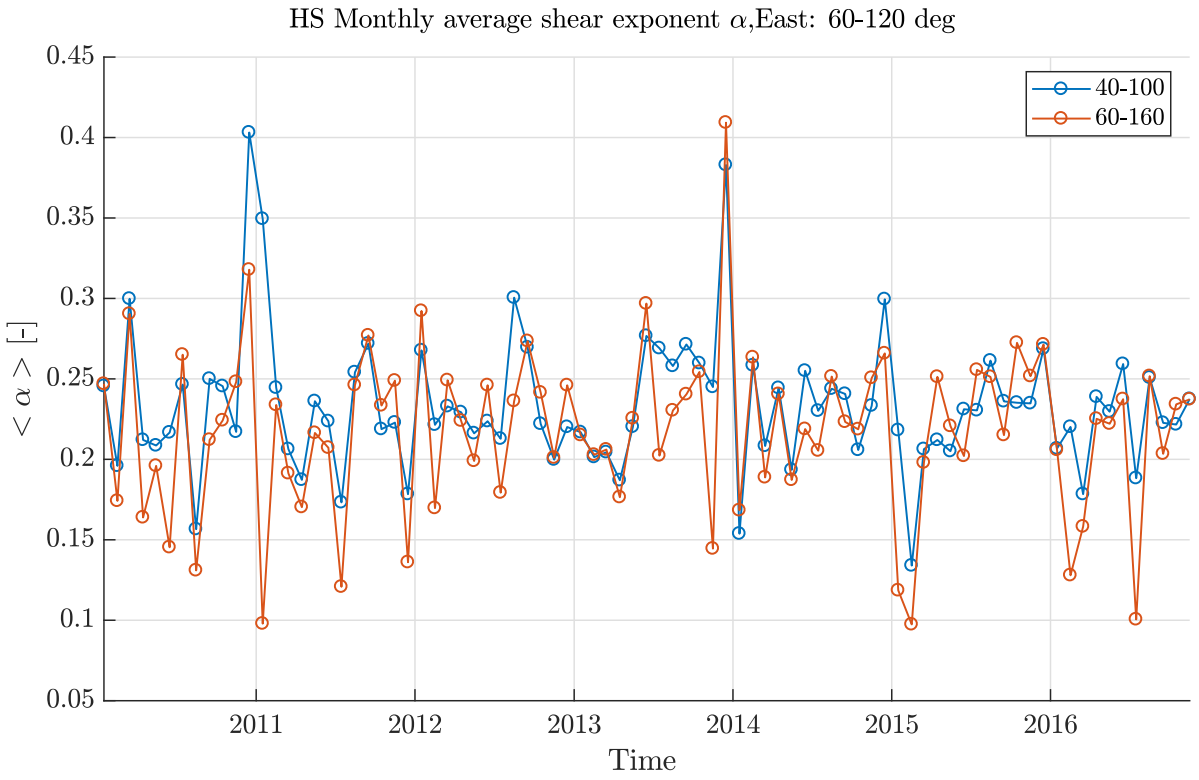


Figure 5.1: Mean shear exponent per month for the eastern sector at Høvsøre

To explain the observation, the shear exponent distribution per month is analyzed. The monthly distributions of $\alpha_{40-100}$ are shown in Fig. 5.2. On the contrary of the mean shear exponent, these distributions show a clear variation on a seasonal scale. In the winter months the shape of the shear exponent distribution has one peak around 0.2. Continuing to the spring, the peak of the distribution shifts towards lower alphas. Simultaneously the distribution becomes wider, implying a decrease of shear exponents around 0.2, and an increase of shear exponents above 0.3.

An interesting result is found for the months July, August and September, in which the distribution has the shape of a bimodal distribution. This observation can be attributed to variation of the wind shear at daily scale. During the nights the wind shear is high, resulting in the peak around 0.38, while the peak at 0.06 results from wind shear measured during the day. Wagner mentions that longer days and stronger heating by the sun are mentioned as causes for the distinct daily variations [41]. These conditions correspond to the conditions in the months July, August and September.

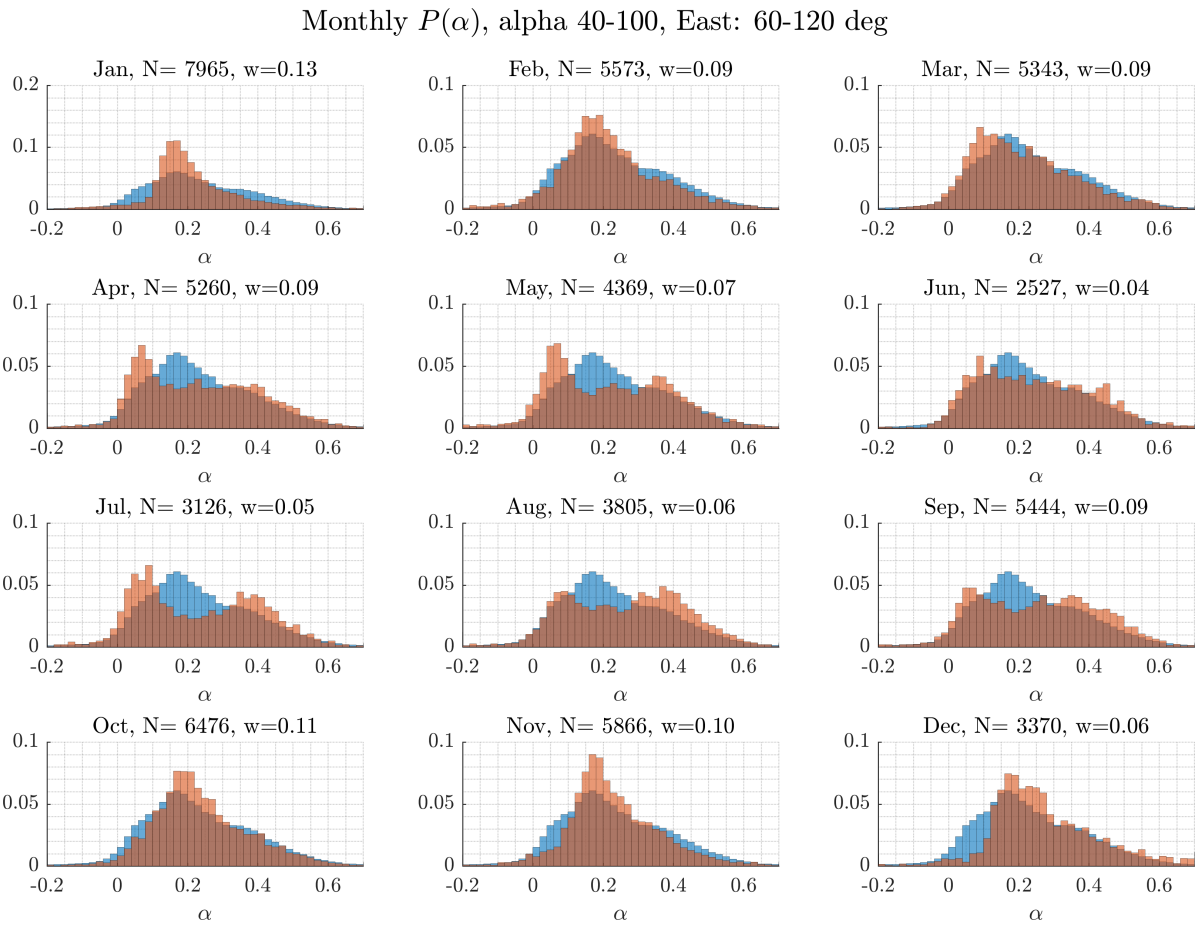


Figure 5.2: Shear exponent distribution, $P(\alpha_{40-100})$ per month for the eastern sector at Høvsøre. The red histograms are showing the distribution for the particular months. The blue histogram is the histogram corresponding to the yearly shear exponent distribution. Seven years of data, 2010-2016, have been included in the distribution.

In Fig. 5.3 the mean shear exponents of the western sector are presented. A fluctuation on seasonal scale is apparent. High mean shear is measured during the winter months, whereas the summer months show low monthly mean shear exponents. Further, it stands out that the winters of 2010 to 2012 result in higher mean shear exponents than the last four years. The monthly mean shear during the summers appears to be similar. An explanation of the higher wind shear during the first three years is the colder winters in this period.

Comparing the $\alpha_{40-100}$ with the $\alpha_{40-160}$ shows that the $\alpha_{40-100}$ is consistently greater than $\alpha_{40-160}$, which implies that the shear in the lower part of the wind profile is higher than the shear in the upper part. The difference between the mean shear exponents fluctuates on the timescale of a year, and is significant over the whole year, i.e. it is is necessary to correct the shear exponent for vertical extrapolation.

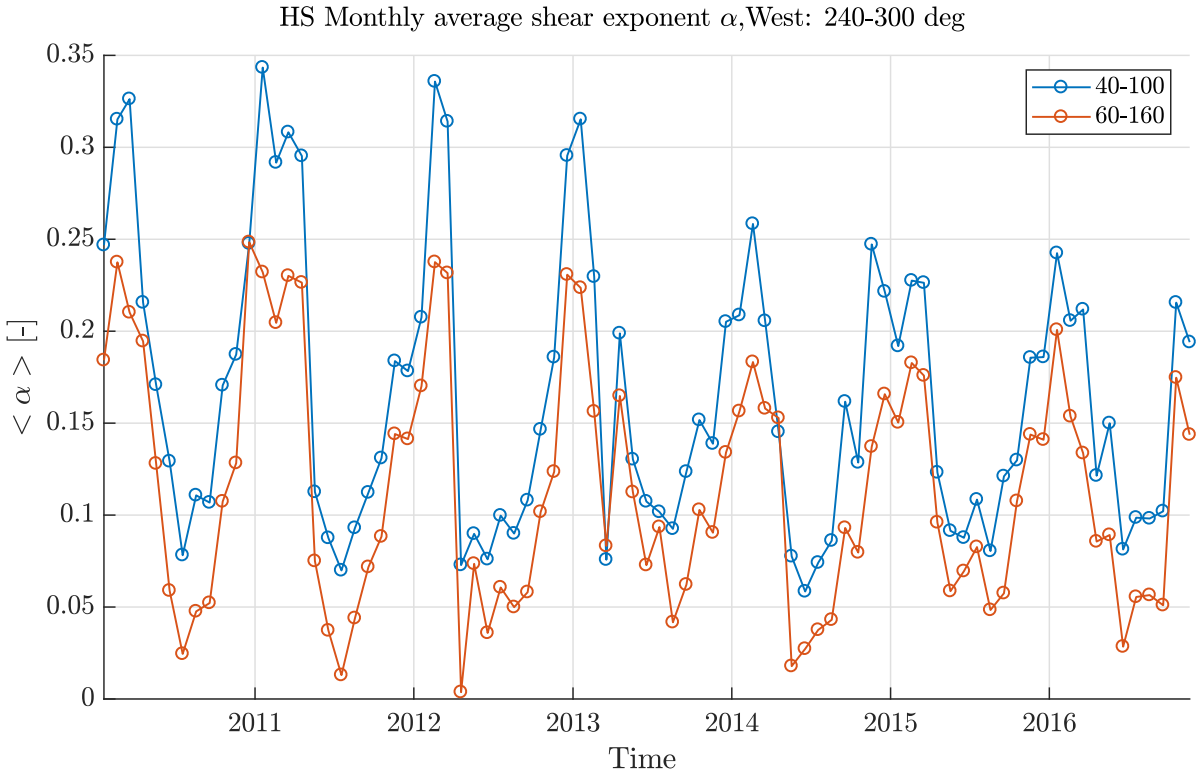


Figure 5.3: Mean shear exponent per month for the western sector at Høvsøre

The 40 to 100 m shear exponent distribution, $P(\alpha_{40-100})$, for the western sector is presented in Fig. 5.4. From the distribution it becomes clear that the width of the distribution changes over the months. From December to May the distribution is wider, meaning higher $\sigma\alpha$ than in the other months. The months with a higher $\sigma\alpha$ are also the months in which the average shear is higher. The wider distributions are caused by the prevailing stable conditions in the winter.

Wagner investigated the wind shear at Høvsøre and included stability [41]. Wind shear distributions per stability class showed that the correlation between stability and wind shear is strong for the eastern sector. For the western sector the correlation is weak due to the presence of the coastline. This finding provides an argument for leaving out stability in the analysis of wind shear.

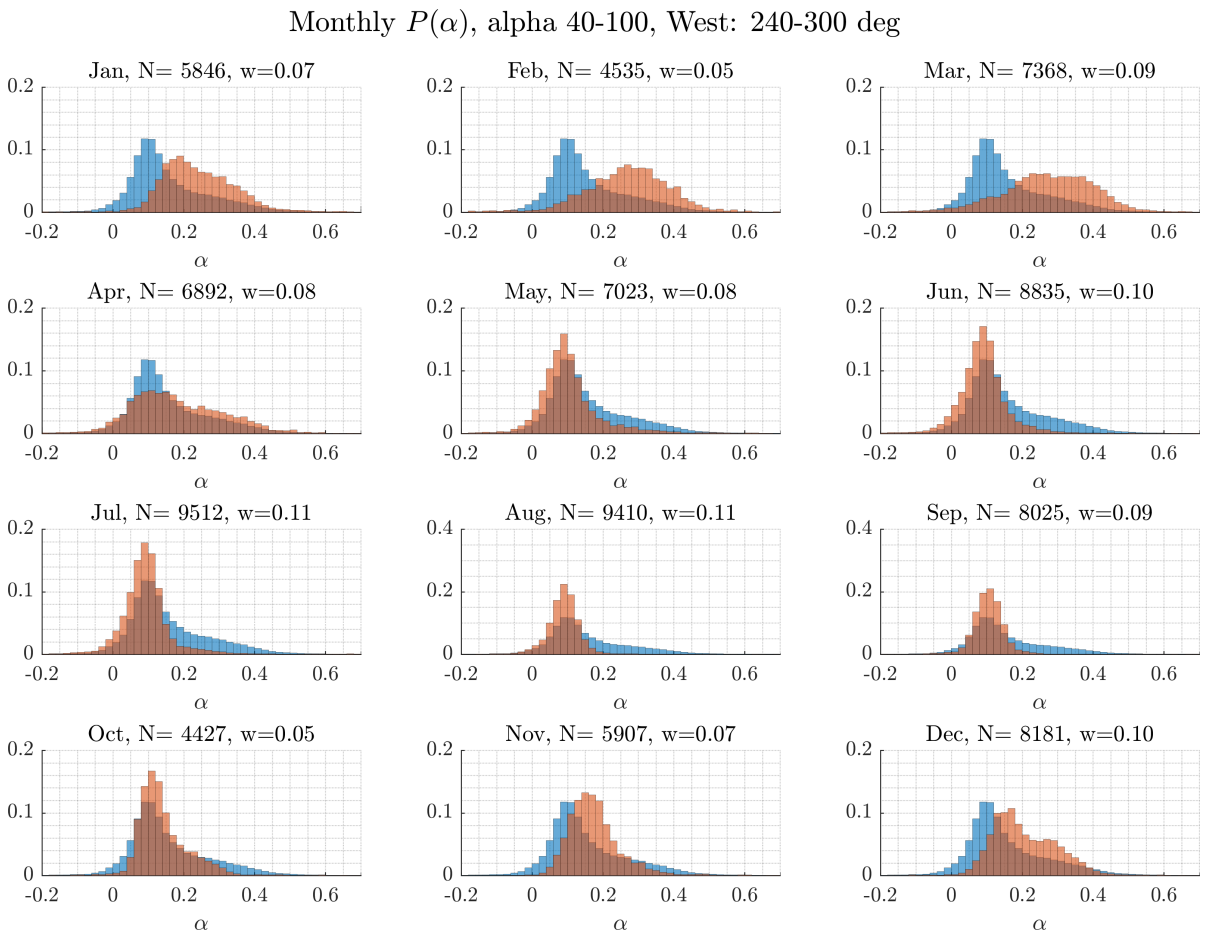


Figure 5.4: Shear exponent distribution, $P(\alpha_{40-100})$, for the western sector at Høvsøre. The red histograms are showing the distribution for the particular months. The blue histogram is the histogram corresponding to the yearly shear exponent distribution. Seven years of data, 2010-2016, have been included in the distribution.

### 5.2.2. Breezanddijk

The lidar data from Breezanddijk has been used to calculate the mean wind shear exponent and the wind shear exponent distribution per month. One and a half year of data was available for the analysis. In order to keep the obtained monthly distributions comparable with the yearly distribution, exclusively data from the year 2016 has been used. In this section, the focus is on the first and the third direction sector as these sectors are the least influenced by obstacles.

As lidar data is used, wind measurements at 11 heights are available, see Table 3.1. For this analysis, three height ranges are used for the shear exponent calculation:

- $\alpha_{40-75}$, is based on wind speed measurements at 40 m and 75 m. These are heights at which typical met masts measure the wind speed.
- $\alpha_{40-200}$, is calculated from wind speed measurements at 40 m and 200 m. The shear exponent would represent the wind shear over a large wind turbine rotor, with a hub height of approximately 120 m.
- $\alpha_{40-120}$ is based on wind speed measurements at 40 m and 120 m. This shear exponent is required for the extrapolation of the wind speed to a typical hub height of 120 m.

Apart from the dyke, Breezanddijk is surrounded by water. The nearest coastline of the IJsselmeer with the main land is located at least 11 km to the north-west. From this observation, it is expected that the average wind shear at Breezanddijk is generally lower than the wind shear at Høvsøre, because the terrain roughness is lower. This hypothesis is confirmed by comparing Fig. 5.5 with Fig. 5.7.

The monthly mean shear exponent of the first sector is shown in Fig. 5.5. The monthly shear average shows a seasonal cycle like the shear for the western sector of Høvsøre. The difference between the minimum and maximum in a yearly cycle is around 0.2, and is similar to the observations for the western section at Høvsøre. The monthly mean shear exponent of the third sector at Breezanddijk (Fig. 5.7 shows the same trend.

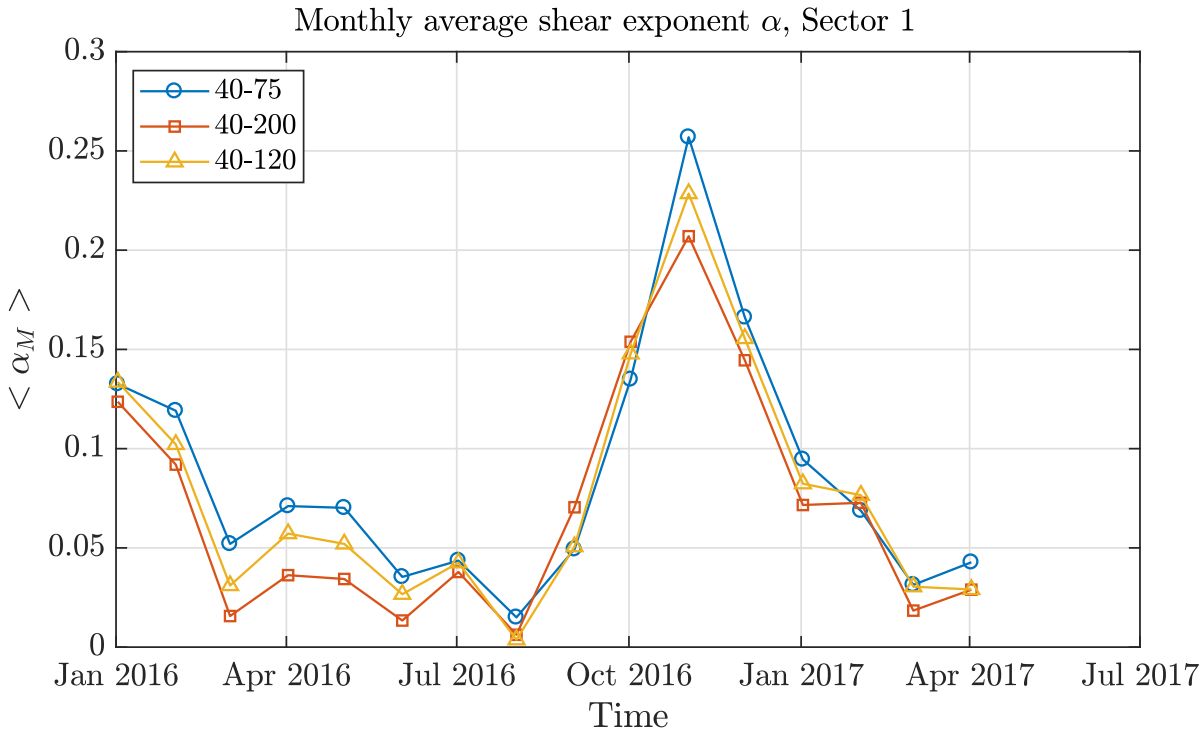


Figure 5.5: Monthly averaged shear exponent $< \alpha_M >$ for sector 1 at Breezanddijk

In Fig. 5.6 the shear exponent distribution for sector 1 is shown. As only one year of wind measurements are used, and sector 1 includes the infrequent northerly winds, a low number of samples is available. Therefore it is hard to obtain an image of the underlying shear exponent distribution. The effect of the lower number of samples is clearly visible when the monthly histograms for Breezanddijk are compared to the histograms for Høvsøre. For example, the months January and December include not enough samples to obtain the distribution. Contrary to these months are May and June, these months include more than 1000 10-min averaged $\alpha_{40-75}$ samples. As a result these months have a weight, $w$ of 0.15, implying that May and June account for 30% of the total number of samples.

Comparing the yearly shear distribution of sector 1 with the distribution of sector 3 shows that the distribution of sector 3 is wider, having more frequent high shear exponents. This difference could be caused by the sampling issue. Direction sector 1 does not include enough samples to construct the $P(\alpha)$ for the winter months December and January (less than 200 data points per month). Another factor could be the presence of the marina. This is unlikely because the dykes of the embankment are not high and will not influence the wind speed at 40 m.

Contrary to sector 1, sector 3 contains enough samples for the winter months January and December. Figure 5.8 clearly shows that the monthly distribution corresponding to the winter months is located at higher shear exponents than the yearly distribution. This is also expected, when one keeps in mind the variation shown in Fig. 5.7.

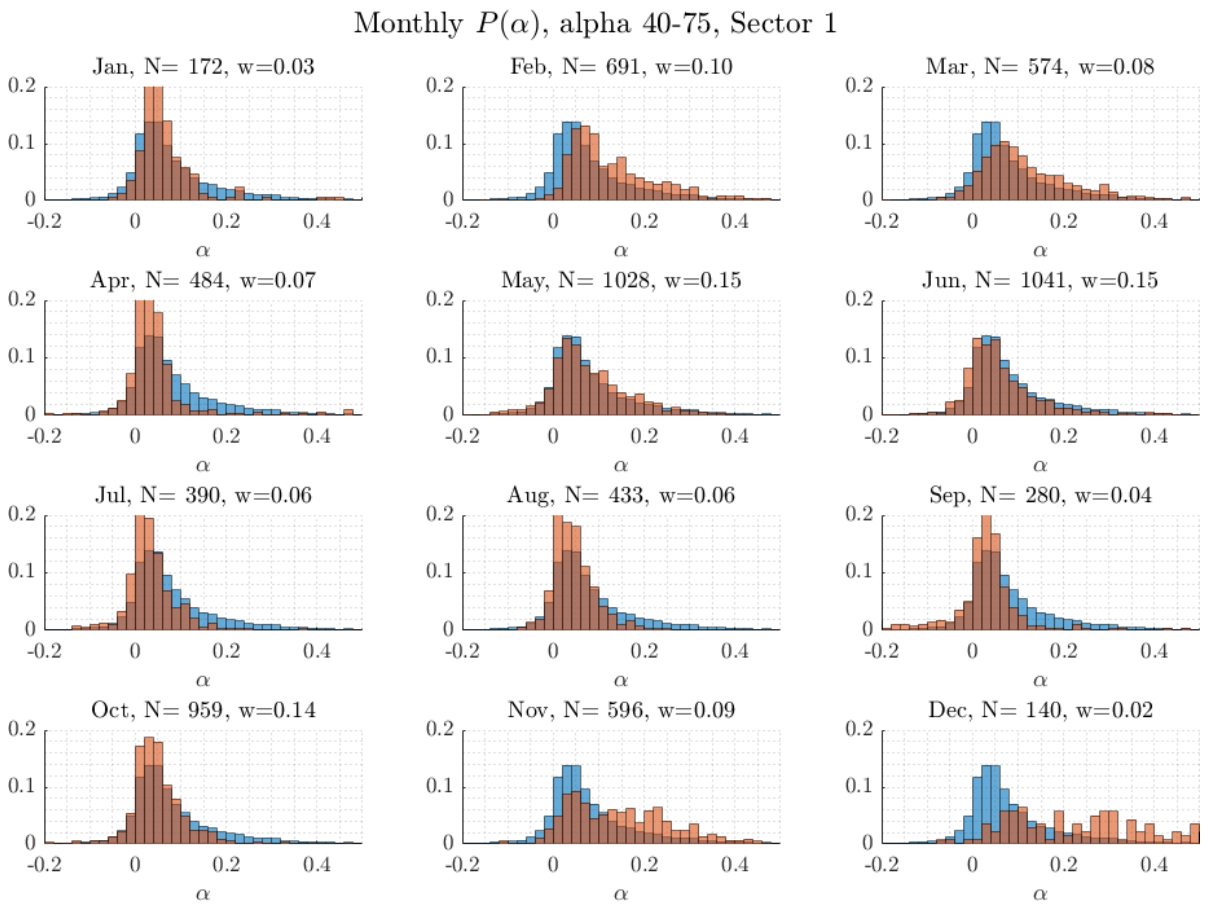


Figure 5.6: Shear exponent distribution, $P(\alpha_{40-75})$, for sector 1 at Breezanddijk. The red histograms are showing the distribution for the particular months. The blue histogram is the histogram corresponding to the yearly shear exponent distribution. One year of data, 2016, has been included in the distribution.

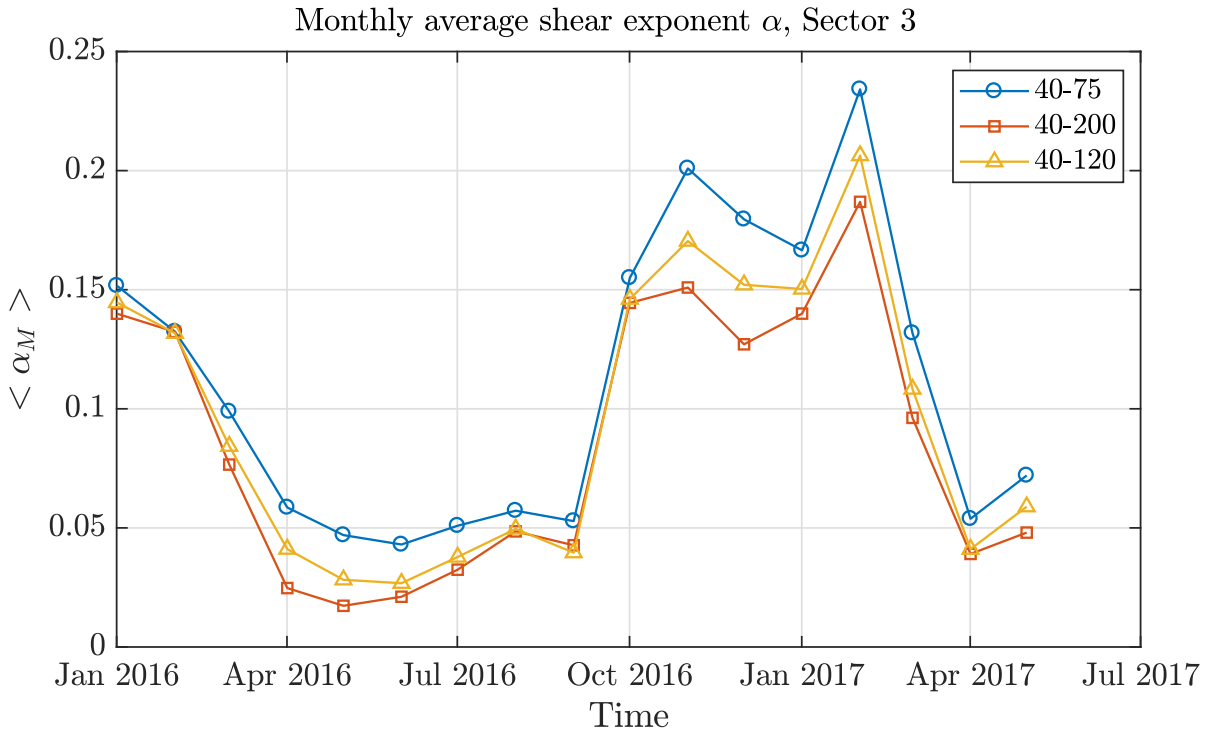


Figure 5.7: Monthly averaged shear exponent $< \alpha_M >$ for sector 3 at Breezanddijk

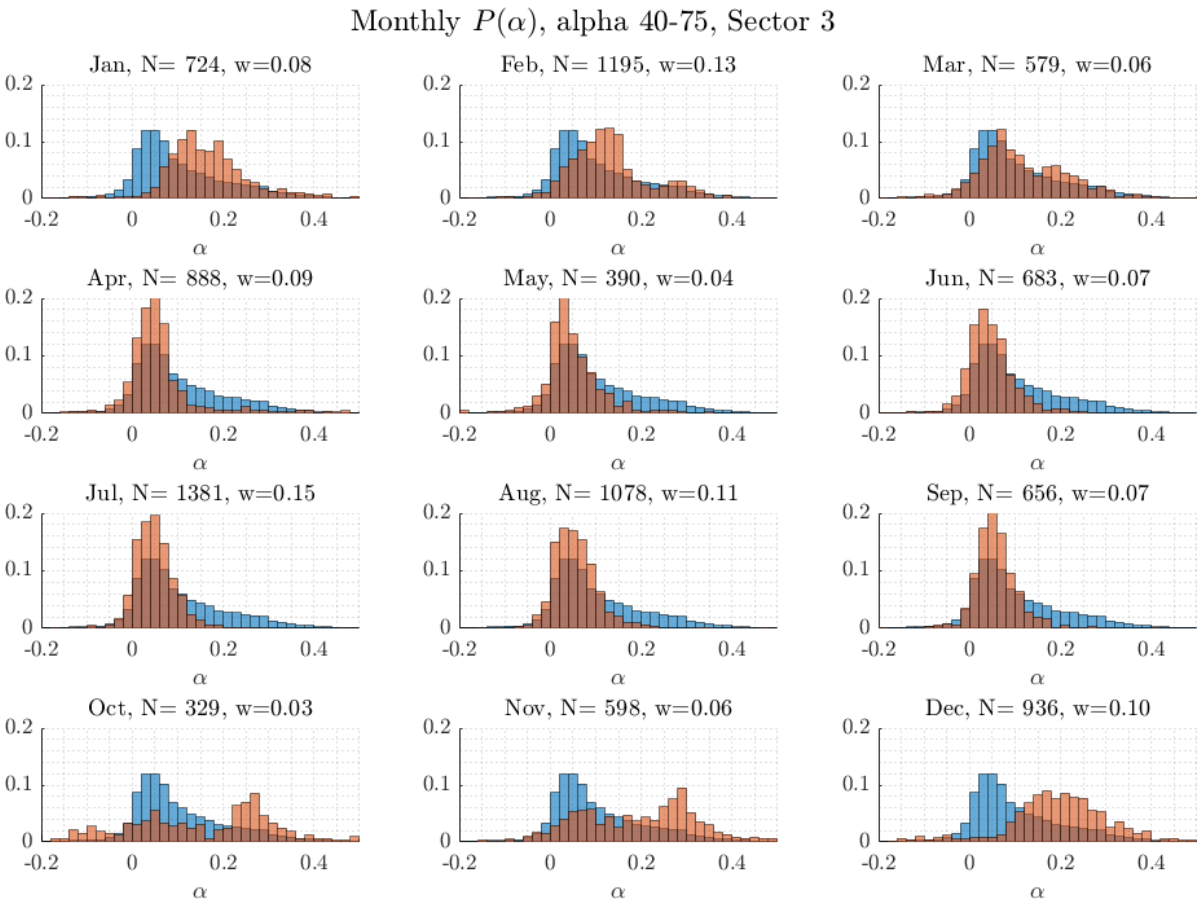


Figure 5.8: Shear exponent distribution, $P(\alpha_{40-75})$, for sector 3 at Breezanddijk. The red histograms are showing the distribution for the particular months. The blue histogram is the histogram corresponding to the yearly shear exponent distribution. One year of data, 2016, has been included in the analysis.

## 5.3. Conclusion

Wind shear exponent distributions vary within a year. The observations at Høvsøre and Breezanddijk show that the shear varies on a seasonal timescale. The variation in wind shear is caused by the difference in the heating of the Earth's surface by the sun from season to season. The surrounding terrain at the measurement site influences the intra-annual variability. At Høvsøre a comparison was made between the eastern and the western sector. Whereas the average wind shear exponent in the western sector shows an obvious seasonal variation, it does not show this trend for the eastern sector. Despite minimal variations in the mean, the shear exponent distributions of the eastern sector do show a seasonal variation. Particularly interesting are the shear exponent distributions in the summer that show 2 maxima due to shear variation on a daily time scale. Fitting a probability density function may be more difficult in this case.

The analysis presented in this chapter has shown that wind shear distributions measured from one season only cannot represent the long-term wind shear. The intra-annual variation confirms the need for an extrapolation of wind shear statistics that are measured during periods shorter than a year. A suitable extrapolation method could be the MCP method. This hypothesis is further tested in the next chapters.

Other consequences of the variable wind shear exponent may be found in wind turbine load calculations. The current IEC standards specify a constant wind shear exponent for the load calculations [16, 17]. As the wind shear exponent is variable, the calculations might be too simple and do not represent the real situation. Especially for large rotors, the variable wind shear could be an important factor. Dimitrov et al. studied the effect of a wind shear model conditional on turbulence on the wind turbine loading [10]. They show that the shear in the design standard may be over-specified in the case of moderate turbulence. The new model could reduce the fatigue loads. Further, they found that the IEC61400-1 wind shear model results in non-conservative estimates of the 50-year extreme blade deflection towards the tower. These are strong arguments to further investigate the potential benefits of a variable wind shear model.

# 6

# Implementation and Validation of the MCP Code

In wind resource assessment it is required to obtain wind statistics that are representative for the long-term wind at the target site. These wind statistics are necessary for the evaluation of the feasibility of a potential wind farm. However, the measurement campaign only provides short-term wind data at the target site. To obtain wind statistics that represent the long-term wind at the target site, an extrapolation is carried out.

This chapter presents the implementation of the MCP method, which can be used to extrapolate short-term wind data to better represent the long-term wind conditions at the target site. Implementation of two existing MCP methods is presented in Section 6.1. To improve the MCP method for the purpose of extrapolating short-term wind shear data, two improvements of the standard MCP method have been considered. Firstly, vertical extrapolation of the wind shear is discussed in Section 6.2. Secondly, a weighted MCP method is presented in Section 6.3. Finally, the implemented MCP code is validated using WindPRO, presented in Section 6.4.

## 6.1. Implementation of the MCP procedure in Matlab

In this section the implementation of the MCP procedure is discussed. The process consists of three main steps and is visualised in Fig. 6.1. Besides, the figure shows the required input, consisting of a short-term and a long-term data set. The following subsections elaborate on the three steps of the MCP procedure.

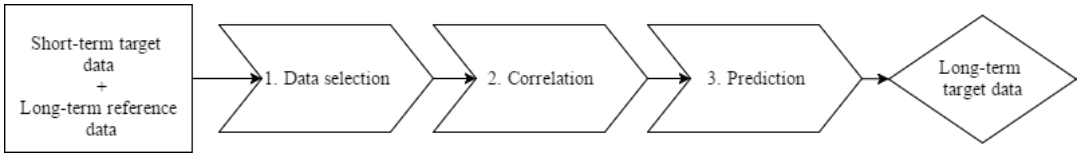


Figure 6.1: Flowchart of the MCP procedure

### 6.1.1. Data selection

In the first step, the target site data and the reference site data are imported and wind direction sectors are defined. By default, twelve direction sectors are used. The first sector ranging from 345 degrees to 15 degrees. The direction sectors will be used to establish a correlation per direction sector. It is assumed that the correlation between the target and reference data depends on the wind direction and that the prediction improves when a separate correlation for each direction sector is used.

This assumption is justified as the terrain influences the wind profile and the terrain changes with direction. Under this assumption, it can be expected that the MCP prediction enhances further when narrow direction sectors are used. The issue which arises for smaller direction sectors is a sampling problem. For smaller direction sectors, the short-term data set may not contain enough data points in each direction sector to establish a reliable correlation. This sampling issue is an important factor to consider when the measurement time in a wind measurement campaign is to be reduced.

### 6.1.2. Correlation

The concurrent data points of the input data are used to establish the correlation. The concurrent data points of the input data are detected and the points are binned using the wind direction data at the reference site. Subsequently, a correlation between the target site and the reference site is established for each direction sector. Two common correlations methods have been implemented: linear regression and the variance ratio method.

Linear regression is implemented, as it is straightforward, and commonly applied in MCP calculations for wind resource assessment. The variance ratio method is implemented as it is better at predicting the distributions than the linear regression method [34]. The difference in the accuracy of the predicted distributions is explained by the fact that linear regression underestimates the variance in the predicted signal (see Appendix B).

The Mortimer method is not implemented, because of the need for enough data to fill the correlation matrix. For short measurement periods, the matrix is not filled out completely, or the bins need to be very large, which reduces the effect of the method. Another way to fill out the correlation matrix is to interpolate and extrapolate the recorded matrix elements, similar to the approach used for WindPRO's matrix method [38].

**Linear Regression**

Linear regression can be performed via the least squares method [13]. The slope and intercept of the linear relation are calculated via:

$$\mathbf{b} = ((\mathbf{X}^T\mathbf{X})^{-1})\mathbf{X}^T\mathbf{y} \tag{6.1}$$

In which $\mathbf{b}$ is the vector containing the slope and intercept of the least squares fit, $\mathbf{X}$ is a matrix containing ones in the first column and the reference data in the second column, and $\mathbf{y}$ is a column vector containing the target data, as shown by:

$$\mathbf{X}^T\mathbf{X} = \begin{pmatrix} 1 & \dots & 1 \\ x_1 & \dots & x_n \end{pmatrix}\begin{pmatrix} 1 & x_1 \\ \vdots & \vdots \\ 1 & x_n \end{pmatrix} \tag{6.2}$$

$$\mathbf{X}^T\mathbf{y} = \begin{pmatrix} 1 & \dots & 1 \\ x_1 & \dots & x_n \end{pmatrix}\begin{pmatrix} y_1 \\ \vdots \\ y_n \end{pmatrix} \tag{6.3}$$

The result of the least squares regression results in the following equations for the slope, $b_1$, and the intercept, $b_0$:

$$b_1 = \frac{\sigma(xy)}{\sigma^2(x)} \tag{6.4}$$

$$b_0 = \overline{y} - b_1\overline{x} \tag{6.5}$$

**Variance Ratio Method**

The variance ratio method was suggested by Rogers [34] to improve the MCP prediction of the target distribution. The correlation established by VRM follows:

$$\hat{y} = \mu_y - \frac{\sigma_y}{\sigma_x}\mu_x + \frac{\sigma_y}{\sigma_x}x \tag{6.6}$$

In which $\mu_y$ and $\mu_x$ are the mean wind speed at the target site and the reference site, respectively. And $\sigma_y$ and $\sigma_x$ are the respective standard deviations of the wind speed at the target site and the reference site. Using Eq. (2.10), the variance of the predicted wind speeds, $\sigma^2(\hat{y})$, is equal to the variance of the observed wind speeds $\sigma^2(y)$. Using Eq. (2.10) for the correlation, results in a better prediction of the wind speed distribution at the target site [34].

### 6.1.3. Prediction

The last step is the prediction of the long-term time series at the target site. The reference data, and the established correlation are used to calculate the long-term time series at the target site. For each time step at which reference data is available, a prediction for the target site is calculated. The algorithm approaches the prediction per direction sector. Firstly, the reference data in and the correlation for the first sector are used for a prediction, then the data and correlation for the second sector, etc.

## 6.2. Vertical extrapolation of the wind shear exponent

For present-day wind energy projects, wind data at heights above 100 m is often necessary. In the ideal case, wind measurements are available at the target hub height for an extended period of time, i.e. multiple years. However, the majority of wind measurements are performed at low altitudes and wind measurements above 100 m are scarce. In particular long-term data is often only available at lower heights. To estimate the long-term wind statistics at higher heights, vertical extrapolation is frequently applied. This vertical extrapolation could be implemented in the MCP method to improve the correlation between the target data and the reference data.

In this section, a simple expression for vertical extrapolation of the wind shear exponent is derived (see Section 6.2.1). In Section 6.2.2 the vertical extrapolation of the shear exponent is compared with observations at Høvsøre.

### 6.2.1. Method

The vertical wind profile is commonly described by the power law profile or the logarithmic profile:

$$u(h) = u_{ref}\left(\frac{z}{z_{ref}}\right)^{\alpha} \tag{6.7}$$

$$u(z) = \frac{u_*}{\kappa}\ln\left(\frac{z}{z_0}\right) \tag{6.8}$$

The shear exponent $\alpha$ of the power law (Eq. (6.7)) can be defined using a centred definition [22], following:

$$\alpha \equiv \frac{\partial u}{\partial z}\frac{z}{u} \tag{6.9}$$

In this definition $\frac{\partial u}{\partial z}$ and $u$ are evaluated at $z$, the geometric mean height.The geometric mean height $z$ is defined as: $z = \sqrt{z_1 z_2}$. Substitution of the logarithmic wind profile for neutral atmospheric stability, Eq. (6.8) in Eq. (6.9) results in the following expression for the wind shear exponent:

$$\alpha = \frac{1}{\ln\left(\frac{z}{z_0}\right)} = \frac{1}{\ln(z) - \ln(z_0)} \tag{6.10}$$

The expression gives the shear exponent as a function of the geometric mean height $z$ and the roughness length $z_0$. When the shear exponent is known from measurements, it can be used to calculate the observed roughness length via:

$$z_0 = \frac{z_{obs}}{e^{\frac{1}{\alpha_{obs}}}} \tag{6.11}$$

In which $z_{obs}$ is the geometric mean height of the observation, and $\alpha_{obs}$ is the observed shear exponent.

The observed roughness length is substituted in Eq. (6.10), resulting in:

$$\alpha(z) = \frac{1}{\ln(z) - \ln(z_{obs}) + \frac{1}{\alpha_{obs}}} = \frac{\alpha_{obs}}{\alpha_{obs} \ln(\frac{z}{z_{obs}}) + 1} \tag{6.12}$$

The advantage of this expression is that it does not contain a roughness length. Therefore a roughness map of the measurement site is not required. The vertically extrapolated $\alpha$ only depends on the observed shear exponent $\alpha_{obs}$, and the ratio of the geometric mean height over over the observed geometric mean height $\frac{z}{z_{obs}}$.

In Fig. 6.2 an example of the application of Eq. (6.12) is shown. The shear exponent as a function of height is calculated using Eq. (6.9). Numerical differentiation has been used to approximate the $\frac{\partial u}{\partial z}$. The shear exponent alpha of the power law is calculated for two height ranges: from 40 to 100 meter and from 40 to 160 m.

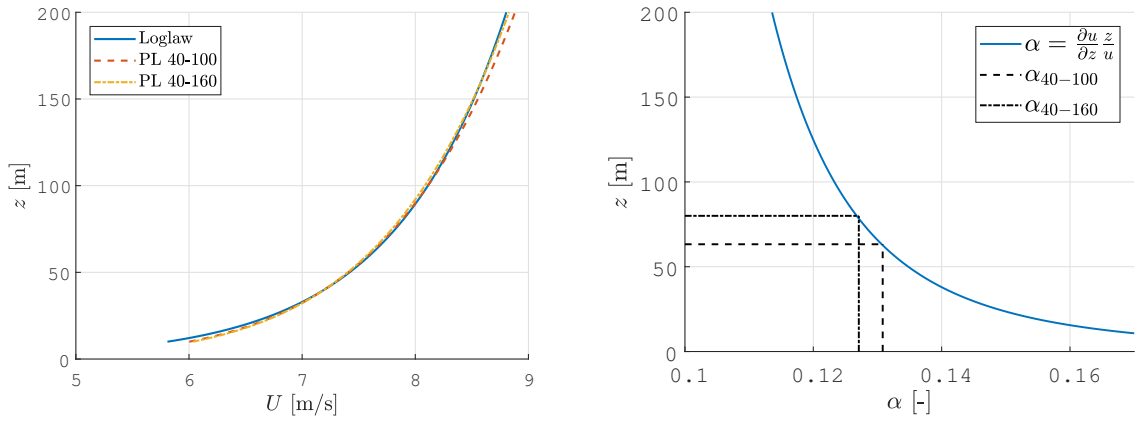


(a) Logarithmic wind profile and two corresponding power law representations of the profile

(b) Shear exponent as function of geometric mean height

Figure 6.2: Example of the application of Eq. (6.12) to a logarithmic wind profile with $u_* = 0.4$ m/s and $z_0 = 0.03$ m

### 6.2.2. Observations

The derived expression, Eq. (6.12) is tested using observations from Høvsøre and Breezanddijk. Only results from the Høvsøre site have been included. In Figs. 6.3 and 6.4 the vertical extrapolation of the shear exponent is shown. Both figures are using the same heights in the extrapolation. The difference is the upwind terrain. The scatter plots show the lower shear exponent on the x-axis and the higher shear exponent on the y-axis.

The expression for the vertical extrapolation, Eq. (6.12), offers only a marginal improvement. In the range of the higher shear exponents, the extrapolation appears to follow the data points better than the linear relations. However, the joint probability density function shows that the conditions for which Eq. (6.12) improves the fit, are not common at this site.

From Fig. 6.3 it can be observed that most of the data is below the curve described by Eq. (6.12). For a better fit, the equation should not go through the origin. An extra term should be added to the equation to enhance the fit. For this reason, the vertical extrapolation by Eq. (6.12) has not been implemented in the MCP.

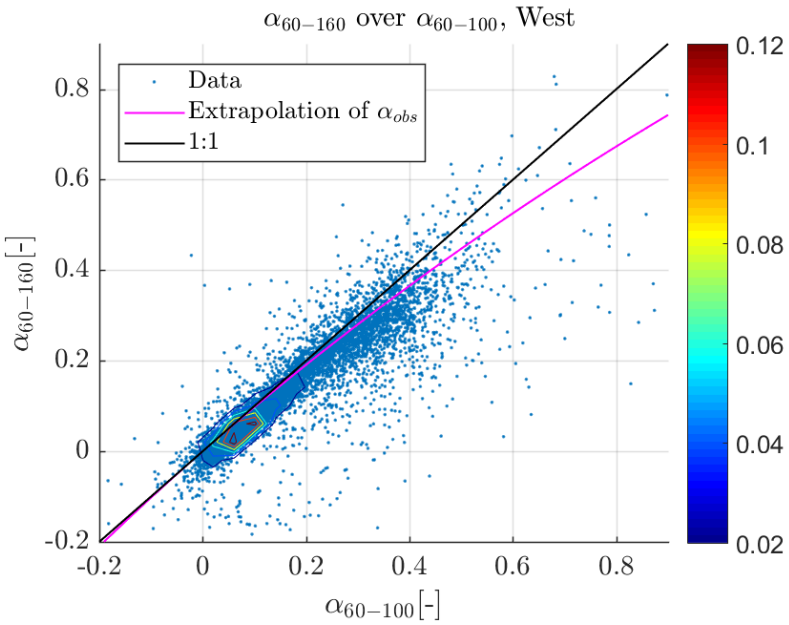


Figure 6.3: Scatter plot of the shear exponent $\alpha_{60-100}$ and the shear exponent $\alpha_{60-160}$ for the western sector at Høvsøre. On top of the data a contour plot shows the joint probability of the shear exponents. The magenta line represents the vertical extrapolation of alpha, given by Eq. (6.12)

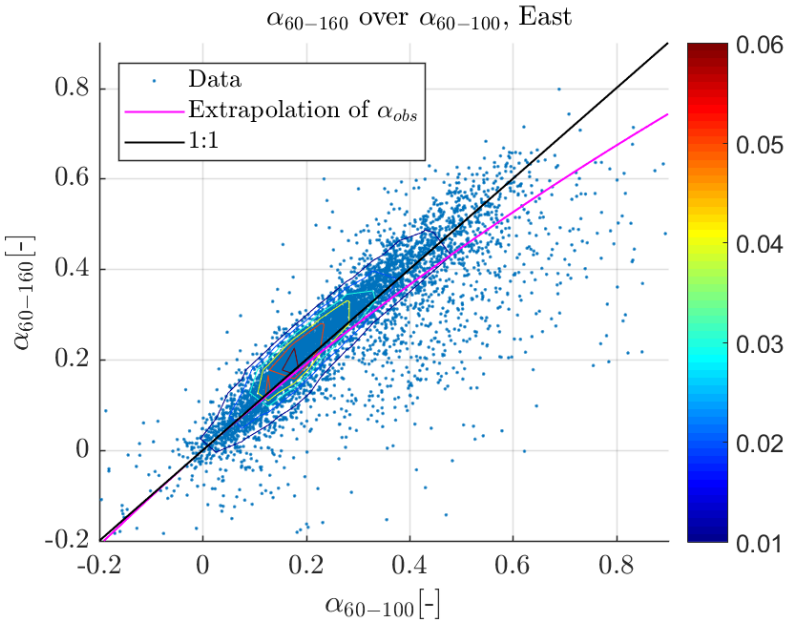


Figure 6.4: Scatter plot of the shear exponent $\alpha_{60-100}$ and the shear exponent $\alpha_{60-160}$ for the eastern sector at Høvsøre. On top of the data a contour plot shows the joint probability of the shear exponents. The magenta line represents the vertical extrapolation of alpha, given by Eq. (6.12)

## 6.3. Weighted MCP

When the concurrent measurement period is reduced, it is more likely that the sample does not represent a full year. Therefore the correlation which is established, could be based on conditions that do not occur as often in the long-term as in the short-term. As a consequence, a bias is introduced in the prediction. The reference data set can be used to mitigate the effect of the unrepresentative measurement period.

As a long-term reference data set is available for the MCP method, it can be determined whether the conditions during the concurrent measurement period are representative for the long-term. Moreover, a weighted correlation can be calculated to account for the long-term. By assigning higher weights to frequent conditions, the correlation improves for the long-term. The weights assigned to the concurrent data points are based on the probability of the reference shear exponent in the long-term distribution, and its probability in the short-term distribution:

$$w = \frac{P(\alpha_{LT})}{P(\alpha_{ST})} \tag{6.13}$$

The probabilities $P(\alpha_{LT})$, and $P(\alpha_{ST})$, are calculated in the same way as the histograms of Chapter 5, following:

$$P(\alpha) = \frac{c_i}{N} \tag{6.14}$$

To ensure that the weights do not become too large, the denominator of the equation has been adapted for its implementation in the MCP procedure. A threshold value was assigned by adding 0.1 to the denominator:

$$w = \frac{P(\alpha_{LT})}{P(\alpha_{ST}) + 0.1} \tag{6.15}$$

The weights can be used both in the linear regression and the variance ratio MCP. In linear regression MCP the weights are used to calculate a weighted least squares fit, following:

$$\mathbf{b} = ((\mathbf{X}^T\mathbf{W}\mathbf{X})^{-1})\mathbf{X}^T\mathbf{W}\mathbf{y} \tag{6.16}$$

In which $\mathbf{b}$ is the vector containing the slope and intercept of the least squares fit, $\mathbf{X}$ is a matrix containing ones in the first column and the reference data in the second column, $\mathbf{W}$ is a matrix containing the weights on the diagonal and zeros at the other locations, and $\mathbf{y}$ is a column vector containing the target data.

In the variance ratio method the weights are used to calculate the weighted mean, $\mu_{x,w}$, and weighted standard deviation, $\sigma_{x,w}$, of the concurrent data set.

$$\mu_{x,w} = \frac{\sum_{i=1}^{N} w_i x_i}{\sum_{i=1}^{N} w_i} \tag{6.17}$$

$$\sigma_{x,w} = \sqrt{\frac{\sum_{i=1}^{N} w_i \left(x_i - \overline{x_w}\right)^2}{\sum_{i=1}^{N} w_i}} \tag{6.18}$$

Substitution of the weighted mean and weighted standard deviation in the VRM correlation results in:

$$\hat{y}_{wVRM} = \mu_{y,w} - \frac{\sigma_{y,w}}{\sigma_{x,w}}\mu_{x,w} + \frac{\sigma_{y,w}}{\sigma_{x,w}}x \tag{6.19}$$

A striking example of the benefit of assigning weights to the short-term data is provided in the second example application of the MCP method in Chapter 7, see Section 7.2.2.

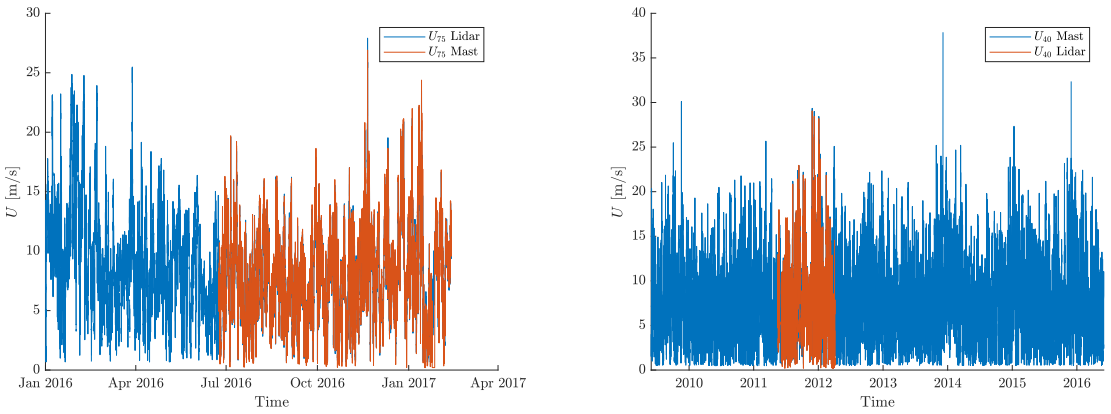


(a) 1. Breezanddijk (b) 2. Høvsøre

Figure 6.5: Visualisation of the wind data used for the validation. Details of the measurement periods are provided in Table 6.1

## 6.4. Validation of the MCP code

Validation of the MCP code is performed by comparing the result of the code with results obtained using the MCP module of the WindPRO software. WindPRO is widely applied in the industry for wind resource calculations. WindPRO has many options for data filtering and data processing, so it is important to set-up the software in the way that it matches the MCP method implemented in Matlab.

For the validation purpose, linear regression MCP is used. The validation is carried out in 2 steps. Firstly, the data selection and calculation of the linear regression are validated by comparing the established linear relations. Secondly, the predictions of the long-term data set is validated, which is done by calculating the difference between the two predicted time series:

$$\epsilon = U_{WP} - U_{Matlab} \tag{6.20}$$

The VRM MCP method is not implemented in WindPRO. Therefor the implemented VRM method cannot be validated directly. However the linear regression and VRM MCP only differ on the established correlation. The data selection and the prediction are carried out in the same way as for the linear regression. Consequently, the validation of the MCP code partially applies to the VRM method.

Two validation cases are carried out using WindPRO and the Matlab code. The cases are listed in Table 6.1. The first case is performed using wind data from the Breezanddijk measurement site. The second case is carried out using wind data from the Høvsøre measurement site. In Fig. 6.5 the input for the MCP method is visualised.

Table 6.1: Validation cases

| **Case** | **Short-term data** | | **Long-term data** | |
|---|---|---|---|---|
| | **Data** | **Period** | **Data** | **Period** |
| 1. Breezanddijk | Lidar, $U_{75}$ | 01-Jul-'16 to 01-Feb-'17 | Mast, $U_{75}$ | 01-Jan-'16 to 01-Feb-'17 |
| 2. Høvsøre | Lidar, $U_{40}$ | 17-May-'11 to 04-May-'12 | Mast, $U_{40}$ | 01-Jun-'09 to 01-Jun-'16 |

Matlab and WindPRO have been used to set-up a linear relation between the target site and the reference site for 12 sectors of 30 degrees. Where the first sector is from 345 to 15 degrees, and the twelfth sector is from 315 to 345 degrees. The calculated linear relation for each sector can be found in Appendix E.

For the first case, the results from Matlab and WindPRO correspond well. The deviation between the slopes and intercepts is in the order of $10^{-5}$ or smaller for the twelve sectors. For the second validation case, the relations calculated in Matlab correspond with the relations calculated in WindPRO for ten out of the twelve sectors. For those sectors, the order of the deviation is similar to the one found for case 1. However, for sectors four and five, the difference in the results of the linear regression is larger. The order of the deviation goes up to $10^{-2}$, and the difference in intercept for sector five is even in the order of $10^{-1}$. Therefore it is expected to observe a difference in the predicted time series as well.

The second part of the validation is the comparison of the predicted time series. The difference between the predicted time series is calculated according to Eq. (6.20). As the output of the WindPRO MCP module is automatically rounded to two decimals, the minimum difference that can be found is 0.01 m/s. The result of the comparison is shown in Fig. 6.6. Note that the vertical axis has a logarithmic scale. It can be observed that for case 1, only at a few time steps a deviation in the order of 0.01 is present. For case 2, the distribution of the difference, $\epsilon$, is wider. From the comparison of the regression line per sector it is expected that the discrepancy is a result of the deviation in the slope and intercept for sectors four and five. Therefore the distribution of $\epsilon$ per sector is visualised in a whisker plot, see Fig. 6.7. The figure confirms the supposition that the deviation is caused by the difference in the linear relations used for the prediction.

Overall, the results of the validation indicate that the implemented MCP procedure works. The results from the Matlab MCP code and the WindPRO MCP module are the same for the major part of the predicted time series. In the remaining part, only a small difference between the predicted time series was found. The median of the difference is around 0.04 m/s and the maximum difference around 0.14 m/s.

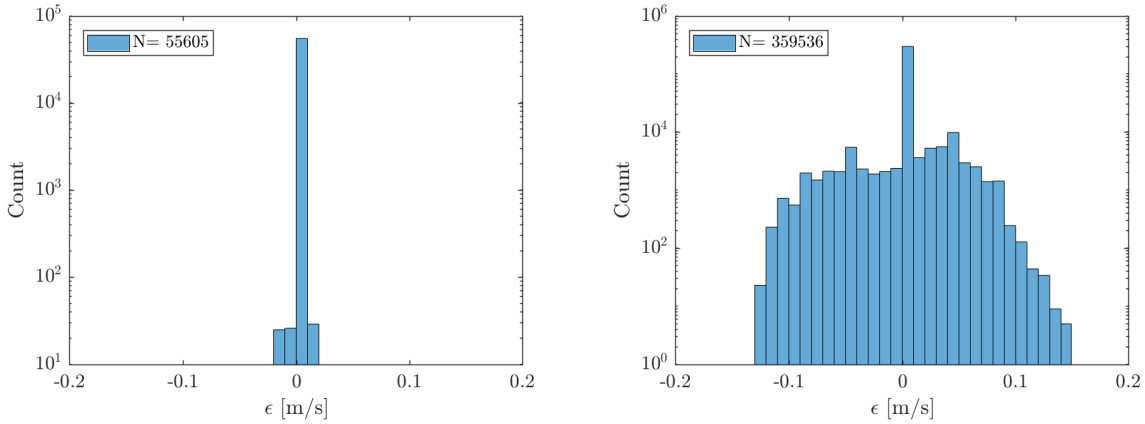


(a) 1. Breezanddijk (b) 2. Høvsøre

Figure 6.6: Histogram of the difference between the predicted time series from WindPRO and Matlab

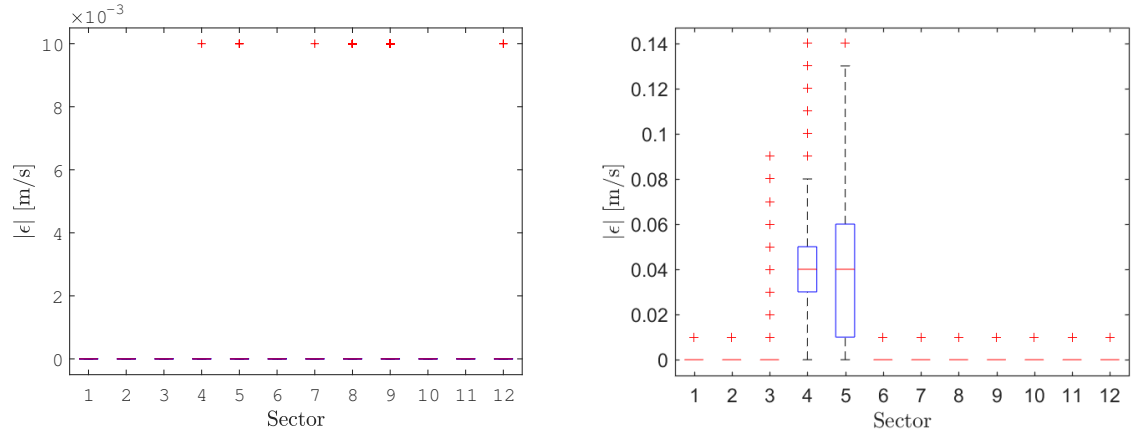


(a) 1. Breezanddijk (b) 2. Høvsøre

Figure 6.7: Box plots of the absolute value of the difference between time series of predicted wind speeds, $|\epsilon|$, per direction sector

# 7

# Application of the MCP Method to Shear Exponent Data

The measure-correlate-predict (MCP) method is applied to obtain wind statistics that represent a period longer than the sample period. In this chapter, the MCP method is tested in various cases to evaluate the performance and the usability of the MCP to extrapolate the short-term shear exponent data. A quantitative assessment of the performance of the MCP methods is made. Performance metrics have been defined to enable a quantitative evaluation. The performance metrics are explained in Section 7.1. Application of the MCP method to predict the wind shear exponent distribution, $P(\alpha)$, is discussed in detail in Section 7.2. Finally, in Section 7.3 an analysis is carried out to assess how good the MCP predictions are in general, and to determine the effect of shorter measurement periods on the result of the MCP prediction.

## 7.1. Performance metrics

To determine to what extent the shear exponent distribution at a target site can be predicted by the MCP method, it is required to have metrics that indicate the performance of the method. Better performance means that the MCP result is a more accurate prediction of the actual wind statistics at the target site and target height. In previous research on MCP methods, a variety of metrics has been used to evaluate to what extent the prediction represents the actual variable. For example, Lackner uses the RMSE and standard deviation of the percentage error [26, 27]. Dinler uses the coefficient of determination, $R^2$, and RMSE applied to the bins of the distributions [11]. Rogers used the Weibull distribution parameters, the normalised mean, and the chi-square goodness of fit test [34]. In addition to those, their research includes derived quantities as the AEP and the capacity factor, [11, 34]. Using derived quantities leads to an indirect comparison of the MCP results, but it shows the significance of the difference in the predictions.

The four performance metrics used to evaluate the MCP predictions in the present analysis are listed below. It has been decided to use three metrics that are directly comparing the predicted distribution with the actual long-term distribution. The fourth metric provides a comparison of the error in the predicted mean wind shear exponent predicted with and without lidar. The effect of the variable wind shear exponent on the AEP calculation is treated separately in Chapter 8.

**Metric 1 - Normalised mean**

The normalised mean indicates how far the predicted mean lies from the real mean, and shows if the MCP method is able to predict the real mean based on the short-term data. It is calculated by:

$$\tilde{\mu}_{\hat{\alpha}} = \frac{\mu_{\hat{\alpha}}}{\mu_{\alpha}} \tag{7.1}$$

In which $\mu\hat{\alpha}$ is the mean of the predicted distribution, and $\mu\alpha$ is the mean of the real long-term distribution.

**Metric 2 - Normalised standard deviation**
The normalised standard deviation is the factor between the real and the predicted standard deviation, calculated via:

$$\tilde{\sigma}_{\hat{\alpha}} = \frac{\sigma_{\hat{\alpha}}}{\sigma_{\alpha}} \tag{7.2}$$

In which $\sigma\hat{\alpha}$ is the standard deviation of the predicted distribution,$P(\hat{\alpha})$, and $\sigma\alpha$ is the standard deviation of the real long-term distribution. The standard deviation of the distribution can be regarded as a measure of the width of the distributions. This metric is calculated to assess whether the MCP method provides an accurate estimate of the width of the distribution.

**Metric 3 - Normalised chi-squared statistic**
The chi-squared goodness of fit test is used to compare the predicted shear exponent distribution with the real shear exponent distribution. The chi-squared goodness of fit test is given by:

$$\chi^2 = \sum_{i=1}^{M} \frac{(O_i - E_i)^2}{E_i} \tag{7.3}$$

In which $M$ is the number of bins, $i$ is the bin number, $O_i$ is the number of observations in bin $i$, and $E_i$ is the expected number of observations in bin $i$. When Eq. (7.3) is used to calculate the $\chi^2$, the outcome depends on the number of observations $N$. Therefore Eq. (7.3) cannot be used to compare samples that differ in sample size, e.g. a short-term observation and a long-term observation.

To make the outcome independent of the number of observations, $O_i$ and $E_i$ are normalised by the respective total number of observations $N_O$ and $N_E$:

$$\tilde{\chi}^2 = \sum_{i=1}^{M} \frac{(O_i/N_O - E_i/N_E)^2}{E_i/N_E} \tag{7.4}$$

The result is the normalised chi-squared statistic, it is equivalent to the chi-squared statistic using ratios instead of the number of observations per bin. An example of the calculation of performance metric $\tilde{\chi}^2$ is given in Table 7.1. In the example, the agreement between an observed and an expected distribution is evaluated. The samples have a different number of observations: The expected distribution is based on a sample of 1000 observations, and the observed sample consists of 100 observations. Figure 7.1 shows a visualisation of the samples. The example calculation of $\tilde{\chi}$ is given in Table 7.1.

Although the normalised chi-square statistic does not depend on the number of observations, it is emphasised that the normalised chi-squared statistic as defined in Eq. (7.4) depends on the bins. The bins used in the analysis of Sections 7.2 and 7.3 are ranging from $\alpha = -0.2$ to $\alpha = 0.6$, and have a width of $\Delta\alpha = 0.02$. From the bin definitions it becomes clear that the predictions also take into account the negative wind shear exponents. A remark on the inclusion of the negative shear exponents is made in the discussion of this chapter (see Section 7.3.4).

Table 7.1: Example calculation of the normalised chi-squared statistic, $\tilde{\chi}^2$

| **Bin Number** | **1** | | **2** | | **3** | | **4** | | **5** | |
|---|---|---|---|---|---|---|---|---|---|---|
| | **Exp** | **Obs** | **Exp** | **Obs** | **Exp** | **Obs** | **Exp** | **Obs** | **Exp** | **Obs** |
| **Count** | 218 | 24 | 422 | 40 | 259 | 23 | 77 | 12 | 24 | 1 |
| **Probability** | 0.22 | 0.24 | 0.42 | 0.40 | 0.26 | 0.23 | 0.08 | 0.12 | 0.02 | 0.01 |
| $\frac{(O_i/N_O - E_i/N_E)^2}{E_i/N_E}$ | 0.0022 | | 0.0011 | | 0.0032 | | 0.0240 | | 0.0082 | |
| **Result** | $\tilde{\chi}^2 = \sum_{i=1}^{M} \frac{(O_i/N_O - E_i/N_E)^2}{E_i/N_E} = 0.039$ | | | | | | | | | |

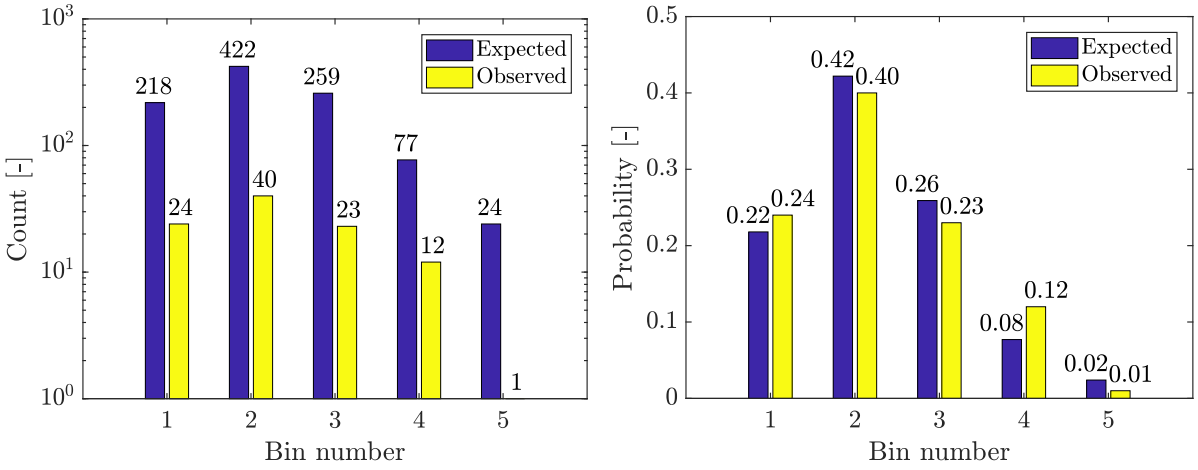


(a) Count per bin

(b) probability

Figure 7.1: Input for the example calculation of the normalised chi-squared statistic, $\tilde{\chi}^2$

**Metric 4 - Normalised error of the predicted mean**

The fourth performance metric is introduced to evaluate the advantage of the lidar in the estimation of the mean wind shear exponent. When no lidar is available, the best estimate of the mean wind shear exponent, is the mean wind shear exponent derived from the mast measurements: $\mu_{\alpha_{M,LT}}$, where the subscript $M, LT$ indicates that it is the wind shear exponent derived from the long-term mast measurement. However, as shown in Chapter 5, the mean wind shear exponent over a greater vertical distance ($\mu_{\alpha_{true,LT}}$) is often smaller than the $\mu_{\alpha_{M,LT}}$. Because of the difference, an error is introduced. This error is notated here as:

$$\epsilon_M = \mu_{\alpha_{M,LT}} - \mu_{\alpha_{true,LT}} \tag{7.5}$$

If a lidar is employed at the measurement site for a short period of time, the estimate of the wind shear exponent can be assisted by measurements above the measurement mast height, e.g. using the MCP approach. This results in a new estimate of the mean wind shear exponent: $\mu\hat{\alpha}$. The new estimate still deviates from the true mean wind shear exponent by the error:

$$\epsilon_L = \mu_{\hat{\alpha}} - \mu_{\alpha_{true,LT}} \tag{7.6}$$

Comparison the error of the case in which a lidar is employed, $\epsilon_L$, and the case in which only a mast is used,$\epsilon_M$, is done by taking the ratio of the errors:

$$\tilde{\epsilon} = \frac{\epsilon_L}{|\epsilon_M|} = \frac{\mu_{\hat{\alpha}} - \mu_{\alpha_{true,LT}}}{|\epsilon_M|} \tag{7.7}$$

This fourth error metric is called the normalised error of the mean, and it indicates the advantage of the new approach using lidar and MCP over the old situation in which only a mast was available. Obviously, an $\tilde{\epsilon}$ in the range of -1 to 1, means that the application of lidar and MCP resulted in a reduced error. Although the $\tilde{\epsilon}$ is closely related to the $\tilde{\mu}$, it is added, since $\tilde{\epsilon}$ includes the comparison with the old situation.

As a major part of the applications of the wind shear exponent are solely using the mean wind shear exponent, $\tilde{\epsilon}$ is particularly relevant. Additionally, $\epsilon_L$ will be used in Chapter 8 for the propagation of uncertainty in the wind shear exponent to the uncertainty in AEP.

## 7.2. Prediction of the wind shear exponent using MCP

Two MCP cases are presented in this section to demonstrate the performance of the MCP method applied to wind shear exponent data. The cases show the application of the MCP method to a 90-day lidar measurement at Høvsøre. The lidar measures the shear over a height range from 40 to 160 m. Subsequently, the MCP method and met mast data are used to extrapolate the 90 day measurement to obtain the long-term shear exponent distribution. The reference data is the wind shear exponent from 40 m to 100 m, measured at the mast.

To assess the quality of the prediction, the prediction is compared with the long-term shear distribution at the obtained from the me which include measurements at the same heights. The metrics discussed in the previous section are used to compare the performance of the implemented MCP methods.

It should be noted that in this section, the performance is evaluated based on the combined result of four direction sectors. This was chosen in order to show the full MCP procedure, so including the correlations per wind direction sectors.

### 7.2.1. Case 1

In Fig. 7.2 the input signals of the MCP procedure are shown. The reference data is eight years of data. The lidar data is measured in a period from 2011-05-17 to 2011-08-15. In Fig. 7.4 the shear exponent distribution, $P(\alpha)$ corresponding to the input is provided. It stands out that the measurement includes mainly lower shear exponents, which corresponds to the fact that the sample period falls in the summer season.

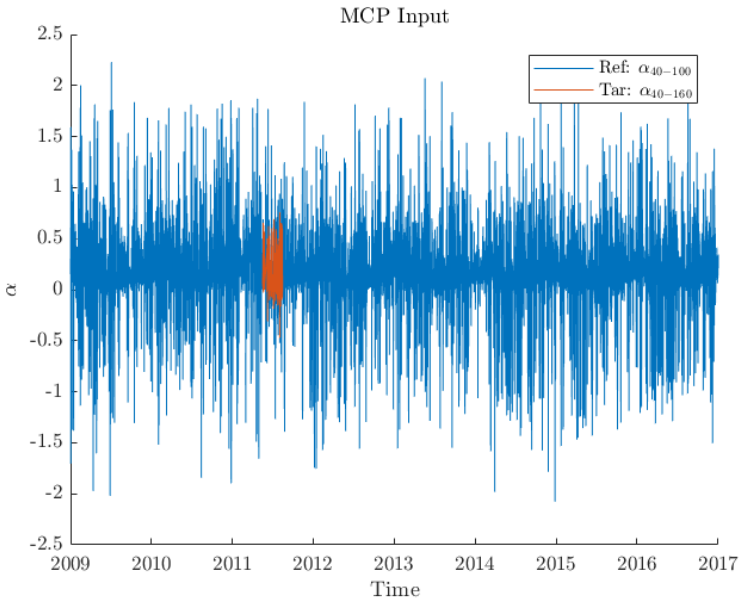


Figure 7.2: Input for the first MCP case. The blue time series is the low shear exponent derived from met mast measurements. The red time series is the high shear exponent derived from the lidar measurement and has a length of 90 days in total (2011-05-17 to 2011-08-15

The input signal is used to establish the MCP correlations. Only 4 direction sectors are used, because in this prediction the directions are limited to the eastern and western direction sector as defined in Section 3.2. The correlations are shown in Fig. 7.3.

The figure shows that there is a significant difference in the number of data points per sector. This is in accordance with the wind rose shown in Fig. 3.4. All sectors include sufficient data for calculation of the correlation. The plots also show the weights assigned to the individual data points. The colour of the data points corresponds with the colour scale on the right side of the plot. Comparison of the four correlations shows that the LR method results in linear relations that have lower slopes and higher intercepts.

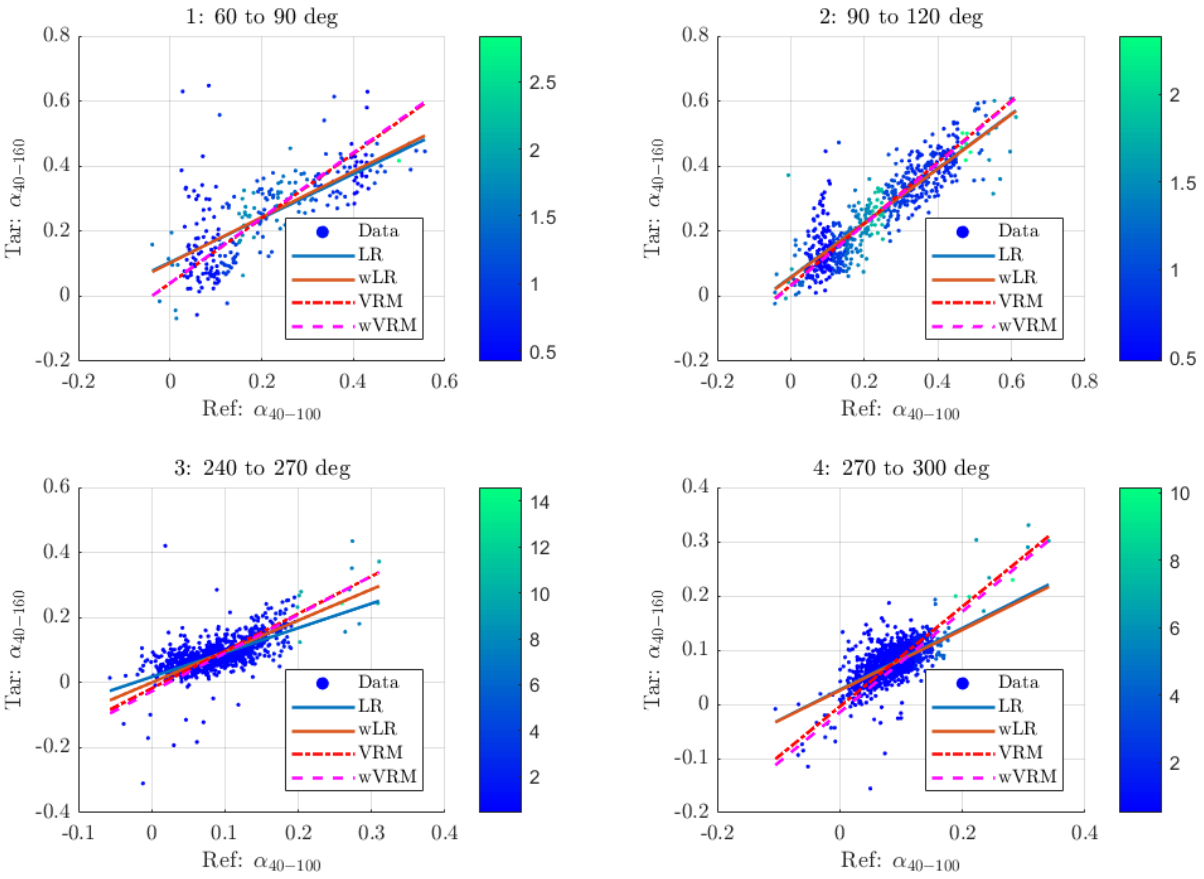


Figure 7.3: Correlations for the first MCP case. The colours of the data points are showing the weights assigned to the individual points. The weights are used for the wLR and wVRM method.

In Fig. 7.4, the predicted distributions are plotted together with the actual measured long-term distribution of $\alpha_{40-160}$. It has to be noted that the discussed result is the combined $P(\alpha)$ of the four direction sectors.

It is observed that all four predictions predicted the mode of the distribution at the same location: $\alpha = 0.1$. However the predicted $P(\alpha)$ differs. Linear regression clearly overestimates the probability corresponding to the mode. Further, all predictions have resulted in underestimations of the probability of the shear exponents in the range of 0 to 0.1.

A second difference is found for shear exponents in the range of 0.15 to 0.25. In this range both the LR and wLR method overestimate the probability, whereas the prediction of the VRM and wVRM method are very accurate. In the tail of the distribution, the VRM and wVRM methods overestimate the probability, and the LR methods seem to be more accurate.

These observations are resembled in the metrics shown in Table 7.2. All methods overestimate the mean of the distribution. The methods based on LR result in the best estimates of the mean in this case. The standard deviation of the distribution is overestimated by the VRM and wVRM method, but underestimated by the LR and wLR methods. The normalised error of the predicted mean wind shear exponent is very high. This is caused by a very small $\epsilon_M$. Probably the effect of assessing the four direction sectors at once, also plays a role. A longer concurrent measurement time is probably needed to improve the estimates. This is discussed in Section 7.3.

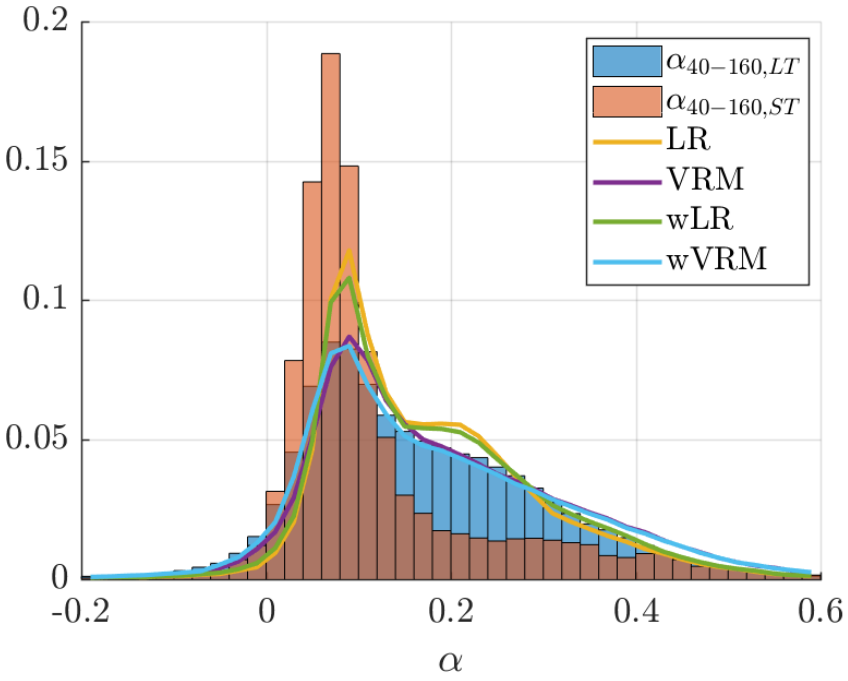


Figure 7.4: Result for the first MCP case. The lines show the four MCP predictions. The blue histogram shows the real long-term distribution obtained from the mast measurement ($\alpha_{40-160,LT}$). The red histogram corresponds to the distribution of the short-term sample, the MCP input ($\alpha_{40-160,ST}$).

Table 7.2: Performance metrics for case 1

| | LR | wLR | VRM | wVRM | ST itself |
|---|---|---|---|---|---|
| **Normalised mean**, $\tilde{\mu}_{\hat{\alpha}}$ | 1.06 | 1.09 | 1.16 | 1.13 | 0.75 |
| **Normalised std**, $\tilde{\sigma}_{\hat{\alpha}}$ | 0.86 | 0.90 | 1.10 | 1.12 | 0.77 |
| **Normalised Chi-squared statistic**, $\tilde{\chi}^2$ | 0.085 | 0.059 | 0.048 | 0.032 | 0.435 |
| **Normalised error statistic**, $\tilde{\epsilon}$ | 18.8 | 45.5 | 25.3 | 37.8 | 73.3 |

### 7.2.2. Case 2

The second case is similar to the first one. The difference is that the 90-day lidar measurement is made during a different season. The lidar data comes from the months January, February and March. Figure 7.5 shows the input for the second case. The stable conditions of the winter months cause that the distribution of the input time series includes a lot of high shear exponents relative to the long-term distribution.

The MCP correlations established for this case are shown in Fig. 7.6. Direction sector four stands out, because the scatter plot contains anomalous data points. These points have a significant influence on the correlation. Ideally, this data is removed from the data set. Instead of removing the data, a similar effect is accomplished by assigning low weights to the particular data points. It is observed that the weighting greatly enhances the correlation established by the VRM. This indicates that the wVRM could be more robust than the unweighted method.

The result of the second MCP execution is shown in Fig. 7.7. In this case, significant differences between the distributions are found. The prediction by the VRM stands out because of the large difference between the predictions and the actual distribution for negative shear exponents. This is a result from the correlation in the fourth direction sector. The intercept of this correlation is too low and the predicted distribution is located too far to the left in Fig. 7.7. The wVRM offers an improvement over the VRM and better resembles the shape of the actual distribution. However, both the LR and wLR method overestimate the probability of the mode, resulting in a high $\tilde{\chi}^2$.

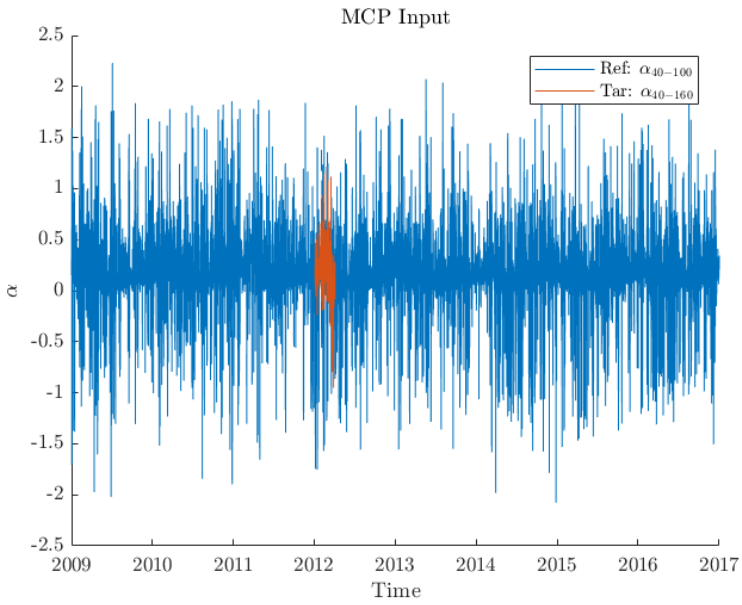


Figure 7.5: Input for the second MCP case. The blue time series is the low shear exponent derived from met mast measurements. The red time series is the high shear exponent derived from the lidar measurement and has a length of 90 days in total (2011-05-17 to 2011-08-15

In Table 7.3 the performance metrics are shown. All methods except VRM overestimate the mean. Furthermore it is observed that the weighted methods are more accurate than the VRM and LR method. The improvement by the weighted methods was expected due to the anomalous data in the fourth direction sector.

A remarkable result is that the LR method results in a better estimate of the standard deviation than the VRM method. This result is opposite of the expectation and is attributed to the large standard deviation of the short-term distribution, $P(\alpha_{40-160} - ST)$. The standard deviation predicted by the VRM method is higher than the standard deviation predicted by the LR methods, which is in accordance with the theory.

Regarding $\tilde{\chi}^2$, the distribution predicted by the wVRM is best in agreement with the real long-term $\alpha_{40-160}$ distribution. As observed from the figure, the distribution predicted by the VRM method deviates the most from the actual distribution, resulting in the largest $\tilde{\chi}^2$. As for the first case, the $\tilde{\epsilon}$ is very high, implying that the error in the estimate is larger than the error resulting from the case without lidar, $\epsilon_M$. This is caused by the effect of calculating the performance metrics for the sum of the sectors.

Table 7.3: Performance metrics for case 2

| | LR | wLR | VRM | wVRM | ST itself |
|---|---|---|---|---|---|
| **Normalised mean**, $\tilde{\mu}_{\hat{\alpha}}$ | 1.11 | 1.08 | 0.62 | 1.03 | 1.35 |
| **Normalised std**, $\tilde{\sigma}_{\hat{\alpha}}$ | 0.89 | 0.92 | 1.59 | 1.16 | 1.00 |
| **Normalised chi-squared statistic**, $\tilde{\chi}^2$ | 0.251 | 0.129 | 1.800 | 0.069 | .435 |
| **Normalised error statistic**, $\tilde{\epsilon}$ | 31.5 | 110.3 | 24.2 | 9.05 | 103.3 |

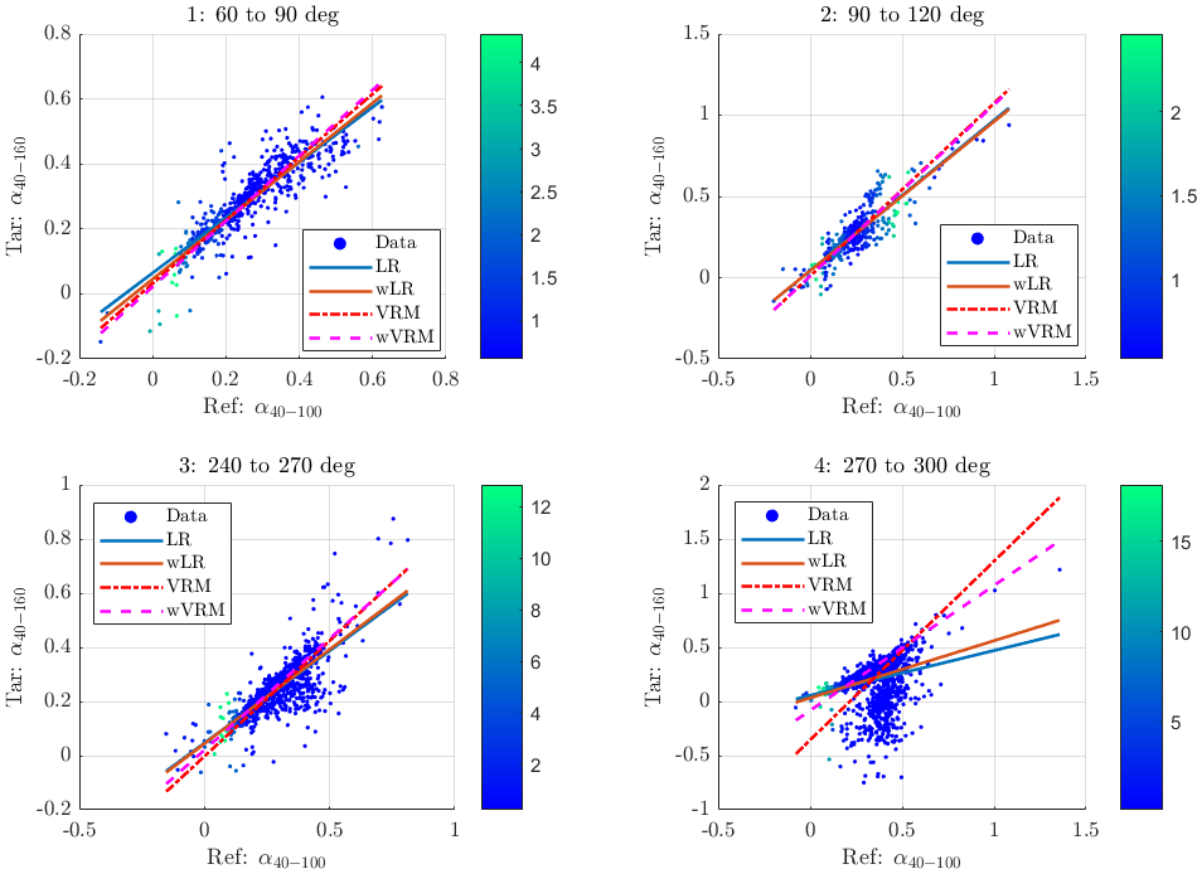


Figure 7.6: Correlations for the second MCP case. The colors of the data points are showing the weights assigned to the individual points. The weights are used for the wLR and wMCP method.

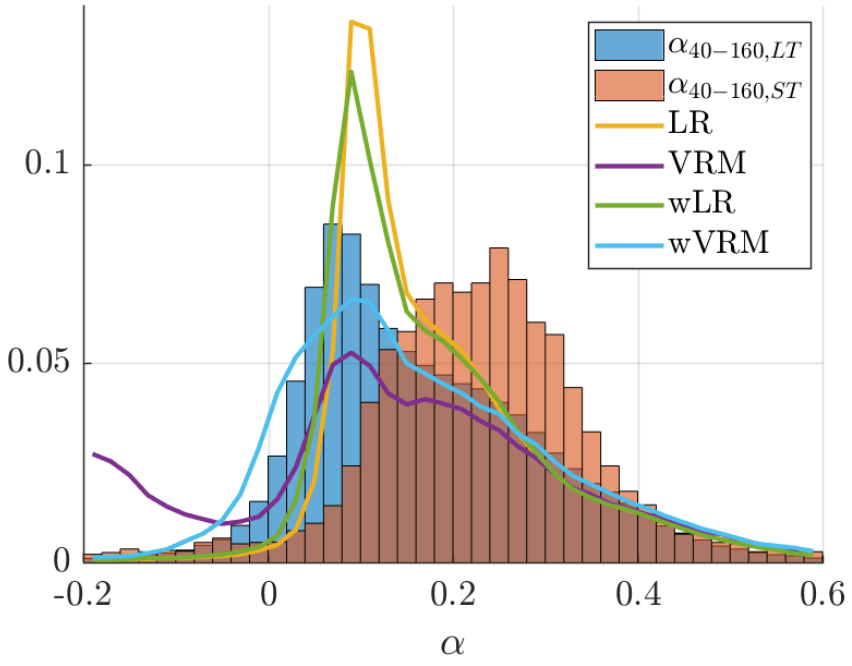


Figure 7.7: Result for the second MCP case. The lines show the four MCP predictions. The histograms show the real long-term distribution obtained from the mast measurement ($\alpha_{40-160}LT$) and the distribution corresponding to the short-term, the MCP input ($\alpha_{40-160}ST$)

## 7.3. Effect of shorter concurrent measurement period

The cases shown in the previous section demonstrate that the implemented MCP methods can correct the measured distribution for the long-term. However, a new question arises: how good are the MCP predictions in general? Whether the MCP is useful in the shear exponent extrapolation or not cannot be based on two cases only. Therefore the MCP is applied in additional, randomly chosen cases. This analysis is combined with the study of the effect of the concurrent measurement time (expressed as $t_C$).

Ideally, multiple years of data should be available to study the effect of reducing the concurrent measurement period on the MCP result. Accordingly, the MCP result can be compared with a real long-term data set and multiple sample periods can be used as MCP input to check the variability in the MCP result due to different input periods. For this reason, measurement data from a tall mast at Høvsøre is used. At Høvsøre at least eight years of data is available for the analysis. Therefore the variability in the MCP result can be tested even for longer periods, e.g. a year, and the outcome of the MCP can be compared with a real long-term measurement.

At Breezanddijk only one and a half year of lidar data is available, so there is only few non-overlapping input for the MCP and there is not an appropriate long-term reference. However, the data set from Breezanddijk is suitable for testing to what extent a lidar measurement of a couple of months can be used to predict the yearly wind shear above the met mast height. Although one and a half year of data is available, only one year of data is used. This is done to ensure that there is no bias due to the seasonality of the data set.

### 7.3.1. Method

The approach used in this analysis is illustrated in the flow chart of Fig. 7.8. Below the figure, the six steps are elaborated on. The third step requires extra attention, as there is a small difference between the approach used for the Breezanddijk case and the approach used for the Høvsøre case.

1. **Define sample period lengths**
   At first the sample period lengths are defined. It was chosen to take steps of 30 days up to 360 days. In this way the added value of every extra measurement month is assessed.

2. **Define measurement periods**
   The measurement periods make up the ensemble for the specific concurrent measurement length. The approach of defining the measurement periods is different for Breezanddijk than for Høvsøre.

   Data of consecutive months is used to simulate that a lidar has been measuring the data during one specific period. In order not to change the effect of the seasonality in the samples, the sampling at Breezanddijk is ”circular”, meaning that the end of the data set is extended using the beginning of the data set. For example, if a period with a length of 3 months is starting in December, January and February of the same year are used to complete the sample. For the Høvsøre data set, this type of ”circular” sampling has not been implemented as multiple years of data are available.

   The second difference is the selection of the start dates of the samples. For the Høvsøre case, 100 random dates are sampled. For Breezanddijk, 12 start dates of the sample periods are evenly distributed over the year, minimising the overlap between the sample periods. This different approach was chosen because of the small data set.

3. **Execution of MCP procedure for each sample period**
   For each sample period the four MCP methods are executed to extrapolate the sample period to a long-term data set.

4. **Calculation of performance metrics**
   For each MCP result the performance metrics are calculated. The metrics are the normalised mean, normalised standard deviation, the normalised chi-squared statistic, and the normalised error of the mean. Additionally, the same metrics are calculated based on the ”ST data itself”. This shows the outcome of the case in which MCP is not applied, but in which the ST data is taken as representative for the long-term.

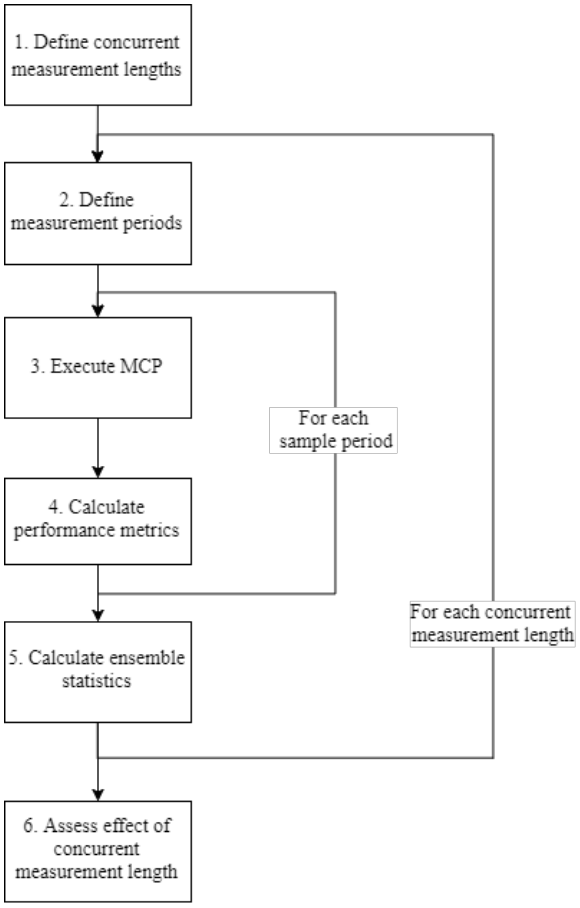


Figure 7.8: Flowchart of the procedure used to assess the effect of the length of the measurement period. The flowchart shows the two loops that are used in the analysis.

5. **Calculation of ensemble statistics over the result**
   Two statistics are calculated for the ensemble corresponding to a specific data length: the ensemble mean and ensemble standard deviation. These statistics are calculated to assess how good the prediction of the MCP method is in general. The ensemble mean provides the bias of the prediction. The ensemble standard deviation should be viewed as an indication of the uncertainty. It shows the variability of the predictions due to the difference in the input periods.

6. **Assessment of ensemble statistics as function of measurement time**
   The ensemble statistics are plotted as function of the length of the concurrent measurement period, $t_C$ to evaluate how $t_C$ influences the performance of the MCP method.

The metrics calculated from the short-term data itself are added to some of the resulting plots to see how the MCP results compares with the uncorrected short-term sample. In principle, any MCP method should provide a more accurate prediction of the real long-term statistics than the short-term data itself [11].

Before moving to the results of the analysis, a remark on the notation is made. The mean and standard deviation of the individual predictions are referred to using $\mu$ and $\sigma$. When discussing ensemble statistics, angle brackets are used to notate the mean and standard deviation, i.e. $\langle x \rangle$ and, $([x - \langle x \rangle]^2)^{\frac{1}{2}}$.

### 7.3.2. Result Breezanddijk

In the first case, the distribution of $\alpha_{40-120}$ of direction sector 3 is predicted (see Section 3.2 for description of the sector). This shear exponent could be required to vertically extrapolate the wind speeds measured at mast height to the hub height of a wind turbine. The ensemble mean of the first metric is shown in Fig. 7.9. It stands out that $\langle \mu_{\hat{\alpha}} \rangle$ is in the order of 1 % for the MCP predictions. The ensemble mean is close to the real mean because the ensemble includes all periods. Due to seasonality, the correlation between the target and reference data varies. This leads to both overpredictions and underpredictions and it is expected that the ensemble mean will be close to the one-year mean.

Comparing the performance of the four MCP method, it can be concluded that the bias of the weighted methods is smaller than the bias of the unweighted methods. Further, it seems that the VRM method benefits more from the weighting than the LR method, but the differences are small. As explained in the method, the Breezanddijk ensemble contains 12 evenly distributed samples for each $t_C$. This implies that all the data is present in the ensemble and one may expect that the ensemble mean of the "ST data" is equal to the one-year mean. However, the individual means in the ensemble are not weighted with the amount of data in the sample month, so a difference exists. When the sample length becomes 12 months, all the data is present in the individual samples, and the exact one-year mean is found.

The scatter plot, which is not included, has shown that the individual $\tilde{\mu}_{\hat{\alpha}}$ of the ensemble are approximately normally distributed. Both overpredictions and underpredictions appear in the ensemble. The ensemble standard deviation of $\tilde{\mu}_{\hat{\alpha}}$ as a function of $t_C$ is given in Fig. 7.10.

This ensemble standard deviation indicates the uncertainty in the predicted mean. The standard deviation of the normalised mean that results from the ST data itself is not shown, as it is much larger than the standard deviation in the MCP results, e.g. the standard deviation of $\mu_{\hat{\alpha}}/\mu\alpha$ is 0.28 for a $t_C$ of 6 months. This is over ten times the value of the VRM method, which is 0.02. The significant difference proofs the advantage of applying the MCP method.

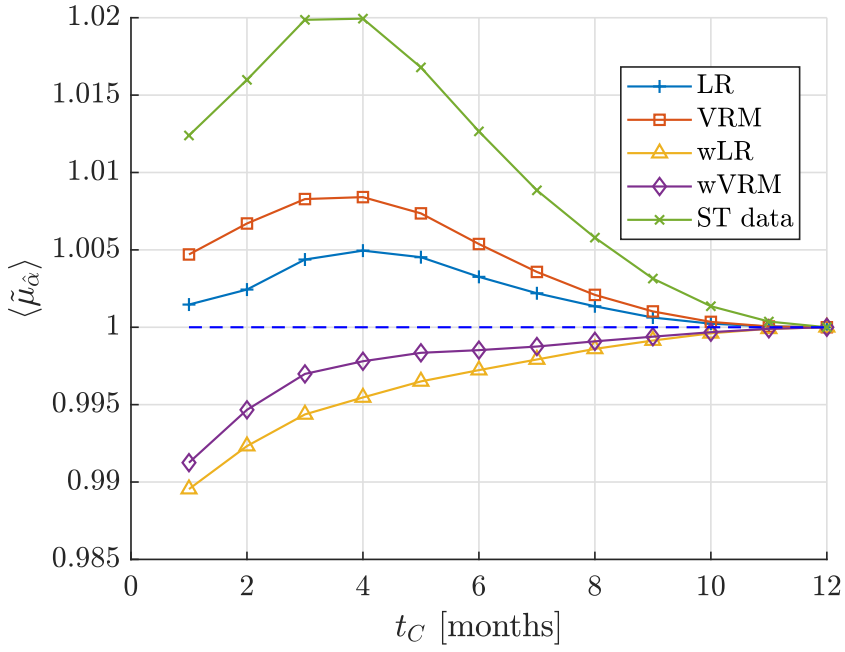


Figure 7.9: Ensemble mean of $\tilde{\mu}_{\hat{\alpha}}$ as a function of concurrent measurement time for Breezanddijk sector 3.

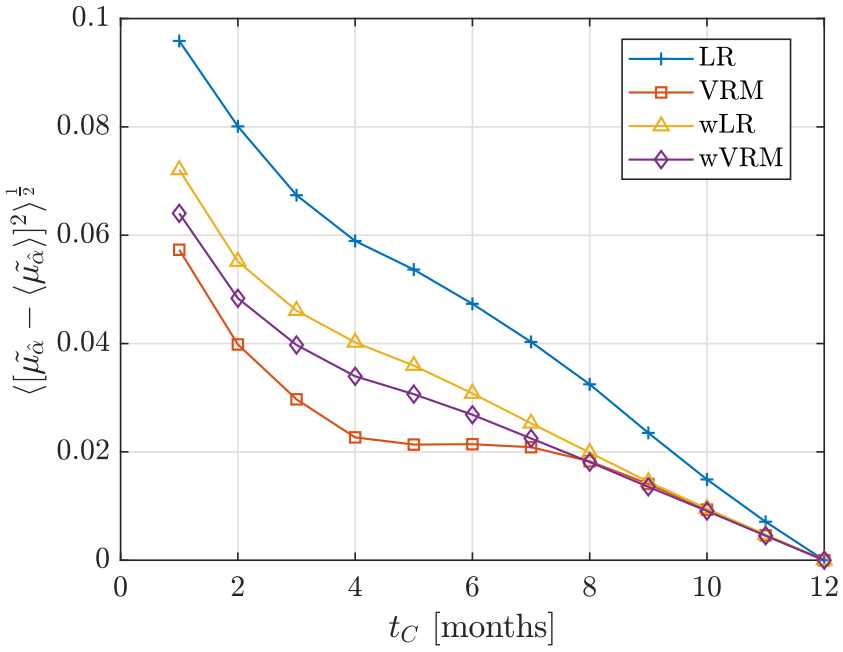


Figure 7.10: Ensemble standard deviation of $\tilde{\mu}_{\hat{\alpha}}$ as a function of concurrent measurement time for Breezanddijk sector 3.

The ensemble mean and ensemble standard deviation of $\tilde{\sigma}_{\hat{\alpha}}$ are shown in Figs. 7.11 and 7.12. Linear regression underestimates the standard deviation of the long-term distribution by 10%. Further, it is observed that the weighted methods result in higher $\sigma_{\hat{\alpha}}$ for this case. The addition of the weights does not result in a better estimation of the $\sigma_{\alpha}$ for the VRM method. The weighting increased the bias in the estimation. Regarding the LR method, the weighting does not significantly change the prediction. If the short-term data is used without the application of MCP, one needs to measure at least 10 months to find the yearly $\sigma_{\alpha}$. It stands out that increasing the length of the measurement period from 7 to 8 months improves the estimate significantly more than an increasing the measurement period from 9 to 10 month.

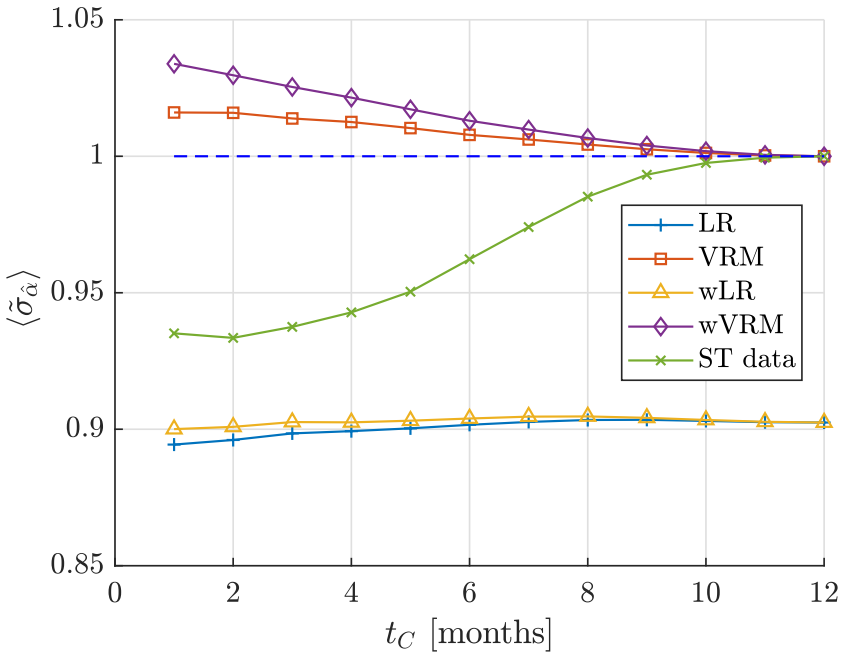


Figure 7.11: Ensemble mean of $\tilde{\sigma}_{\hat{\alpha}}$ as a function of concurrent measurement time for Breezanddijk sector 3.

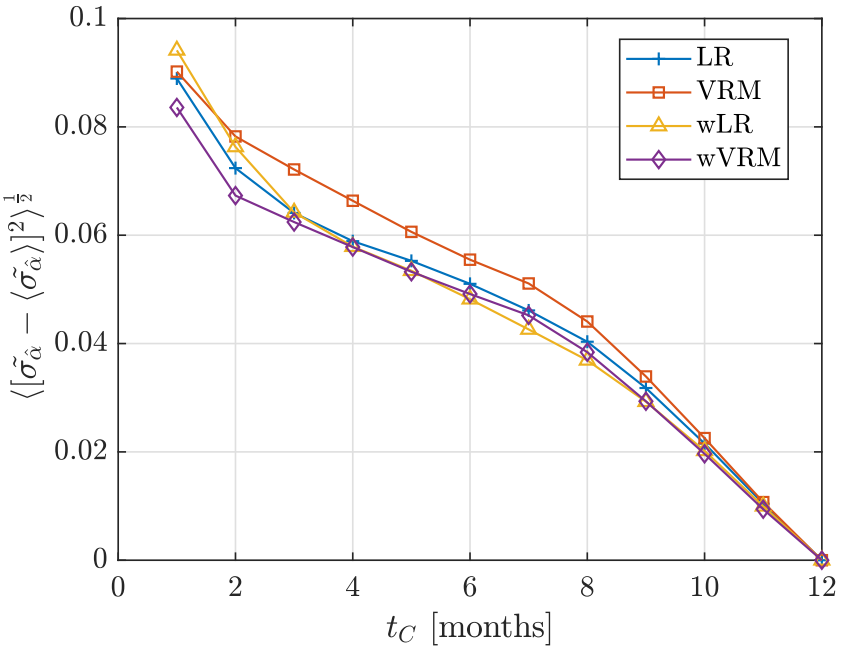


Figure 7.12: Ensemble standard deviation of $\tilde{\sigma}_{\hat{\alpha}}$ as a function of concurrent measurement time for Breezanddijk sector 3.

In order to evaluate the agreement between the predicted distributions and the measured long-term distribution, the ensemble mean of the chi-squared metric is provided in Fig. 7.13. It is observed that the distributions predicted by the VRM methods are consistently better than the ones predicted by linear regression.

The chi-squared metric that compares the short-term distribution with the long-term distribution is also plotted in Fig. 7.13. It shows that the agreement between the one-year distribution and the ST data is better than the agreement between the one-year distribution and the prediction by the LR method for a $t_C$ of 9 months, and the VRM methods for a $t_C$ of 10 months. So in this particular case, in which the yearly distribution is estimated, the estimation mostly benefits from the MCP application for a $t_C$ shorter than 9 months.

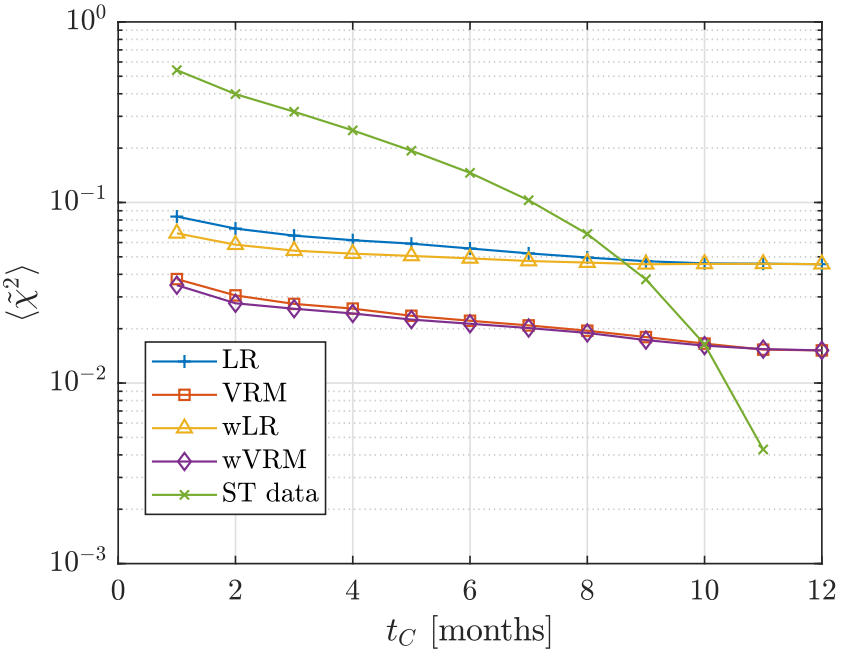


Figure 7.13: Ensemble mean of $\tilde{\chi}^2$ as a function of concurrent measurement time for Breezanddijk sector 3.

Lastly, the ensemble statistics of the normalised error in the predicted mean, $\tilde{\epsilon}$, is shown in Figs. 7.14 and 7.15. Although it is expected that the predictions are unbiased, the plot of the ensemble mean shows that a bias exists. The bias is largest for a $t_C$ of one month. There it is around 0.06. The bias decreases for increasing $t_C$.

The ensemble standard deviation of the normalised error is smaller than 1. The majority of the individual $\tilde{\epsilon}$ is smaller than 1, which means that the application of short-term lidar data and MCP reduces the error. The best result is obtained using the VRM, e.g. 1 month of lidar data decreases the error by more than 50%, and 4 months of lidar data reduces the error by more than 85% with respect to the $\epsilon_M$. Further, it is observed that the weighting only improves the LR method. The wVRM is not better than the VRM.

The reduction of the error can also be supported by the calculation of the mean absolute deviation of $\tilde{\epsilon}$. This calculation is not shown here, as it is closely related to the ensemble standard deviation, shown in Fig. 7.15.

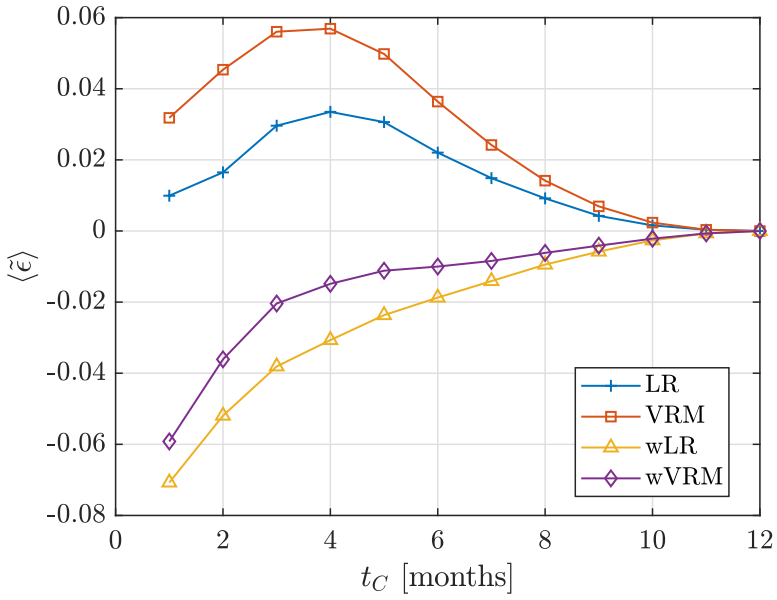


Figure 7.14: Ensemble mean of $\tilde{\epsilon}$ as a function of concurrent measurement time for Breezanddijk sector 3.

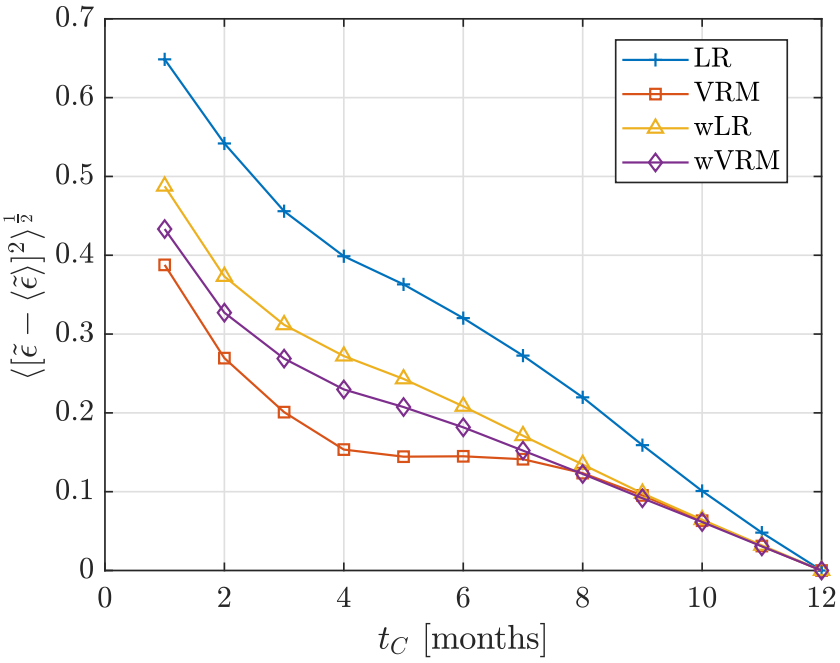


Figure 7.15: Ensemble standard deviation of $\tilde{\epsilon}$ as a function of concurrent measurement time for Breezanddijk sector 3.

### 7.3.3. Results Høvsøre

The long-term shear exponent distribution, $P(\alpha_{40-160})$ of a 30-degree sector centred at 270 degrees, is predicted using short-term measurements of $\alpha_{40-160}$ and the MCP method. The short-term measurements represent lidar measurements, although they originate from the mast. The reference data in this MCP prediction is the time series of the shear exponent $\alpha_{40-100}$.

As described in Section 7.3.1, the MCP method is executed 100 times per ensemble. As eight years of data are available, inter-annual variability of the shear exponent is now included in the predictions, and the performance metrics will not converge like the performance metrics of the Breezanddijk case. Chapter 5 has shown that the mean shear exponent varies on a yearly scale as well, so the inter-annual variability is expected to affect the predictions.

The ensemble mean of $\tilde{\mu_{\hat{\alpha}}}$ is shown in Fig. 7.16. Comparing the performance of the four MCP methods shows that the linear regression seems to be better at predicting the mean for a $t_C$ below 6 months. The ensemble mean corresponding to the data itself is oscillating due to the variability in the random samples. Further, the weighting appears to be an improvement. Especially for the measurement periods shorter than 6 months.

Fig. 7.17 shows the ensemble standard deviation of $\tilde{\mu}\hat{\alpha}$. An interesting difference with the previous case is, that VRM results in the largest ensemble standard deviation, whereas in the Breezanddijk case it resulted in the lowest ensemble standard deviation. The differences between are in the order of 0.01

The ensemble standard deviation corresponding to the ST data itself is not shown, as it is much larger and falls outside this plot, e.g. for a $t_C$ of 6 months, the ensemble standard deviation is 0.22 and for $t_C$ equal to 12 months, it is 0.10. This difference illustrates the benefit of the MCP. The application of the MCP method reduces the uncertainty in the prediction of the long-term mean. When measuring a full year, the ensemble deviation reduces to approximately 3%, which is the variation due to inter-annual variability.

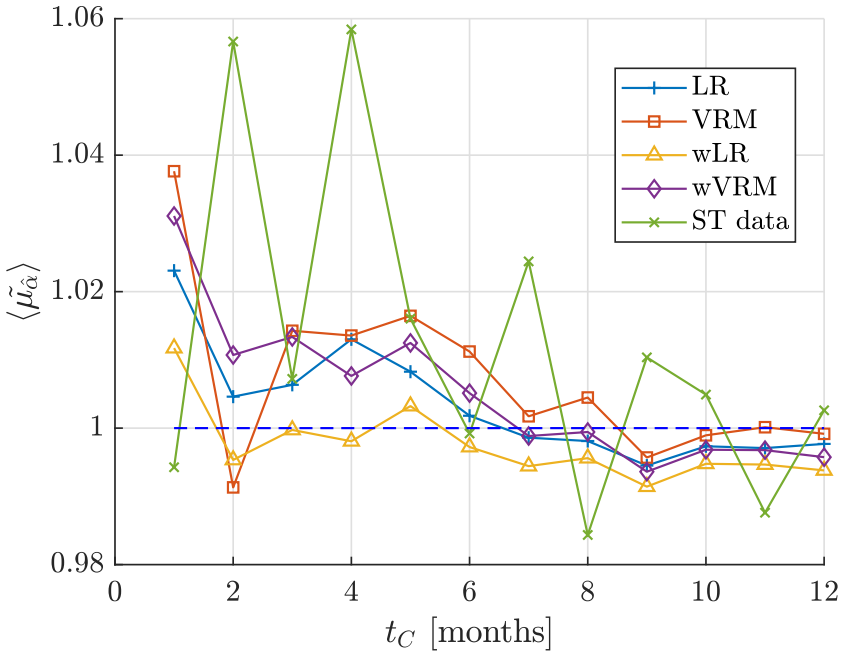


Figure 7.16: Ensemble mean of $\tilde{\mu}_{\hat{\alpha}}$ as a function of concurrent measurement time for the western sector at Høvsøre.

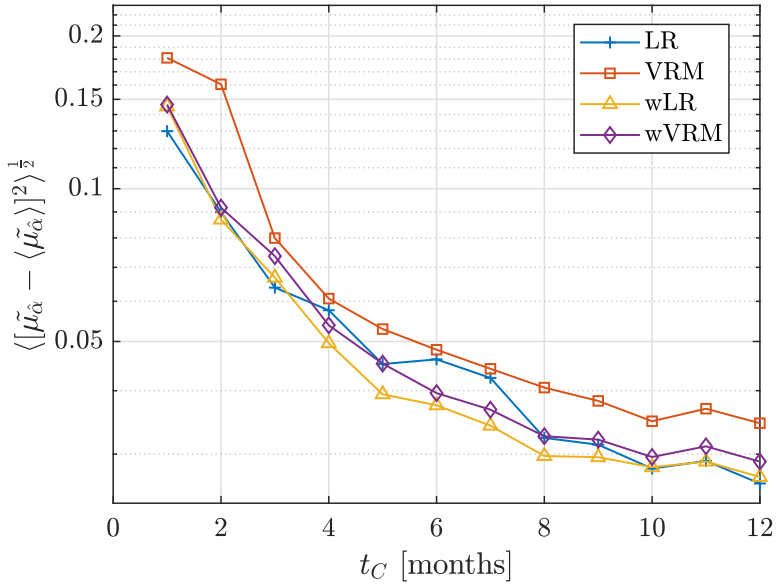


Figure 7.17: Ensemble standard deviation of $\tilde{\mu}_{\hat{\alpha}}$ as function of concurrent measurement time for the western sector at Høvsøre.

From Fig. 7.18 it is observed that one needs to measure at least 9 months to reduce the bias in the prediction of $\sigma_\alpha$ when VRM MCP is used. As explained in Appendix B, linear regression MCP is not able to predict the $\sigma\alpha$ without a negative bias.

As for the first case, Fig. 7.18 can be used to estimate the minimum measurement length if MCP would not be applied. According to the result, at least 10 months of measurement time are required to reduce the bias to approximately 1%. Although an estimate of the long-term $\sigma_\alpha$ may be found without applying MCP, the uncertainty of this estimate is higher. This can be observed from the ensemble standard deviation of $\tilde{\sigma}_{\hat{\alpha}}$, shown in Fig. 7.19.

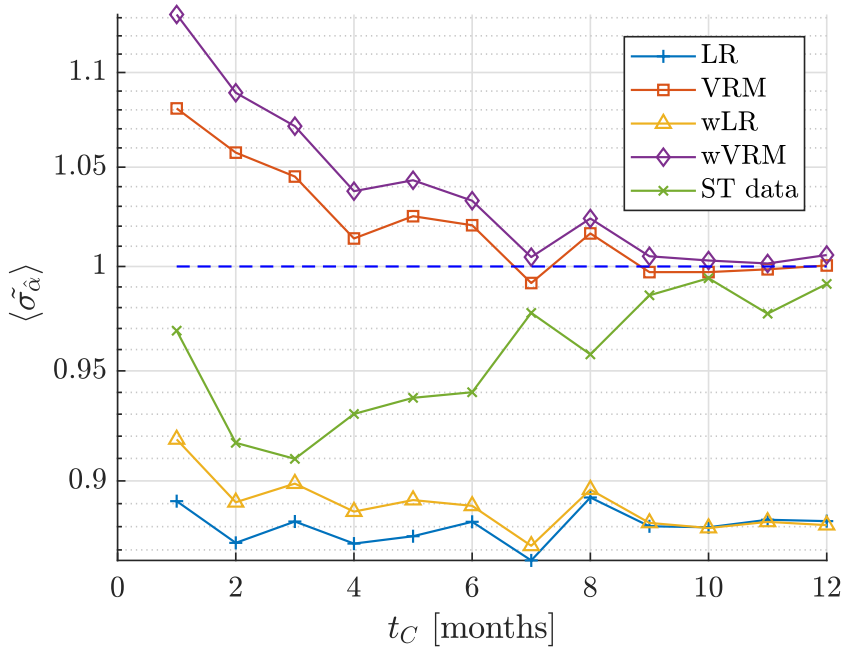


Figure 7.18: Ensemble mean of $\tilde{\sigma}_{\hat{\alpha}}$ as a function of concurrent measurement time for the western sector at Høvsøre.

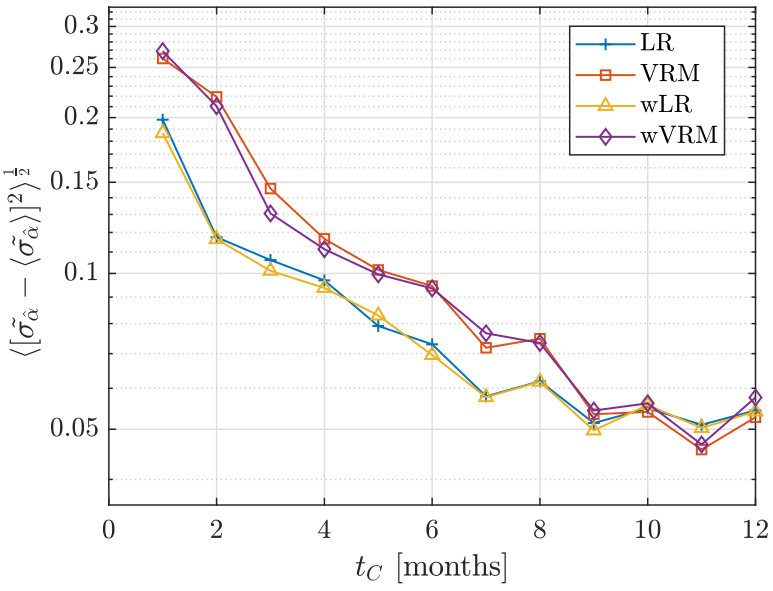


Figure 7.19: Ensemble standard deviation of $\tilde{\sigma}_{\hat{\alpha}}$ as a function of concurrent measurement time for the western sector at Høvsøre

The ensemble mean of the chi-squared statistic is plotted in Fig. 7.20. The VRM gives the best predictions. It stands out that the $\langle\tilde{\chi}^2\rangle$ does not reduce after a $t_C$ of 9 months. A remarkable difference with the Breezanddijk case is that the ST data plot does not surpass the MCP methods in this figure. This is explained by the inter-annual variability, which was already observed in Fig. 5.3. The inter-annual variability cannot be accounted for in the predictions by the ST data only, but is included in the MCP prediction. It confirms that the prediction of the long-term distribution benefits from the MCP application.

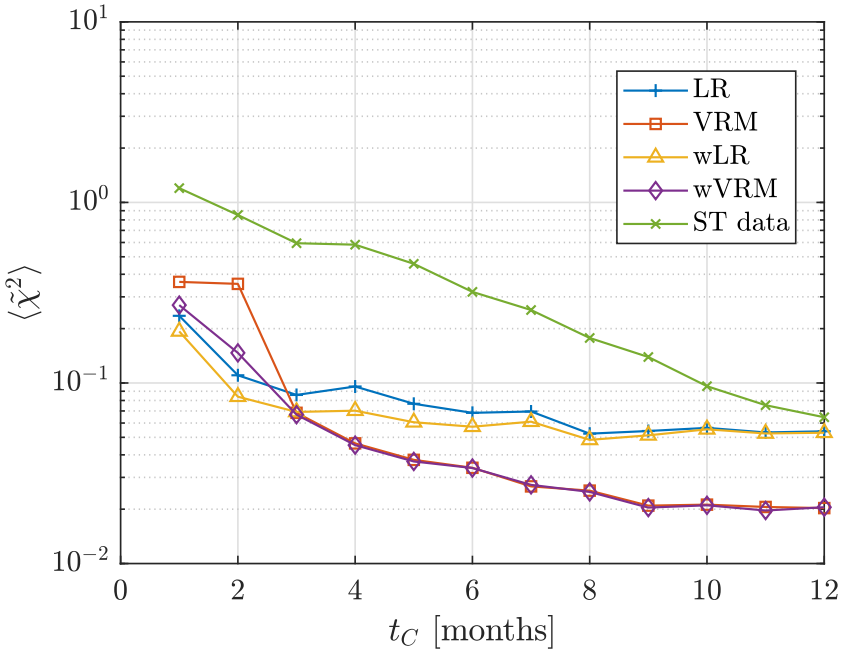


Figure 7.20: Ensemble mean of $\tilde{\chi}^2$ as a function of concurrent measurement time for the western sector at Høvsøre.

To compare the error in the predicted mean in the case with lidar to the case without lidar, $\tilde{\epsilon}$ is calculated. The ensemble mean of $\tilde{\epsilon}$ is plotted in Fig. 7.21. The figure shows that a bias exists for a $t_C$ of 1 month. When only 1 month of lidar data is used, the MCP method overestimates the true mean wind shear exponent. As the $t_C$ is increases, the bias decreases. It is remarkable that the bias is the largest for the VRM, because in the Breezanddijk case, the VRM gave the best result in comparison to the other three methods.

The same conclusion can be drawn from Fig. 7.22. The VRM decreases the error in the predicted mean, but its performance is worse than the other methods. The figure also shows that the weighted MCP methods offer a small improvement over the unweighted ones.

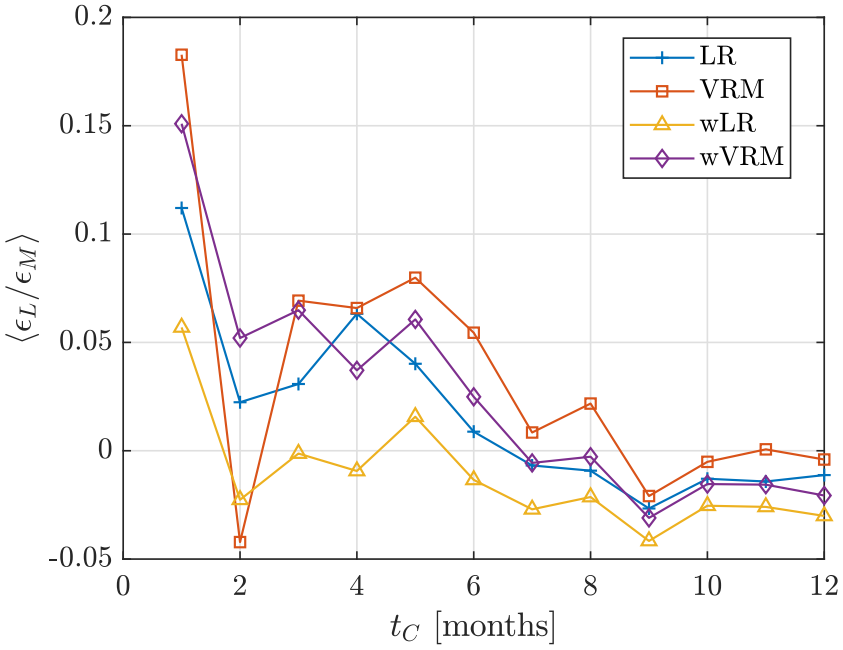


Figure 7.21: Ensemble mean of $\tilde{\epsilon}$ as a function of concurrent measurement time for the western sector at Høvsøre.

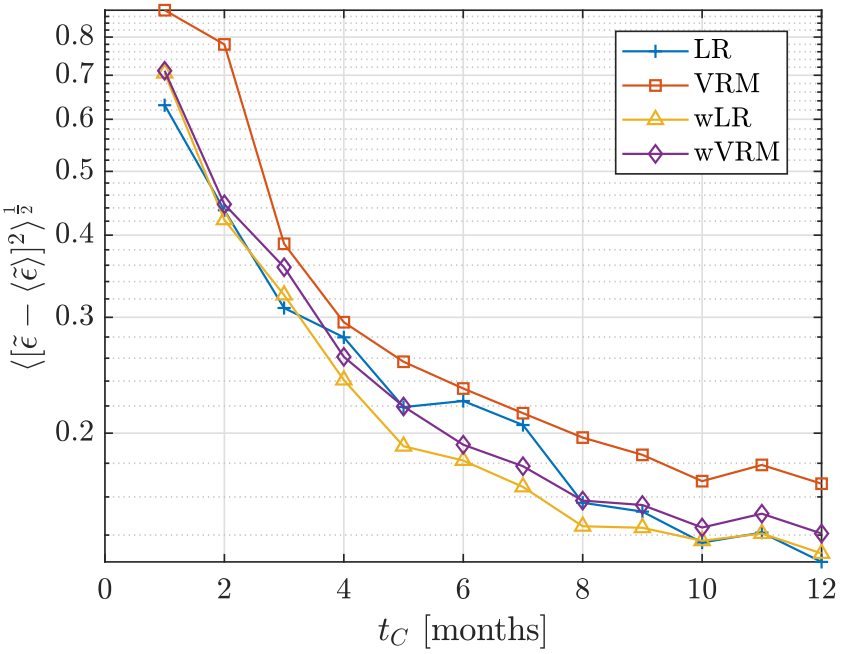


Figure 7.22: Ensemble standard deviation of $\tilde{\epsilon}$ as a function of concurrent measurement time for the western sector at Høvsøre.

In addition to the result of the western sector, selected plots for the eastern sector are shown. The same analysis as for the west has been performed on wind shear data from a 30-degree wind direction sector centred at 90 deg. The first three metrics, $\tilde{\mu}_{\hat{\alpha}}$, $\tilde{\sigma}_{\hat{\alpha}}$, and $\tilde{\chi}^2$ show a similar behaviour as the western sector. However, the ensemble statistics of $\tilde{\epsilon}$ as function of $t_C$ show some significant differences that shows the limits of the suggested MCP procedure. For this reason, the ensemble statistics are shown in Figs. 7.23 and 7.24. It is observed that the application of the lidar data and the MCP method is less successful in reducing the error. Two factors may explain the difference with the western sector. Firstly, the wind profile in the east is more affected by stable atmospheric conditions. Secondly, the prevailing wind direction at Høvsøre is the west, so more months of lidar data are necessary to record the same amount of data as for the western sector.

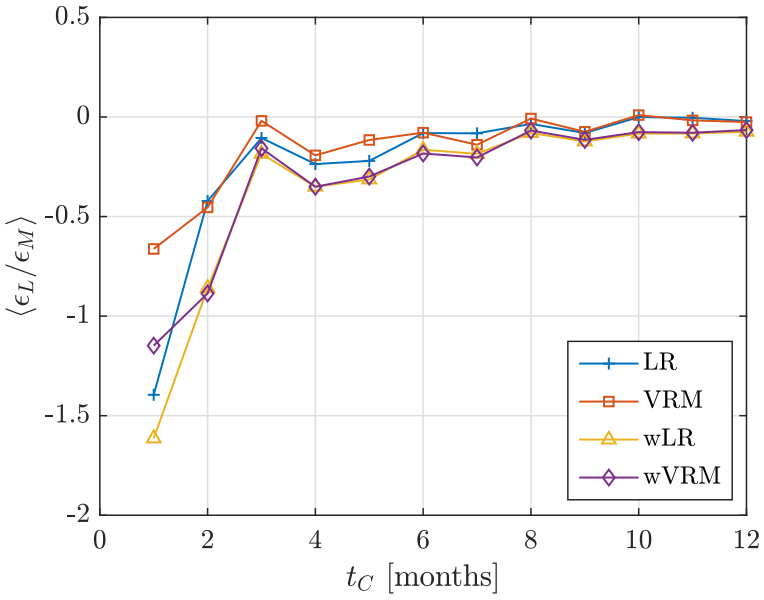


Figure 7.23: Ensemble mean of $\tilde{\epsilon}$ as a function of concurrent measurement time for the eastern sector at Høvsøre.

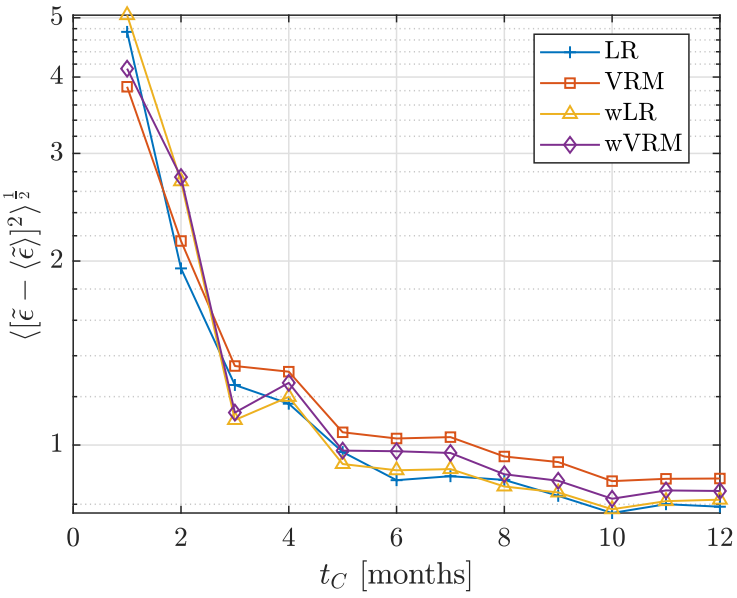


Figure 7.24: Ensemble standard deviation of $\tilde{\epsilon}$ as a function of concurrent measurement time for the eastern sector at Høvsøre.

### 7.3.4. Conclusion and Discussion

This section has shown the effect of the length of the concurrent measurement period $t_C$ on the MCP outcome, as well as, the convergence of the performance metrics without the application of MCP. At Breezanddijk, the MCP method has been used to find the one-year wind shear exponent distribution. At Høvsøre, MCP has been used to find a long-term (eight-year) wind shear exponent distribution. Therefor a $t_C$ of 12 months leaves an uncertainty due to inter-annual variability.

A comparison of the performance of four MCP methods was made using four performance metrics: the normalised mean, normalised standard deviation and the chi-squared statistic, and the normalised error of the mean. As expected, wind shear exponent distributions are better predicted by VRM methods. This is consistent with the findings of Rogers when he applied MCP to predict wind speed distributions [34]. However, it is acknowledged that the majority of application of the wind shear exponent require just the mean wind shear exponent.

The bias in the prediction of the mean wind shear exponent by the methods was small, and is in the order of 1%, even in the case where $t_C$ is only a few months.The uncertainty in the predictions also shows small differences. In the Breezanddijk case the LR method produced the largest uncertainty, whereas in the Høvsøre case the VRM method did. Assigning weights to the data results in minor improvements, and reduces the bias and uncertainty, in particular for the LR method

Results of the MCP method have been compared with the results of taking the short-term data as representative for the long-term. If MCP is not applied, the bias and uncertainty are significantly larger. Nevertheless, the metrics also converge without application of MCP, and the present study can be used to determine what period is required to get a good estimate of the mean and standard deviation of the shear exponent distribution. Thereby one has to keep in mind that the presented analysis used a direction selection. The $t_C$ does not indicate the actual number of data points within the selected sector. Depending on the wind direction distribution at a site, the convergence of the metrics for increasing $t_C$ may be different.

Using the normalised error in the mean wind shear exponent, the prediction of the mean using the proposed MCP procedure has been compared to the situation in which no lidar is available. When no lidar is available, the best estimate of the wind shear exponent above measurement mast height, is the wind shear exponent derived from mast measurements. This estimate often results in too high wind shear exponents, so an error exists. The proposed method of using MCP in combination with short-term lidar measurements can reduce this error. For the western sector the method was particularly successful and reduces the error by 50% for two months of lidar data. However, for the eastern sector 8 to 10 months of lidar data were necessary to reduce the error approximately 10%.

The present analysis also includes negative wind shear exponents. One would in general not use negative wind shear exponents for vertically extrapolating the wind resource, but there are reasons to include the negative part of the distribution. The share of negative shear exponents in the long-term distribution used in the examples of Section 7.2 is 4.5%. Excluding those measurements results in an overestimation of the mean wind shear exponent. Furthermore, as the lidar measures the wind speed directly at the prediction height the shear exponent resembles a relation between the wind speed measured at the two heights.

Finally, a remark is made on the perception of the presented MCP application. MCP in the way demonstrated here can be viewed as a typical MCP application of extrapolating observed wind shear exponents in time. However, one could also argue that the implemented MCP methods can be viewed as a first-order vertical extrapolation model for wind shear exponents: the long-term data is extrapolated to the height of the short-term data. It is noted that in the case of a MCP application on wind speed data, it is common to have a reference data set which is measured at a different, usually lower, height.

# 8

# The Effect of Wind Shear on the Prediction of Annual Energy Production

In this chapter, the role of the wind shear exponent in AEP estimations is discussed. Firstly, in Section 8.1 it is shown how the extrapolation of the wind speed depends on the wind shear exponent and the extrapolation distance, expressed by the height ratio $r = \frac{z_{pred}}{z_{obs}}$. Secondly, the uncertainty propagation from wind shear exponent to AEP is presented in Section 8.2.

## 8.1. Vertical Extrapolation of the Wind Speed

It is demonstrated how the vertical extrapolation of wind speeds depends on alpha and the ratio between the predicted and observed height.

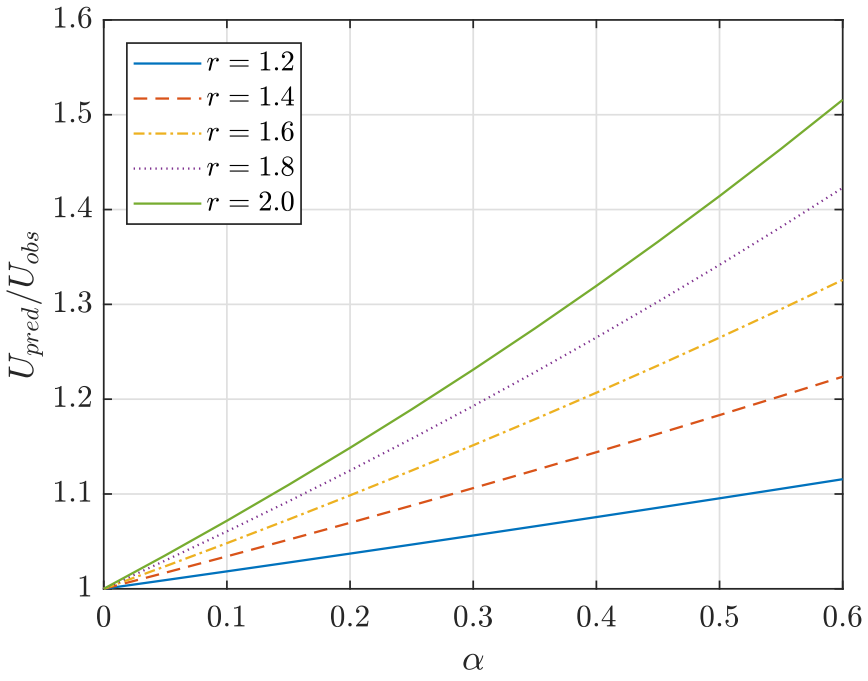


Figure 8.1: The effect of changing alpha on the ratio of the predicted wind speed and the observed wind speed for multiple height ratios, $r = \frac{z_{pred}}{z_{obs}}$.

## 8.2. Uncertainty Propagation

As shown in Section 7.3, the long-term mean wind shear exponent can be predicted using MCP. However, the outcome of the prediction varies. Therefor the predicted mean wind shear exponent is uncertain. In this section the propagation of the uncertainty in the wind shear exponent towards the uncertainty in the AEP is analysed. First the propagation to uncertainty in wind speed is discussed. Subsequently, the uncertainty in wind speed is used to find the uncertainty in the AEP.

### 8.2.1. Propagation to Wind Speed

Starting from the power law wind profile, Kelly derived an expression for the uncertainty in the predicted wind speed due to the uncertainty in the observed wind speed, and the uncertainty in the wind shear exponent [18]. The result is:

$$\tilde{\sigma}^2_{U_{pred}} \simeq \tilde{\sigma}^2_{U_{obs}} + \sigma^2_{\alpha}[\ln\left(\frac{z_{pred}}{z_{obs}}\right)] \tag{8.1}$$

In which $\sigma_{U_{obs}}$ is the uncertainty in the observed wind speed, $z_{obs}$ and $z_{pred}$ are the heights of the observed and the predicted wind speed respectively. The tildes indicate non-dimensional quantities. The dimensional uncertainty, $\sigma^2_{\alpha}$, can be related to a normalised uncertainty via:

$$\sigma^2_{\alpha} = \alpha^2 \tilde{\sigma}^2_{\alpha} \tag{8.2}$$

To study the effect of $\sigma_{\alpha}$ on the $\tilde{\sigma}_{U_{pred}}$, the uncertainty in the observed mean wind speed was assumed to be 1%. This allows direct calculation of the $\tilde{\sigma}_{U_{pred}}$. The result is given in Fig. 8.2.

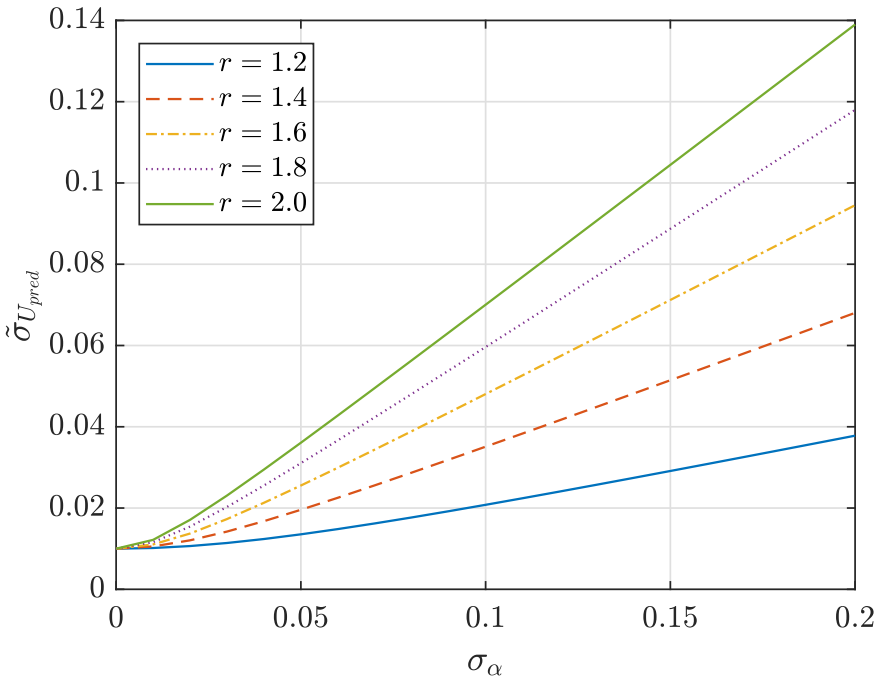


Figure 8.2: Non-dimensional uncertainty of the predicted wind speed, $U_pred$ as function of the uncertainty in the shear exponent, $\sigma\alpha$, following Eq. (8.1). For multiple height ratios, $r = \frac{z_{pred}}{z_{obs}}$.

### 8.2.2. Propagation to AEP

Propagation of the uncertainty in wind speed towards uncertainty in the AEP prediction is done by means of a method presented by Kelly et al. [20]. They state that the relation between mean wind speed, $\langle U \rangle$ and the AEP depend on the ratio of mean wind speed over rated wind speed, $\langle U \rangle / V_{\mathrm{rat}}$, and it can be expressed via:

$$\text{AEP} = \langle U \rangle^p \tag{8.3}$$

In the paper an expression for the exponent $p$ is derived. Here only the result is shown:

$$p = \frac{\pi(A/V_{\text{rat}})\text{sech}^2\left(\pi(A/V_{\text{rat}}) - \frac{1}{\sqrt{2}}\right)}{1 + \tanh\left(\pi(A/V_{\text{rat}}) - \frac{1}{\sqrt{2}}\right)} \tag{8.4}$$

If one takes into account that the Weibull scale parameter, $A$ is directly related to the mean wind speed for a given shape parameter, $k$ (see Eq. (8.5)), the exponent $p$ only depends on the ratio $\langle U \rangle / V_{\text{rat}}$. The function is plotted for a Weibull shape parameter of 2 in Fig. 8.3.

$$\langle U \rangle = A\Gamma(1 + 1/k) \tag{8.5}$$

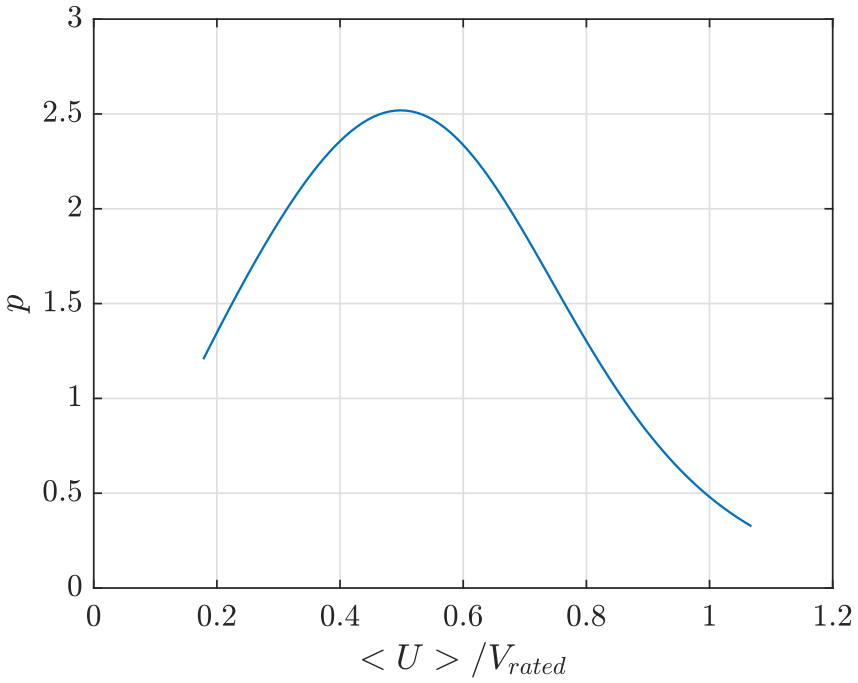


Figure 8.3: The exponent $p$ as function of the ratio mean wind speed over rated wind speed. For this $p$ curve a Weibull shape factor of 2 is assumed.

The model for the AEP,Eq. (8.3) is combined with the power law representation of the wind profile, to express the AEP as function of the wind shear exponent, the observed wind speed and the height ratio:

$$\text{AEP} = \langle U \rangle^p = [U_{obs} r^{\alpha}]^p \tag{8.6}$$

Equation (8.6) can be used to evaluate the uncertainty in AEP due to the uncertainty in the wind shear exponent:

$$\text{AEP} = \text{AEP}(\alpha_0) + \left(\frac{\partial \text{AEP}}{\partial \alpha}\right)[\alpha - \alpha_0] \tag{8.7}$$

$$\sigma_{\text{AEP}} = \frac{\partial \text{AEP}}{\partial \alpha}\sigma_\alpha \tag{8.8}$$

A resulting expression for normalised uncertainty in AEP,$\tilde{\sigma}_{\text{AEP}}$ due to uncertainty in $\alpha$ is found:

$$\tilde{\sigma}_{\text{AEP}} = p \ln(r)\sigma_\alpha \tag{8.9}$$

The $\tilde{\sigma}_{\text{AEP}}$ has been calculated for two height ratios and three values of the $p$-exponent. The result is shown in Fig. 8.4.

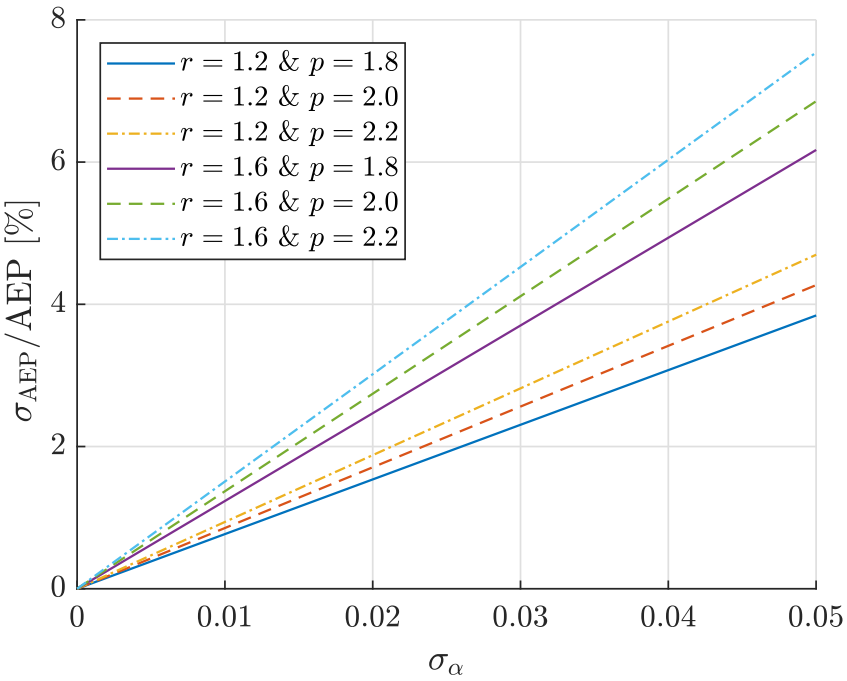


Figure 8.4: Uncertainty in AEP due to the uncertainty in the mean wind shear exponent for two height ratios, and three values of the $p$-exponent

## 8.3. Example of uncertainty propagation

The outcome of the previous section, which is Fig. 8.4, can be connected to the uncertainty in the mean wind shear exponent due to variable MCP input, as discussed in Section 7.3, to estimate the effect of the length of the measurement period on the uncertainty in AEP due to the uncertain mean wind shear exponent. In Section 7.1, the error $\epsilon_L$ was defined:

$$\epsilon_L = \mu_{\hat{\alpha}} - \mu_{\alpha_{true,LT}} \tag{8.10}$$

The standard deviation of $\mu_{\hat{\alpha}}$ is equal to the standard deviation of $\epsilon_L$. The measure for the uncertainty of the predicted mean wind shear exponent is the ensemble standard deviation of $\epsilon_L$.

This can be found by multiplying $\tilde{\epsilon}$ with $\epsilon_M$. If the results of the analysis of the third sector at Breezanddijk is taken as an example, it follows that $\epsilon_M$=0.0159. Using the data from Fig. 7.15, a $\sigma_\alpha$ can be calculated. Subsequently, Fig. 8.4 can be used to find the $\sigma_{AEP}$. The result is provided in Table 8.1.

Table 8.1: Example of uncertainty propagation, using the ensemble standard deviation of $\tilde{\epsilon}$ of the Breezanddijk case (see Fig. 7.15), and $r$ =1.6 and $p$ =2.0

| $t_C$ [months] | $\langle[\tilde{\epsilon} - \langle\tilde{\epsilon}\rangle]^2\rangle^{\frac{1}{2}}$ | $\sigma_\alpha = \sigma_{\epsilon_L}$ | $\sigma_{AEP}$ [%] |
|---|---|---|---|
| 1 | 0.5 | 0.008 | 1.1 |
| 3 | 0.3 | 0.005 | 0.7 |
| 6 | 0.2 | 0.003 | 0.4 |

# 9

# Conclusion and Recommendations

## 9.1. Conclusion

Lidar is a relatively new technique in wind resource assessment. The measurement principle of the lidar is different from the measurement principle of the traditional cup anemometer. The lidar measures the wind speed over a volume, whereas the cup measurement is considered to be a point measurement.

Data from two measurement sites have been used in this study: the Høvsøre test facility in Denmark, and the industrial measurement site Breezanddijk in the Netherlands. Lidar and mast pairs at the sites have been used to evaluate if the difference in measurement principle causes a difference in the derived wind shear exponents. In general, the shear exponents derived from mast and lidar are in good agreement. However, deviations arise due to the spatial separation between lidar and mast, and due to obstacles at the sites. For an ideal comparison, the lidar should be placed directly next to the mast, which causes a significant improvement in the correlation between mast and lidar.

When the length of a measurement period is reduced below one year, seasonality in the wind statistics becomes a concern. Therefore a detailed analysis of the variation of wind shear exponents has been made. It is shown that the mean shear exponent varies from season to season, in particular for the directions that are affected by the presence of the sea. The eastern sector at Høvsøre did not show high variation in the mean wind shear, but the shape of the wind shear exponent distribution varies from season to season. Particularly interesting are the distributions corresponding to the summer, as those distributions show two maxima. One could question the usefulness of a mean shear exponent for this situation.

Two standard MCP methods have been implemented for prediction of the long-term wind exponent distributions: the linear regression MCP and the variance ratio MCP. For the present application, two improvements have been considered of which one has been implemented, namely the assigning of weights to the concurrent data points. Only the linear regression MCP has been validated, as this method is available in the commercial wind software WindPRO.

In literature, no other examples have been found of the application of MCP to extrapolate the shear exponent distribution. This thesis has shown that the application of MCP can be used to predict long-term shear exponent distributions. The results can be used to make a recommendation on the required measurement period for obtaining wind statistics that are representative of the long-term.

The reduction of the measurement time of the lidar has a significant effect on the predictions. The variability of the MCP outcome is a function of the measurement time. This dependency means that the uncertainty of the prediction reduces when the measurement time is increased. The results of this research can be used to determine the required measurement time of the lidar. Furthermore, it has been shown that the estimation of the mean wind shear exponent can benefit from short-term lidar measurements. For the Breezanddijk case and the Høvsøre-West case, a reduction of the error was possible even using 1 or 2 months of lidar data in combination with MCP. This reduction is with respect to the case in which no lidar is available, and measurements performed below the prediction height are used.

Lastly, the propagation of uncertainty in the mean wind shear exponent to uncertainty in the AEP is analysed. The uncertainty due to vertical extrapolation is one out of the numerous uncertainties that are involved in the estimation of the wind resource at a potential site. An example has shown that the uncertainty is reduced when the amount of lidar data is increased. Increasing the measurement time from 1 month to 6 months yielded a decrease from $\sigma_{AEP} = 1.1\%$ to $\sigma_{AEP} = 0.4\%$.

## 9.2. Recommendations

Regarding recommendations for further work, it is suggested to keep looking into the effects of a variable wind shear exponent. The analysis performed in this thesis has shown that the wind shear and its distribution vary from season to season. The assumption that the wind shear is well represented by a mean wind shear exponent should be challenged.

It is suggested to look further into the extrapolation of the wind shear exponents using the MCP method. The presented evaluation of the MCP performance focused on the prediction of the distribution. More research is needed to assess the quality of the predicted time series.

Another part of the continuation of research could be on the improvement of the MCP method. Based on the analysis of the seasonal variation, it is suggested to include seasonal terms in the MCP method. Likewise, one could investigate the possibility of improving the MCP methods using additional input variables, or the possibility of enhancing the weighted MCP method which was presented here. More advanced correlation methods can be found in literature, and have been applied to extrapolate wind speed statistics. It would be interesting to see if these methods can improve the predictions.

Also, it would be good to look into the effect of choosing a different reference data set. It would be interesting to know to what extent the shear exponent distribution can be predicted when e.g. a mesoscale model is used to generate the reference data. Expanding the possible sources of reference data would increase the usability of the application of MCP to extrapolate wind shear statistics.

# Bibliography


[1] Allen Back. Variance of residuals in simple linear regression, 2011. URL `http://www.math.cornell.edu/~back/m171/sumsq_residuals/`. Retrieved on: 27-06-2017.

[2] José A. Carta, Sergio Velázquez, and Pedro Cabrera. A review of measure-correlate-predict (MCP) methods used to estimate long-term wind characteristics at a target site. *Renewable and Sustainable Energy Reviews*, 27:362–400, 2013.

[3] José A. Carta, Pedro Cabrera, José M. Matías, and Fernando Castellano. Comparison of feature selection methods using ANNs in MCP-wind speed methods. A case study. *Applied Energy*, 158: 490–507, 2015.

[4] A. Clifton, A. Smith, and M. Fields. Wind Plant Preconstruction Energy Estimates : Current Practice and Opportunities. Technical Report April, National Renewable Energy Laboratory, Golden, 2016.

[5] Peter J M Clive. Non-linearity in MCP with Weibull Distributed Wind Speeds. *Wind Engineering*, 32(3):319–323, 2009.

[6] G. A. Cool. Floating lidar technology. Master's thesis, Delft University of Technology, Delft, The Netherlands, September 2016.

[7] M Courtney, Rozenn Wagner, and P Lindelöw. Testing and comparison of lidars for profile and turbulence measurements in wind energy. *IOP Conference Series: Earth and Environmental Science*, 1:012021, 2008.

[8] A Crockford, M Müller, E Holtslag, and H Villanueva. Shorter Wind Measurement Campaigns. Speeding up wind farm developments with LiDAR, 2013.

[9] A. Derrick. Development of the measure-correlate-predict strategy for site assessment. In *Proc. BWEA*, 1992.

[10] Nikolay Dimitrov, Anand Natarajan, and Mark Kelly. Model of wind shear conditional on turbulence and its impact on wind turbine loads. *Wind Energy*, 18(11):1917–1931, 11 2015.

[11] Ali Dinler. A new low-correlation MCP (measure-correlate-predict) method for wind energy forecasting. *Energy*, 63:152–160, 2013.

[12] Stefan Emeis. Current issues in wind energy meteorology. *Meteorological Applications*, 21(4): 803–819, 2014.

[13] Michael Havbro Faber. *Statistics and probability theory : in pursuit of engineering decision support : Topics in Safety, Risk, Reliability and Quality*. Springer Science+Business Media B.V, Dordrecht, 2012.

[14] Sven Erik Gryning, Ekaterina Batchvarova, Burghard Brümmer, Hans Jørgensen, and Søren Larsen. On the extension of the wind profile over homogeneous terrain beyond the surface boundary layer. *Boundary-Layer Meteorology*, 124(2):251–268, 2007.

[15] M C Holtslag, W A A M Bierbooms, and G J W van Bussel. Estimating atmospheric stability from observations and correcting wind shear models accordingly. *Journal of Physics: Conference Series*, 555(1):12052, 2014.

[16] International Electrotechnical Commission. "IEC 61400-1 Wind turbines – Part 1: Design requirements, 2009.

[17] International Electrotechnical Commission. IEC: 61400-3 Wind turbines - Part 3: Design requirements for offshore wind turbines, 2009.

[18] Mark Kelly. Uncertainty in vertical extrapolation of wind statistics: shear-exponent and WAsP/EWA methods. Technical report, Technical Unicersity of Denmark, 2016.

[19] Mark Kelly and Sven Erik Gryning. Long-Term Mean Wind Profiles Based on Similarity Theory. *Boundary-Layer Meteorology*, 136(3):377–390, 2010.

[20] Mark Kelly and Hans Ejsing Jørgensen. Statistical characterization of roughness uncertainty and impact on wind resource estimation. *Wind Energy Science*, 2(1):189–209, 4 2017.

[21] Mark Kelly and Ib Troen. Probabilistic stability and 'tall' wind profiles: Theory and method for use in wind resource assessment. *Wind Energy*, 19(2):227–241, 2016.

[22] Mark Kelly, G Larsen, N K Dimitrov, and A Natarajan. Probabilistic Meteorological Characterization for Turbine Loads. *Journal of Physics: Conference Series*, 524(1):012076, 2014.

[23] Daeyoung Kim, Taewan Kim, Gwanjun Oh, Jongchul Huh, and Kyungnam Ko. A comparison of ground-based LiDAR and met mast wind measurements for wind resource assessment over various terrain conditions. *Journal of Wind Engineering and Industrial Aerodynamics*, 158 (September):109–121, 2016.

[24] Soon-Duck Kwon. Uncertainty analysis of wind energy potential assessment. *Applied Energy*, 87 (3):856–865, 2010.

[25] M. A. Lackner, A. L. Rogers, and J. F. Manwell. Uncertainty Analysis in MCP-Based Wind Resource Assessment and Energy Production Estimation. *Journal of Solar Energy Engineering*, 130 (3):031006, 2008.

[26] Matthew A. Lackner, Anthony L. Rogers, and James F. Manwell. The round robin site assessment method: A new approach to wind energy site assessment. *Renewable Energy*, 33(9):2019–2026, 2008.

[27] Matthew A. Lackner, Anthony L. Rogers, James F. Manwell, and Jon G. McGowan. A new method for improved hub height mean wind speed estimates using short-term hub height data. *Renewable Energy*, 35(10):2340–2347, 10 2010.

[28] MEASNET. MEASNET Procedure: Evaluation of Site-Specific Wind Conditions. Version 2, 4 2016.

[29] Torben Krogh Mikkelsen. Lidar-based Research and Innovation at DTU Wind Energy – a Review. *Journal of Physics: Conference Series*, 524(1):012007, 2014.

[30] A. A. Mortimer. A new correlation/prediction method for potential wind farm sites. In *Proc. BWEA*, 1994.

[31] M. Nielsen, L. Landberg, N.G. Mortensen, R.J. Barthelmie, and A. Joensen. Application of the measure-correlate-predict approach for wind resource assessment. In P. Helm and A. Zervos, editors, *Wind energy for the new millennium. Proceedings*, pages 773–776. WIP Renewable Energies, 2001.

[32] Alfredo Peña, Charlotte B Hasager, Merete Badger, Rebecca J Barthelmie, Ferhat Bingöl, Jean-Pierre Cariou, Stefan Emeis, Sten T Frandsen, Michael Harris, Ioanna Karagali, Søren E Larsen, Jakob Mann, Torben Mikkelsen, Mark Pitter, Sara Pryor, Ameya Sathe, David Schlipf, Chris Slinger, and Rozenn Wagner. Remote Sensing for Wind Energy. Technical report, Technical University of Denmark, Roskilde, 2015.

[33] Alfredo Peña, Rogier Floors, Ameya Sathe, Sven Erik Gryning, Rozenn Wagner, Michael S. Courtney, Xiaoli G. Larsén, Andrea N. Hahmann, and Charlotte B. Hasager. Ten Years of Boundary-Layer and Wind-Power Meteorology at Høvsøre, Denmark. *Boundary-Layer Meteorology*, 158(1): 1–26, 2016.

[34] Anthony L Rogers, John W Rogers, and James F Manwell. Comparison of the performance of four measure–correlate–predict algorithms. *Journal of Wind Engineering and Industrial Aerodynamics*, 93:243–264, 2005.

[35] J. Sanz Rodrigo, F. Borbón Guillén, P. Gómez Arranz, M. S. Courtney, Rozenn Wagner, and E. Dupont. Multi-site testing and evaluation of remote sensing instruments for wind energy applications. *Renewable Energy*, 53:200–210, 2013.

[36] David A Smith, Michael Harris, Adrian S Coffey, Torben Mikkelsen, Hans E. Jørgensen, Jakob Mann, and Régis Danielian. Wind lidar evaluation at the Danish wind test site in Høvsøre. *Wind Energy*, 9(1-2):87–93, 1 2006.

[37] R B Stull. *An Introduction to Boundary Layer Meteorology*. Kluwer Academic Publishers, Dordrecht, 1988. ISBN 978-90-277-2769-5.

[38] Motta M. Sørensen T. Thøgersen, M.L. and P. Nielsen. Measure-correlate-predict methods: case studies and software implementation. *European Wind Energy Conference & Exhibition*, 2007.

[39] Sergio Velázquez, José A. Carta, and J. M. Matías. Comparison between ANNs and linear MCP algorithms in the long-term estimation of the cost per kWh produced by a wind turbine at a candidate site: A case study in the Canary Islands. *Applied Energy*, 88(11):3869–3881, 2011.

[40] Jacobus Wouter Verkaik. *On Wind and Roughness over Land*. PhD thesis, Wageningen University, 2006.

[41] Rozenn Wagner. *Accounting for the speed shear in wind turbine power performance measurement*. PhD thesis, Technical University of Denmark, 2010.

[42] Harry L. Wegley, James V. Ramsdell, Montie M. Orgill, and Drake Ron L. A siting handbook for small wind energy conversion systems. Technical report, Pacific Northwest Laboratory, Richland, Washington, 3 1980.

[43] Jie Zhang, Souma Chowdhury, Achille Messac, and Bri Mathias Hodge. A hybrid measure-correlate-predict method for long-term wind condition assessment. *Energy Conversion and Management*, 87:697–710, 2014.

# A

# Simple example of the MCP method

In this appendix the application of three MCP methods is shown in a simple situation to illustrate the principle of the MCP method. A set of reference and target wind speeds and directions has been generated using Matlab's built-in multivariate normal random number generator. The set has a total length of 50 points. The input for the random number generator consists of a vector of mean values of the wind speed and wind direction time series, and a corresponding covariance matrix:

$$\mu = \begin{bmatrix} 9 & 11 & 190 & 160 \end{bmatrix} \qquad \mathbb{C} = \begin{bmatrix} 1 & 0.7 & 0.5 & 0 \\ 0.7 & 1 & 0.5 & 0.5 \\ 0.5 & 0.5 & 3600 & 2520 \\ 0 & 0 & 2520 & 3600 \end{bmatrix}$$

It is assumed that only the last 20 data points were measured at the target site, see Fig. A.1. The MCP method is applied to estimate the first 30 data points at the target site. The correlation methods used in this example are: linear regression, variance ratio method and the Mortimer method. The methods are explained in Section 2.3. The linear regression and the variance ratio method were applied without taking into account the wind speed directions. Therefor the correlation does not depend on the direction of the wind speed.

The correlation via the variance ratio method is given by

$$\hat{y} = \mu_y - \frac{\sigma_y}{\sigma_x}\mu_x + \frac{\sigma_y}{\sigma_x}x \tag{A.1}$$

The standard deviations and mean values from the sample can be found in Table A.1. In the table it is shown that the variance ratio method results in $\sigma(\hat{y}_{\text{VRM}}) = \sigma(y)$, ensuring that the standard deviation of the predicted wind speed is equal to the standard deviation of the observations. Further, it is shown that the standard deviation of the prediction via linear regression, is significantly lower.

A visualisation of the correlations is shown in Fig. A.2. It is observed that the slope of the linear regression fit is lower than the slope of the variance ratio method. This results in significant differences in the correlation for reference wind speeds below 8 m/s or above 11 m/s.

Table A.1: Mean values and standard deviations corresponding to the input and the results of the MCP example

| | **Input** | | **MCP Results** | | |
|---|---|---|---|---|---|
| | $x = U_{ref}$ | $y = U_{target}$ | $\hat{y}_{\text{LR}}$ | $\hat{y}_{\text{VRM}}$ | $\hat{y}_{\text{Mortimer}}$ |
| $\mu$ | 8.98 | 10.83 | 11.08 | 10.97 | 10.99 |
| $\sigma$ | 0.9083 | 1.0318 | 0.7011 | 1.0318 | 1.5714 |

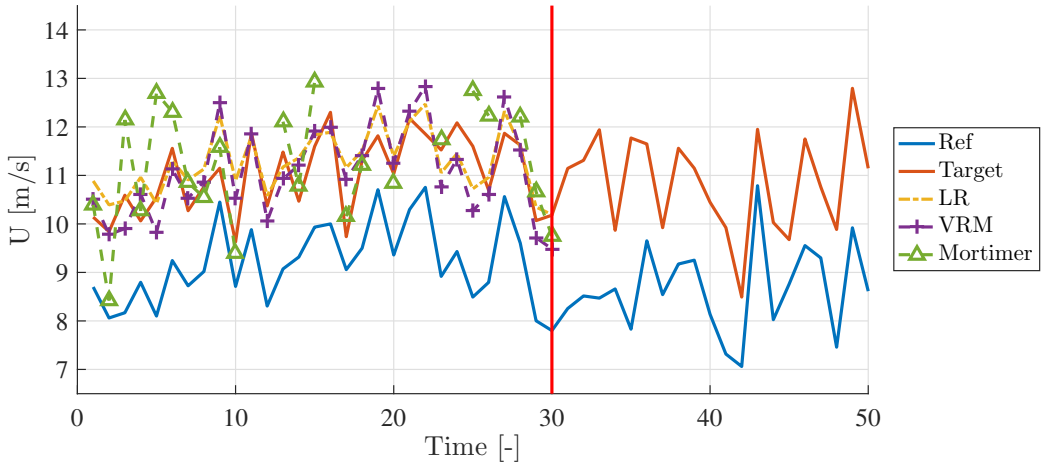


Figure A.1: Results of the MCP example using three methods: linear regression (LR), variance ratio method (VRM) and the Mortimer method. Furthermore the wind speeds at the target site and reference site are plotted.

As described in Section 2.3 the Mortimer method bins the wind speed measurements according to the wind speed and wind direction at the reference site. For this example three bins for the wind directions were established (0-120,120-240,240-360) and four bins for wind speed were established (0-8, 8-9, 9-10, 10-18). The reason for the large bins is the small data set. If the bins would be smaller, a lot of empty bins will exist, and the correlation for the corresponding wind speeds has to be estimated in a different way.

The binned data is used to construct two matrices, $R$ and $e$. The matrix $R$ contains the average of the wind speed ratios in each bin. The elements of $R$ and $e$ are calculated using:

$$R_{i,j} = \frac{1}{N} \sum_{n=1}^{N} \frac{y_{i,j}^{n}}{x_{i,j}^{n}} \tag{A.2}$$

$$e_{i,j} = \sqrt{\frac{1}{N} \sum_{n=1}^{N} (\frac{y_{i,j}^{n}}{x_{i,j}^{n}} - R_{i,j})^2} \tag{A.3}$$

In which $x$ is the wind speed at the reference site and $y$ is the wind speed at the target site. The subscripts $i$ and $j$ are used to indicate the direction bins and wind speed bins respectively. The $N$ represents the total number of wind speed ratios in the bin.

The resulting matrices for the example of Fig. A.1 are given below. Five of the matrix elements could not be calculated due to a lack of data. These matrix elements show ”Not a Number” (NaN) as the result. Other bins contain only very few data, which causes $e$ to be equal to zero. This directly shows the drawback of the Mortimer method. The concurrent measurement period has to be long enough to record a sufficient amount of data to construct the matrices. Alternatively, wider bins could be chosen or the missing elements of the matrices could be estimated using the known elements of the matrix, but these methods are not demonstrated here.

$$\mathrm{R} = \begin{bmatrix} 1.35 & \mathrm{NaN} & 1.16 & 1.11 \\ 1.33 & 1.23 & 1.24 & \mathrm{NaN} \\ \mathrm{NaN} & 1.35 & \mathrm{NaN} & \mathrm{NaN} \end{bmatrix}$$

$$\mathrm{e} = \begin{bmatrix} 0.21 & \mathrm{NaN} & 0 & 0 \\ 0.03 & 0.10 & 0.04 & \mathrm{NaN} \\ \mathrm{NaN} & 0.09 & \mathrm{NaN} & \mathrm{NaN} \end{bmatrix}$$

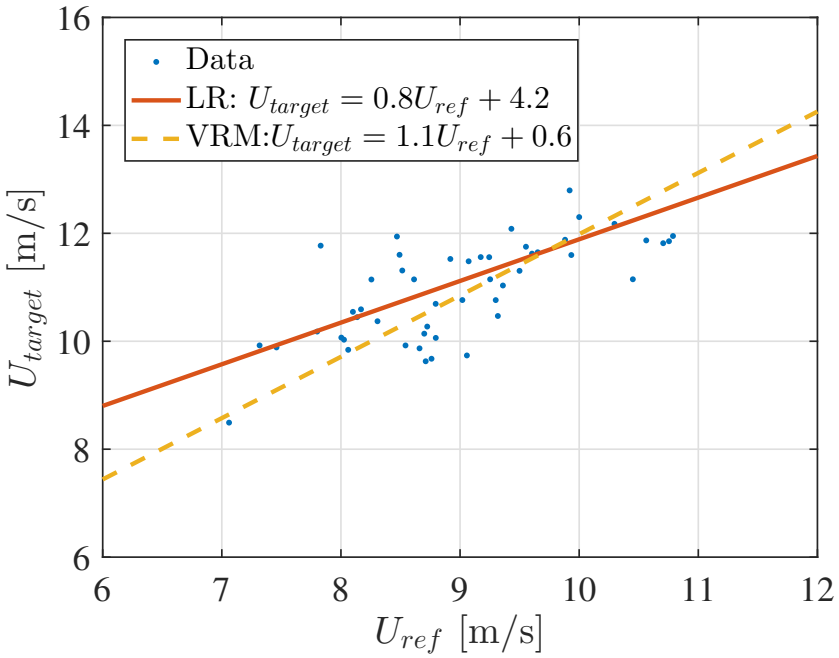


Figure A.2: The correlations found through linear regression (LR) and the variance ratio method (VRM).

# B

# Variance of the residuals in linear regression

This appendix shows how the variance of the residuals in linear regression relates to the variance of the dependent variable $y$, as derived by Back [1].

The result from linear regression is:

$$\hat{y}_i = b_1 x_i + b_0 \tag{B.1}$$

In which the slope $b_1$ is:

$$b_1 = \frac{\sigma(xy)}{\sigma^2(x)} = r\frac{\sigma(y)}{\sigma(x)} \tag{B.2}$$

In which the correlation coefficient $r$ is:

$$r = \frac{\sigma(xy)}{\sigma(x)\sigma(y)} \tag{B.3}$$

And the intercept $b_0$ is:

$$b_0 = \overline{y} - b_1\overline{x} \tag{B.4}$$

The residuals in linear regression are:

$$d = y_i - \hat{y}_i \tag{B.5}$$

Then the variance of the residuals of linear regression can be written as:

$$\begin{aligned}
\sigma^2(d) &= \sigma^2(y_i - \hat{y}_i) && \text{(B.6)}\\
&= \sigma^2(y_i - (b_1 x_i + \bar{y} - b_1\bar{x})) && \text{(B.7)}\\
&= \sigma^2(y_i - \bar{y} - b_1(x_i - \bar{x})) && \text{(B.8)}\\
&= \sigma^2{}_{y_i} + b_1^2\sigma^2{}_{x_i} - 2b_1\mathrm{Cov}(y_i - \bar{y}, x_i - \bar{x})) && \text{(B.9)}\\
&= \sigma^2{}_{y_i} + r^2\frac{\sigma^2{}_{y_i}}{\sigma^2{}_{x_i}}\sigma^2{}_{x_i} - 2r\frac{\sigma_{y_i}}{\sigma_{x_i}}(r\sigma_{y_i}\sigma_{x_i}) && \text{(B.10)}\\
&= \sigma^2{}_{y_i} - r^2\sigma^2{}_{y_i} && \text{(B.11)}\\
&= \sigma^2{}_{y_i}(1 - r^2) && \text{(B.12)}
\end{aligned}$$

The variance of the residuals, $\sigma^2(d)$ is smaller than the variance of the dependent variable $\sigma^2(y)$, when the correlation coefficient $r$, is unequal to zero.

# C

# Power law representation of observed wind profiles

The power law representation of wind profiles is probably the most used wind profile representation for engineering purposes. An example of its application is the IEC standard, in which the wind shear exponent of the power law is used to specify the wind shear over the rotor.

$$u(z) = u_{ref}\left(\frac{z}{z_{ref}}\right)^{\alpha} \tag{C.1}$$

The power law is fitted using the log ratio method. This method uses wind speed measurements at two heights to calculate the wind shear exponent via:

$$\alpha = \frac{\ln(u_2/u_1)}{\ln(h_2/h_1)} \tag{C.2}$$

In this appendix, the power law representation of wind profiles observed at Breezanddijk is discussed in Appendix C.1. Further, the power law wind profile is shown for a range of wind shear exponents in Appendix C.2.

## C.1. Power law fit to Wind profiles observed at Breezanddijk

The power law is limited to increasing wind speeds over height, i.e. for negative wind shear exponents the wind profile is not correctly described by the power law. However, current wind turbine rotors are large, reaching heights from 40 to 200 m. In this height regime, the wind speed is not always strictly increasing with height, and the assumption of a constant shear exponent does not hold. As the extrapolation distance increases, the accuracy of the wind profile representation decreases. Therefor the estimated wind speeds over the rotor can significantly deviate from the observed wind speed. In Fig. C.1 four observed 10-min averaged wind profiles are plotted along with three corresponding fits of the power law. The fits have been calculated using the log ratio method, but using different heights.

- The first shear exponent, $\alpha_{40-75}$, is based on wind speed measurements at 40 m and 75 m. These are heights at which typical met masts measure the wind speed.
- The second shear exponent, $\alpha_{40-200}$, is based on wind speed measurements at 40 m and 200 m. This shear exponent could be used to represent the wind shear over a large wind turbine rotor, with a hub height of approximately 120 m.
- The third shear exponent, $\alpha_{40-120}$ is based on wind speed measurements at 40 m and 120 m. This shear exponent is necessary for the extrapolation of the wind speed to a typical hub height of 120 m.

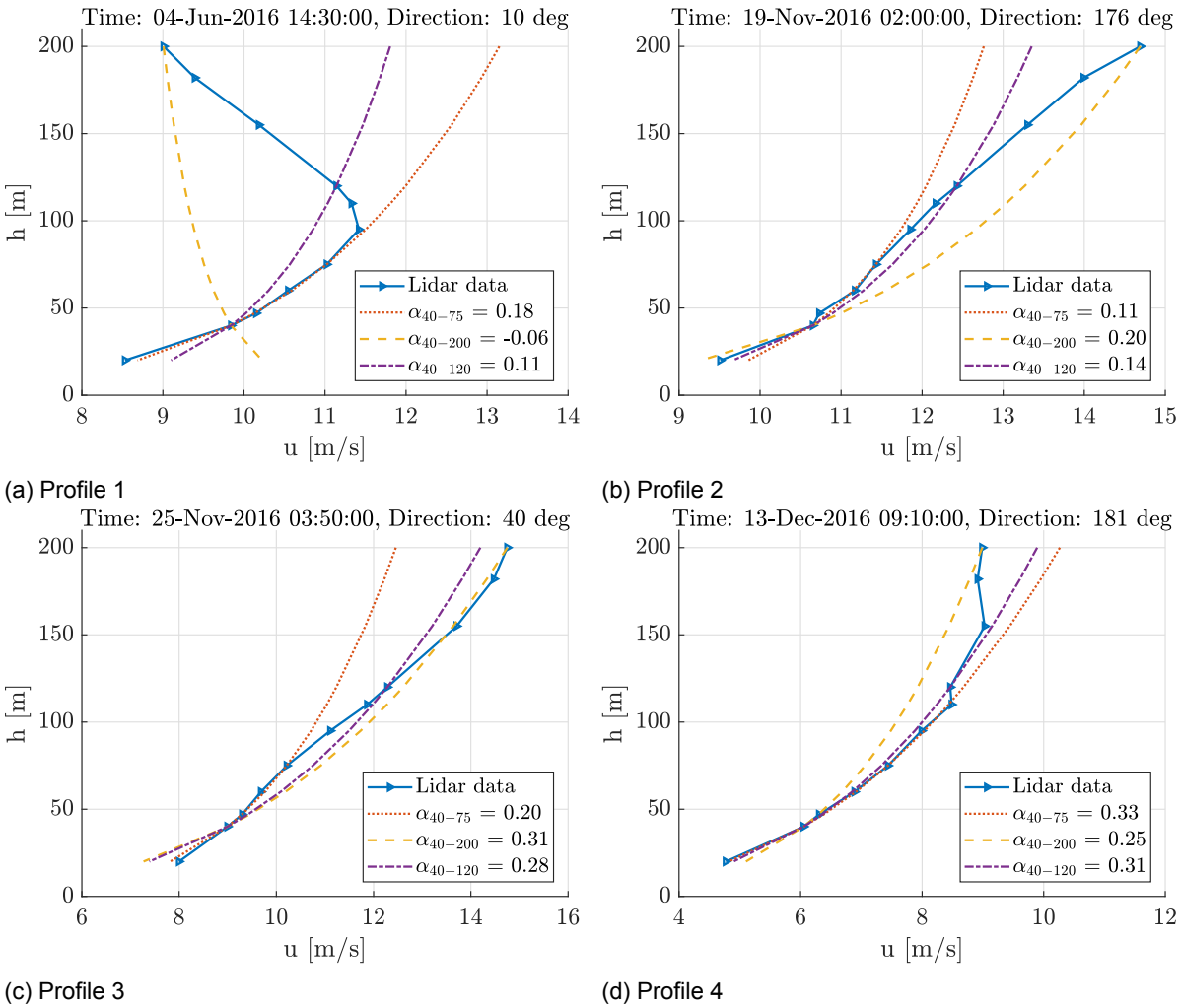


(a) Profile 1

(b) Profile 2

(c) Profile 3

(d) Profile 4

Figure C.1: Log ratio fit of the power law to four observed 10-min averaged wind profiles at Breezanddijk. The time stamp and mean wind direction at 95 m of the 10-min period is provided for each wind profile.

The observed wind profile of Fig. C.1a shows a low-level jet. The wind speed increases from ground level to 95 m and a decreases for heights above 100 m. The power law profile using $\alpha_{40-75}$ drastically overestimates the wind speed at heights above 100 m. The $\alpha_{40-200}$ is negative and the corresponding power law profile fails to represent the observed profile.

The wind profile in Fig. C.1b shows an increasing wind shear with height. The power law based on $\alpha_{40-75}$ leads to an underestimation of wind speed around hub height. Using $\alpha_{40-200}$ leads to an overestimation of the wind speed over the rotor plane. Another example of $\alpha_{40-75}$ leading to underestimation of the wind speed is provided in Fig. C.1c. However in this case the wind over the rotor plane is well represented by the power law using $\alpha_{40-200}$ or $\alpha_{40-120}$.

## C.2. Examples of the power law wind profile

In Fig. C.2 the power law profile is plotted for a range of shear exponents.

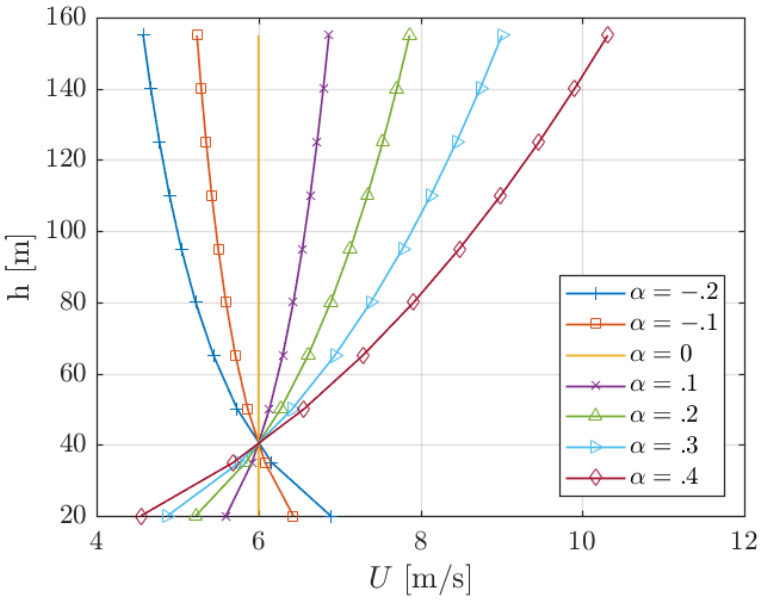


Figure C.2: The power law wind profile for a shear exponent ranging from -0.2 to 0.4

# D

# Comparison of shear measured at met mast and lightning mast

This appendix includes the results of the analysis in which the shear derived at the met mast is compared to the shear derived at the lightning mast. The masts are located at the Høvsøre measurement site. A description of the site is provided in Section 3.2. The method used for the analysis is similar to the method used in Chapter 4 and is described in Section 4.1.

Table D.1: Comparison of the shear exponent $\alpha_{100-160}$ measured at the met mast and at the lightning mast per direction sector at Høvsøre

| | | **East** | | **West** | |
|---|---|---|---|---|---|
| **Parameter** | **Indicator** | MM | Sonic | MM | Sonic |
| | # Samples | 6488 | 6488 | 13252 | 13252 |
| | # vs MM | | 6488 | | 13252 |
| $\alpha$ 60-100 | Mean [-] | 0.2388 | 0.2346 | 0.1560 | 0.1545 |
| | BIAS [-] | | -0.0042 | | -0.0015 |
| | RMSE [-] | | 0.0534 | | 0.0336 |
| | Slope [-] | | 0.9304 | | 0.9682 |
| | $R$ [-] | | 0.9013 | | 0.9457 |

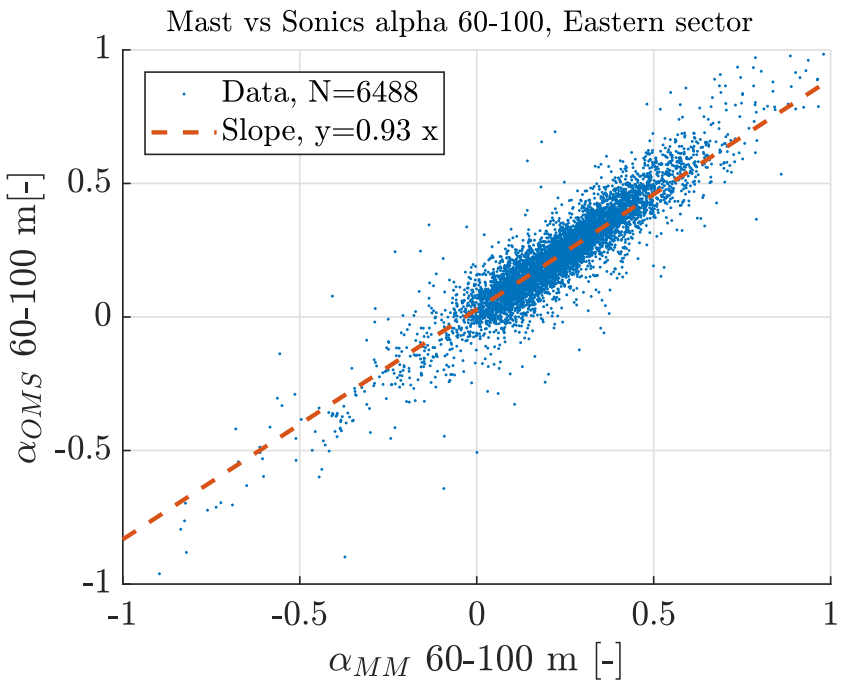


Figure D.1: Comparison of the shear exponent $\alpha_{60-100}$ measured at the met mast and at the lightning mast for the eastern sector.

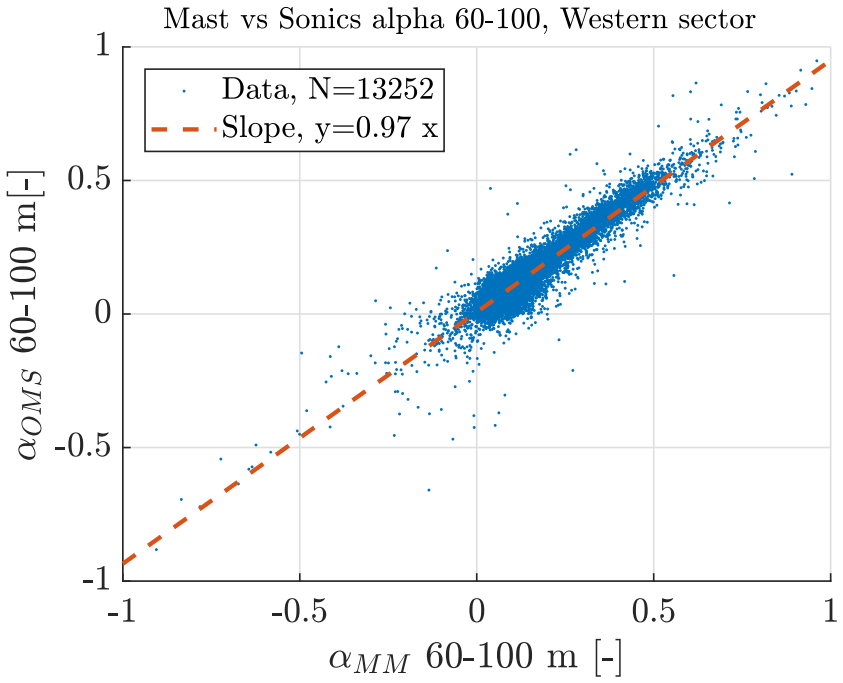


Figure D.2: Comparison of the shear exponent $\alpha_{60-100}$ measured at the met mast and at the lightning mast for the western sector

# E

# WindPRO and Matlab linear regression MCP results

This appendix includes the correlations established for the linear regression MCP in Matlab and WindPRO. The anomalous results, for which the Matlab and WindPRO result show a deviation of the order $10^{-2}$, have been highlighted.

Table E.1: Validation case 1: Comparison of MCP correlations for 12 sectors at Breezanddijk by Matlab and WindPRO

| **Sector** | **Slope** | | **Intercept** | |
|---|---|---|---|---|
| | Matlab | WindPRO | Matlab | WindPRO |
| 1 | 1.0182 | 1.0182 | -0.0238 | -0.0238 |
| 2 | 1.0292 | 1.0292 | -0.1166 | -0.1166 |
| 3 | 1.0194 | 1.0194 | -0.0330 | -0.0330 |
| 4 | 1.0083 | 1.0083 | 0.0640 | 0.0640 |
| 5 | 0.8023 | 0.8023 | 0.4034 | 0.4034 |
| 6 | 1.0426 | 1.0426 | -0.5461 | -0.5461 |
| 7 | 1.1088 | 1.1088 | -1.1470 | -1.1469 |
| 8 | 1.0319 | 1.0318 | -0.2138 | -0.2130 |
| 9 | 1.0169 | 1.0169 | 0.0137 | 0.0137 |
| 10 | 1.0096 | 1.0096 | 0.0369 | 0.0369 |
| 11 | 1.0099 | 1.0099 | 0.0210 | 0.0210 |
| 12 | 0.9945 | 0.9945 | 0.1231 | 0.1231 |

Table E.2: Validation case 2: Comparison of MCP correlations for 12 sectors at Høvsøre by Matlab and WindPRO

| **Sector** | **Slope** | | **Intercept** | |
|---|---|---|---|---|
| | Matlab | WindPRO | Matlab | WindPRO |
| 1 | 0.5657 | 0.5656 | 2.9728 | 2.9729 |
| 2 | 0.8729 | 0.8729 | 0.9891 | 0.9891 |
| 3 | 0.9822 | 0.9822 | -0.1564 | -0.1564 |
| **4** | **0.9848** | **0.9922** | **-0.1402** | **-0.1525** |
| **5** | **0.9711** | **0.9860** | **0.1083** | **-0.0232** |
| 6 | 1.0275 | 1.0277 | -0.1656 | -0.1669 |
| 7 | 1.0015 | 1.0015 | -0.0413 | -0.0413 |
| 8 | 1.0035 | 1.0035 | -0.1351 | -0.1351 |
| 9 | 1.0031 | 1.0031 | -0.0353 | -0.0353 |
| 10 | 1.0105 | 1.0105 | -0.2128 | -0.2128 |
| 11 | 0.9692 | 0.9692 | -0.5425 | -0.5425 |
| 12 | 0.6375 | 0.6375 | 1.5207 | 1.5207 |